CHAPTER 9

STABLE AND RADIOGENIC ISOTOPES

9.1 INTRODUCTION

This section presents new stable and radiogenic isotopic data for ore and gangue minerals from El Teniente. These isotopic datasets are used to constrain the sources of the fluids involved in the magmatic-hydrothermal system and to investigate their temporal and spatial variations in order to evaluate potential ore depositional mechanisms.

9.2 SULFUR ISOTOPES

Introduction

Due to the significant difference in atomic mass between stable isotopes of sulfur, oxygen, hydrogen, and carbon, their individual isotopes can be distributed unevenly among phases during chemical reactions. This partitioning is known as fractionation, and is responsible for creating reservoirs of homogenous isotopic composition involved in geological processes (Campbell and Larson, 1998). Fractionation is also influenced by physico-chemical effects including changes in temperature, oxidation potential (redox), pH, and by processes such as phase separation (e.g., Ohmoto and Goldhaber, 1997).

Data obtained from sulfur isotope analysis of sulfide and sulfate minerals can be used to help interpret sources of sulfur, temperatures of deposition, and chemical conditions of ore formation (e.g., Ohmoto and Rye, 1979, Ohmoto and Goldhaber, 1997). Using samples constrained paragenetically, it is also possible to investigate spatial and temporal variations in sulfur isotope compositions, and to use this information to help infer processes of fluid evolution.

Porphyry copper systems typically have sulfide $\delta^{34}S$ values near zero ($\pm$ 5‰) and co-precipitated anhydrite values mostly from 8‰ to 15‰ (e.g., Ohmoto and Rye, 1979; Ohmoto and Goldhaber 1997). SO_2 and H_2S are the predominant sulfur species

in high temperature (> 350° - 400°C) magmatic-derived fluids. At temperatures below ~350° - 400°C, SO_4^{2-} becomes the predominant oxidized sulfur species. Under oxidizing conditions ($SO_4/H_2S > 1$) the ^{34}S isotope will preferentially fractionate into the oxidized sulfur species (Ohmoto and Goldhaber, 1997) and be incorporated into anhydrite. Sulfide species precipitating from the oxidized fluid will be enriched in ^{32}S and have isotopically light $\delta^{34}S$ values (Rye et al., 1993). Cooling of an oxidized fluid results in a wide spread of $\delta^{34}S$ $_{sulfide}$ values and a narrow range of coprecipitated $\delta^{34}S_{sulfate}$ values (Rye et al., 1993). A narrow range of $\delta^{34}S$ $_{sulfide}$ values and a wider range of $^{34}S_{sulfate}$ values reflects reducing fluid conditions ($SO_4/H_2S < 1$). Variations in the redox state of the fluid have been interpreted to explain arrays of $\delta^{34}S$ sulfide values reported from porphyry copper deposits at Goonumbla, (Heithersay and Walshe, 1995; Lickfold, 2002) and Cadia (Harper, 2000; Wilson, 2003) in the Lachlan Fold Belt, central NSW, and from the Sur-Sur breccia at Río Blanco (Frikken et al., submitted). Mixing of isotopically distinct sulfur sources can also generate variable $\delta^{34}S_{sulfide}$ values (e.g., Ohmoto and Goldhaber, 1997).

Previous Work

Kusakabe et al. (1984) analyzed 42 sulfide (chalcopyrite, pyrite, galena) and 31 anhydrite samples in their study of oxygen and sulfur isotopic compositions from El Teniente. Sulfide and sulfate $\delta^{34}S$ values varied from -6.5‰ to +1.6‰ and +8.6‰ to +15.5‰ respectively (Fig. 9.2F). The most negative ^{34}S values were from LH stage galena (Kusakabe et al., 1984). The average calculated $\delta^{34}S$ fractionation between anhydrite and chalcopyrite ($\Delta_{anh-cpy}$) increased from 12.8‰ from the LM stage to 16.8‰ for the *Postuma* stage (LH vein stage 4c and 4d). Based on $\Delta_{anh-cpy}$, Kusakabe et al. (1984) calculated depositional temperatures of 460°C (± 41°C) for the LM stage, to 420-410°C (± 35°C) for the PH and LH stages, and 360°C for the *postuma* stage. In order to determine the $\delta^{34}S_{\Sigma S}$ fluid value for the Teniente system, Kusakabe et al. (1984) plotted data from sulfide-sulfate mineral pairs on a $\delta^{34}S$ vs $\Delta\delta^{34}S_{sulfate-sulfide}$ diagram (Fig. 9.1). According to the method of Field and Gustafson (1976), the point at which the sulfide and sulfate trendlines intersect the Y-axis represents the bulk sulfur composition of the fluid. Assuming that the sulfide and sulfate were precipitated in equilibrium, Kusakabe et al. (1984) calculated a bulk sulfur composition of +4.5‰ and a SO_4/H_2S ratio of approximately 1 for Teniente (Fig. 9.1). However, Ohmoto (1986) argues against the use of this methodology as the axes and the intersecting trendlines
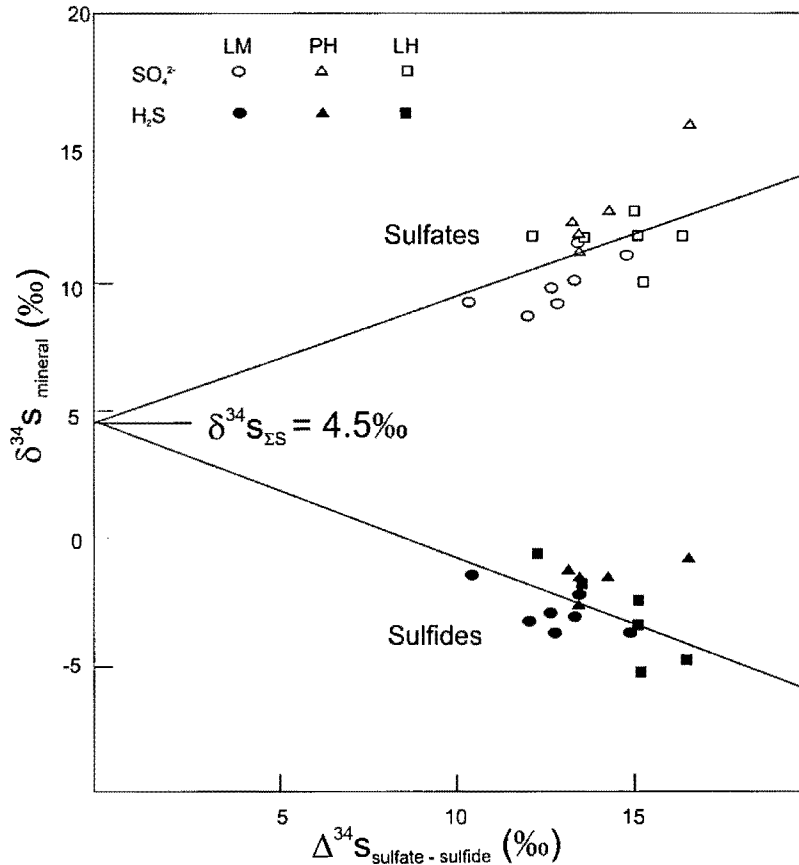
Figure 9.1. δ^{34}S (sulfide and sulfate) vs $\Delta\delta^{34}$S$_{sulfate-sulfide}$ diagram from Kusakabe et al. (1984). From this dataset Kusakabe et al. (1984) estimate a bulk sulfur composition of 4.5‰ and a sulfate/sulfide ratio of 1:1.

are mathematically dependent. Consequently, this methodology will not be used in the current study.

Methodology

In this study a total of 59 sulfur isotope analyses of sulfides (chalcopyrite, bornite, pyrite, molybdenite) and 21 sulfates (anhydrite) have been obtained from 45 samples. Samples were chosen predominantly from section-83 (1000N), in order to investigate the spatial variations of the sulfide and sulfate ^{34}S values existing in the Teniente hydrothermal system. The current study aims to provide more detailed spatial resolution of the sulphur isotope systematics than the study of Kusakabe et al. (1984). Where possible, analyses of sulfide/sulfate mineral pairs from anhydrite breccias and anhydrite-bearing veins has been undertaken for sulfur isotope geothermometry.

Of the 80 sulfide and sulfate samples analyzed, 64 samples contained coarse sulfide and/or sulfate amenable to hand drilling. These were analysed by using the con-

ventional techniques of Robinson and Kusakabe (1975). Sixteen samples, from veins and disseminated in alteration assemblages, contained sulfides that were too fine grained (<1mm) to be hand drilled. These were analyzed by laser ablation, according to the method of Huston et al. (1995). Conventional and laser ablation analyses were performed by Keith Harris of the Central Science Laboratory (CSL), University of Tasmania. Analytical methods are contained in Appendix 6A, and all results are listed in Appendix 6E.

Results

The laser ablation and conventional $\delta^{34}S$ isotope datasets, summarised in Table 9.1, have overlapping ranges (Appendix 5B). The laser ablation data are more variable and on average 0.7‰ - 1.3‰ lighter than the conventional dataset. Pyrite from a stage 2-distal vein was analysed by conventional methods ($\delta^{34}S$ = -0.2‰) and by laser ablation methods ($\delta^{34}S$ = -1.81‰). A laser ablation repeat analysis returned $\delta^{34}S$ values of –0.48‰ and -1.83‰ from adjacent chalcopyrite crystals from the same vein. These differences are probably due to fine scale $\delta^{34}S$ variations in the sulfide crystals that are only detectable by laser ablation analyses (Keith Harris, pers. comm., 2002).

Stage	Mineral	No. samples	$\delta^{34}S_{min}$	$\delta^{34}S_{max}$	$\delta^{34}S_{mean}$
Late Magmatic	bornite	9	-5.3	-1.0	-2.9
	chalcopyrite	16	-5.9	0.2	-1.8
	molybdenite	3	-0.6	0.7	-0.1
	anhydrite	9	10.1	12.8	11.4
Late Magmatic – transitional - propylitic zones	chalcopyrite	2	-2.9	0.1	-1.4
	pyrite	8	-1.8	0.7	-0.6
	anhydrite	1			14.6
Principal Hydrothermal	chalcopyrite	7	-2.1	-0.3	-1.4
	pyrite	1			-1.5
	anhydrite	3	11.7	13.4	12.7
Late Hydrothermal	bornite	1			-3.7
	chalcopyrite	5	-5.7	-0.8	-3.8
	pyrite	2	-1.2	-1.3	-1.2
	molybdenite	2	-1.8	2.4	0.3
	anhydrite	6	10.0	12.6	11.7
Agua Amarga	chalcopyrite	1			-1.1
	pyrite	2	-5.2	0.3	-2.5
	anhydrite	1			9.9

Table 9.1. Summary of $\delta^{34}S$ results for El Teniente from the current study. Errors are ± 0.2‰ for conventional and ± 0.4‰ for laser ablation analysis.

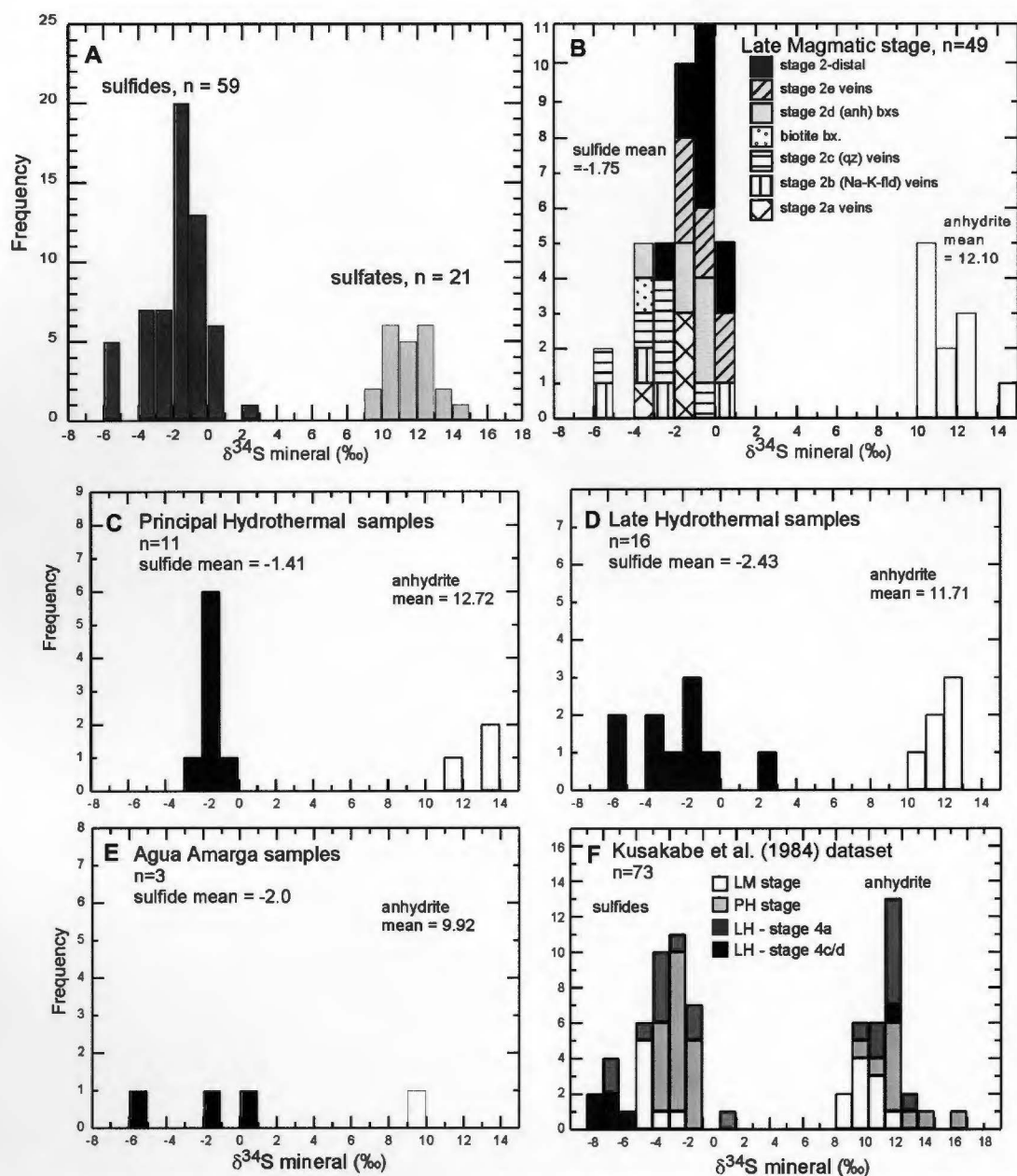**Figure 9.2.** Histograms of $\delta^{34}S_{sulfide}$ and $\delta^{34}S_{sulfate}$ values for the different stages at El Teniente. A to E are from the current study. All data are contained in Appendix 6E.

A) All sulfides and sulfates analysed in the current study.   D) Late Hydrothermal stage

B) Late Magmatic stage   E) Agua Amarga

C) Principal Hydrothermal stage   F) Dataset of Kusakabe et al. (1984)

Late Magmatic sulfides and sulfates

A total of 37 LM sulfides analysed in the current study have a $\delta^{34}S$ mean of -2.0‰, and a range from -5.9 to +0.7‰. Bornite and chalcopyrite have a similar range of $\delta^{34}S$ values (Table 9.1); however, bornite has a lower $\delta^{34}S$ mean (-2.9‰) than chalcopyrite (-1.8‰). Three molybdenite sample cluster near zero (-0.6 to +0.7‰). Nine anhydrite

229

samples have a mean $\delta^{34}S$ value of 11.5‰, with the dataset ranging from 10.1 to 12.8‰.

Samples from the different LM paragenetic stages have overlapping ranges of $\delta^{34}S$ sulfide values (Figure 9.2B). In general sulfides from stage 2b (Na-K-feldspar) veins, stage 2c (quartz) veins, and biotite breccias have more negative $\delta^{34}S$ values than the stage 2e veins and LM distal veins. The lightest $\delta^{34}S$ values are from stage 2b and 2c veins (-5.9‰ and -5.3‰) from the zone of intense pervasive Na-K-feldspar alteration associated with the dacite pipe on section-124 (Figs. 4.9 and 8.1). The heaviest values are from LM veins from the transitional and propylitic zones (Figs. 4.9 and 8.1), which have a $\delta^{34}S$ mean of -0.7‰ and a range from -2.9 to +0.7‰ (Table 9.1). A LM anhydrite sample from the propylitic zone has the highest $\delta^{34}S$ value (14.6‰) recorded from the deposit.

A well-defined sulfur isotope zonation exists for the LM stage copper-iron sulfides on section-83 (1000N). The most negative sulfide $\delta^{34}S$ values (< -3‰) occur close to and within the dacite porphyry. The copper-sulfides have progressively heavier $\delta^{34}S$ values peripheral to the dacite and upwards throughout the deposit. In the transitional and propylitic zones, greater than 400m away from the dacite contacts, the $\delta^{34}S$ values are consistently > -1‰.

Principal Hydrothermal and Late Hydrothermal sulfides and sulfates

Eight sulfide samples from chalcopyrite-rich PH veins have a $\delta^{34}S$ mean of -1.4‰, ranging from -2.1 to -0.3‰ (Table 9.1, Fig. 9.2C). The compositions of chalcopyrite and pyrite overlap. LH sulfides are on average isotopically lighter and more variable than PH sulfides (Table 9.1, Fig. 9.2D). Ten LH sulfide samples have a $\delta^{34}S$ mean of -2.4‰, ranging from   −5.7‰ to +2.4‰. Bornite and chalcopyrite have lighter $\delta^{34}S$ values (mean = -3.7‰ and -3.8‰ respectively) than pyrite and molybdenite (mean = -1.2‰ and 0.3‰ respectively). Anhydrite from PH and LH stage veins has $\delta^{34}S$ values from 10.0‰ to 13.4‰.

$\delta^{34}S_{sulfide}$ values from PH and LH stage have a negative relationship with elevation (Fig. 9.4). For both the PH and LH datasets more negative $\delta^{34}S_{sulfide}$ values occur at higher elevations, and less negative values occur deeper in the deposit, with the excep-
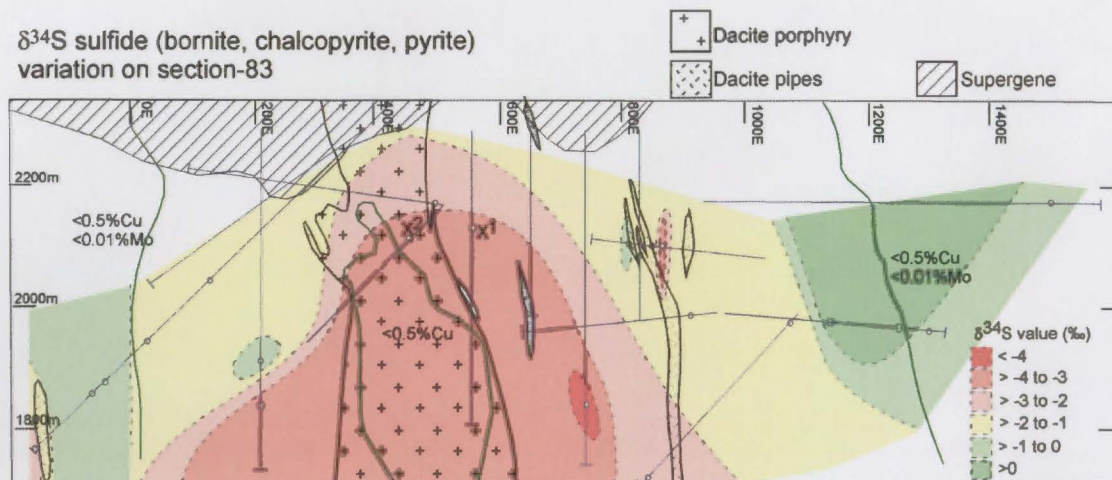
Figure 9.3. Spatial zonation of 22 Late Magmatic stage δ^{34}S Cu-Fe sulfide values on section-83 (1000N). Where more than one δ^{34}S value exists for a sample, the chalcopyrite value is used. Point X^1 is from Kusakabe et al. (1984), and is the only LM stage δ^{34}S sulfide sample on this section from their study. Point X^2 (from this study) is projected 400m from the south (from DDH1505, 7m, section-600N). The molybdenite data do not conform to this zonation.
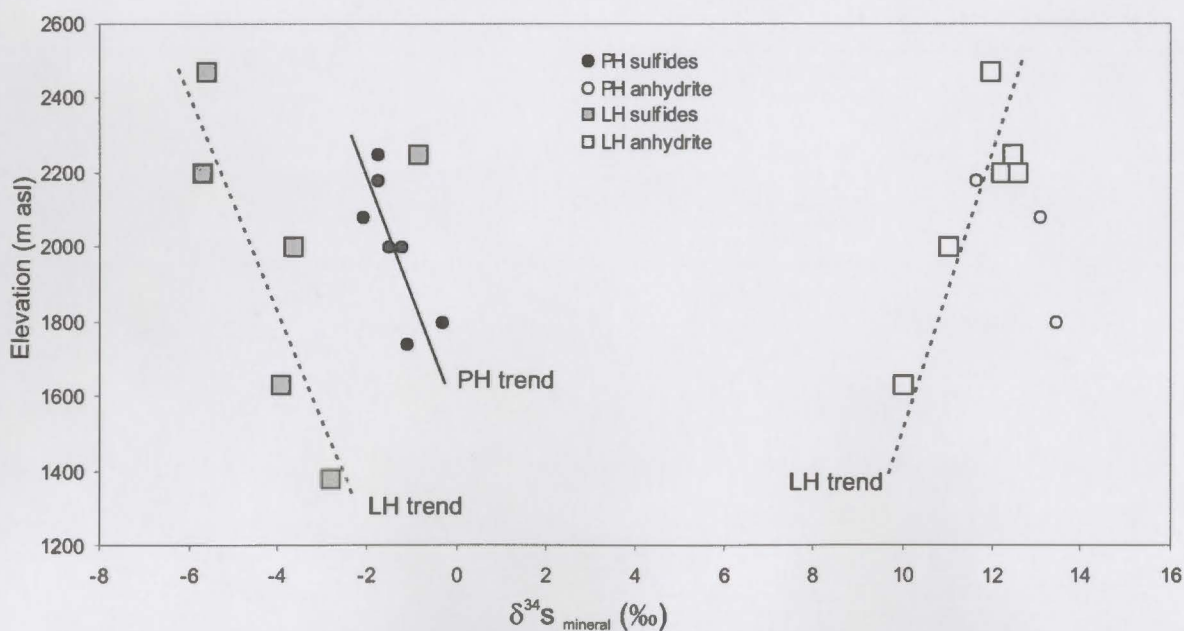
Figure 9.4. PH and LH δ^{34}S $_{sulfide}$ and δ^{34}S $_{sulfate}$ values compared to elevation (metres above sea level). The sulfides analysed are all chalcopyrite, with the exception of one bornite from the LH dataset. The PH δ^{34}S values and all except one LH δ^{34}S$_{sulfide}$ values trend to lower values at higher elevations. The LH anhydrite data show an opposite linear trend to higher values at higher elevations. Molybdenite and pyrite analyses generally do not conform to this pattern.

tion of a single LH sulfide sample (Fig. 9.4). The PH and LH data both lie on a trend line with a gradient of approximately -1‰ for every 350m elevation. The LH values are shifted by approximately 3‰ to more negative $\delta^{34}S$ values in comparison to the PH values. Sulfates from the LH stage have an antithetic relationship with LH sulfides, with higher $\delta^{34}S$ values occurring at higher elevations. Possible causes for the spatial zonations evident in the LM, PH, and LH sulfur isotopic datasets are discussed in section 9.5.

Agua Amarga samples

Limited samples were collected from the Agua Amarga prospect to the SW of Teniente (Fig. 2.6). The three analysed sulfide samples have variable $\delta^{34}S$ values ranging from -5.2 to 0.3 ‰ (mean = -2.0‰). One anhydrite sample from Agua Amarga has a low anhydrite $\delta^{34}S$ value of 9.9‰.

Sulfur isotope geothermometry

Temperatures of formation have been calculated using the fractionation equations for co-precipitating sulfides and sulfates (Table 9.2). Chalcopyrite-anhydrite was the principal mineral pair used in this study, with additional data coming from bornite-, pyrite-, and molybdenite-anhydrite pairs. Where possible, mineral pairs displaying apparent textural equilibrium were selected for analysis (Fig. 9.5), for example non-corroded euhedral crystal contacts. However, for most of the samples it could not be confidently asserted that the minerals were co-precipitated. Sulfide-sulfate mineral pairs with embayed contacts were not analysed. The results are plotted in Figure 9.6.

Calculated temperatures for sulfide-sulfate mineral pairs from LM veins range from 436° to 499°C, with an average of 460°C (Table 9.2, Fig. 9.6). The highest temperature was obtained from a biotite – anhydrite – sulfide breccia sample located around the grey porphyry. The lowest temperature sample (381°C) is from a stage 2 distal vein located 750m east of the dacite porphyry on section-83 (1000N) in the propylitic zone.

Calculated temperatures from three PH stage chalcopyrite-pairs are significantly lower than for the LM stage. They range from 395° to 439°C, with a mean of 420°C (Table 9.2, Fig. 9.6). No obvious spatial zonation exists in the limited dataset.

A total of seven sulfide-sulfate mineral pairs were analysed from LH veins and breccias. Of these, four temperatures calculated from chalcopyrite-anhydrite pairs range from 340° to 443°C and average 388°C (Table 9.2, Fig. 9.6). The highest temperature from the LH veins was recorded from a stage 4c anhydrite-sulfide breccia zone on section-238. This breccia surrounds a swarm of thin, altered late dacite dykes. The second highest temperature sample (425°C) is from the late dacite body located beneath the Braden Pipe. The lower temperatures (340°C and 345°C) were obtained from LH veins hosted in the THS. Temperatures of 416°C and 428°C from bornite-anhydrite and molybdenite-anhydrite geothermometers respectively (Table 9.2, Fig. 9.6) were obtained from a sulfide – sulfate cemented stage 4c breccia zone adjacent to a late dacite dyke on section-238.

The sulfide and sulfate $\delta^{34}S$ values determined during the current study are consistently about 1‰ heavier than comparable values from Kusakabe et al. (1984). This

Vein stage	Mineral pair	No. pairs	Temperature		
			min (°C)	max (°C)	average (°C)
Late Magmatic (500°C ± 100°C)					
bt-anh-sulf bx	cpy-anh	3	438	499	463
2b	cpy-anh	1			463
2c	cpy-anh	1			464
	bn-anh	1			467
2d	bpy-anh	2	446	450	448
	bn-anh	1			456
2e	cpy-anh	2	436	493	460
average		*11*	*436*	*499*	*460*
2-distal (275° - 440°C)	py-anh	1			381
Principal Hydrothermal (380°C ± 80°C)					
3	cpy-anh	3	395	439	421
Late Hydrothermal (330°C ± 60°C)					
	cpy-anh	4	340	443	388
	py-anh	1			404
4c	bn-anh*	1			416
	mo-anh*	1			428

Table 9.2. Sulfur isotope geothermometry results for individual vein stages from El Teniente. Estimated temperature ranges from the fluid inclusion study are shown in brackets for comparison. Chalcopyrite - anhydrite geothermometer from Ohmoto and Lasaga (1982). Bornite - anhydrite, molybdenite - anhydrite, and pyrite-anhydrite geothermometers from Ohmoto and Rye (1979). Two bornite-anhyrite, one pyrite-anhydrite, and one molybdenite-anhydrite temperature estimates were discarded as they supplied unreasonably high temperatures, and were assumed to have been precipitated out of equilibrium. All the $\delta^{34}S$ sulfide values for the mineral pairs were obtained from conventional analysis except a single bornite-anhydrite pair from a type 2c vein. * mineral pairs are from the same sample, and have similar temperature estimates.

Abbreviations: anh = anhydrite, bn = bornite, cpy = chalcopyrite, mo = molybdenite, py = pyrite.
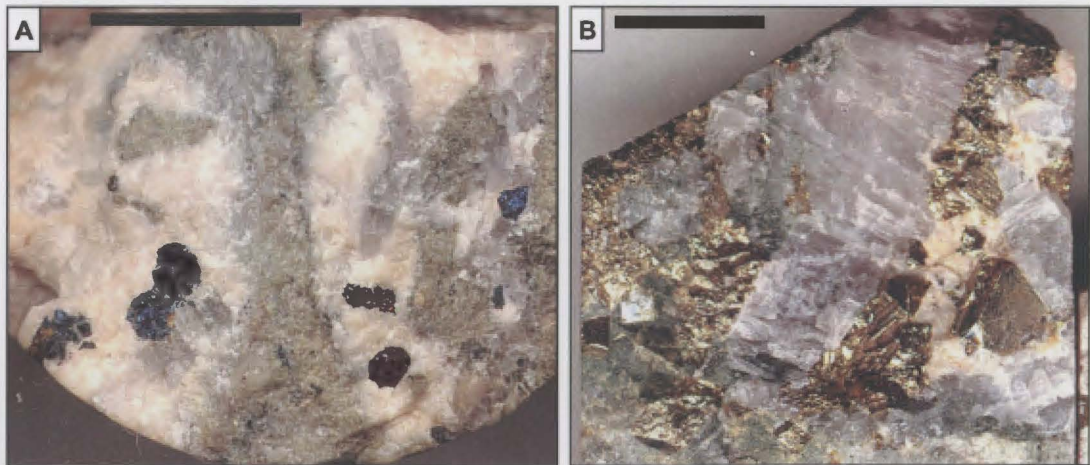
Figure 9.5. Interpreted equilibrium textures between sulfides and sulfates. Scale bar = 1cm.

A) Polygonal bornite crystals (blue) occurring in a carbonate (white) and anhydrite (light grey) cement in a LH stage 4c breccia with light green sericite altered wall rock clasts. Note the lack or evidence of corrosion at the sulfide contacts. ET744, DDH1272, 21.0m.

B) Euhedral anhydrite (pinkish grey), euhedral pyrite, and white carbonate in a stage 4c breccia cement in the Braden Pipe. Note the straight contacts between the sulfides and sulfates. ET618, DDH2047, 205m.
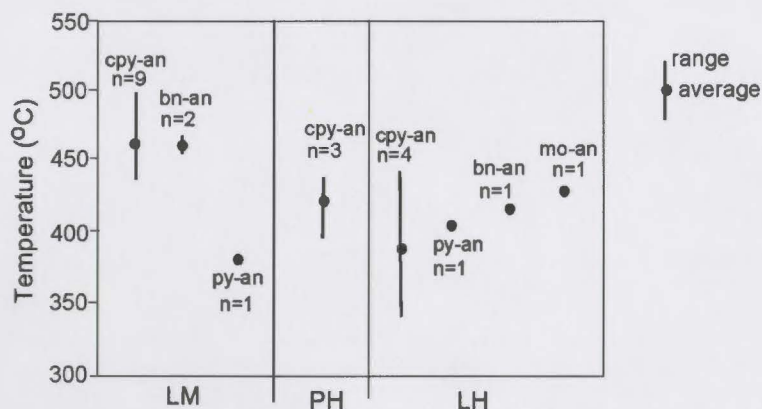

Figure 9.6. Temperature estimates based on sulfide-sulfate geothermometry for the LM, PH and LH stages of mineralization at Teniente. The co-existing sulfide-sulfate pair is indicated above the data range. Abbreviations: an = anhydrite, bn = bornite, cp = chalcopyrite, py = pyrite.

may be a function of the different analytical procedures or laboratories used in the two studies. Nonetheless the $\Delta_{sulfate-sulfide}$ values and calculated temperatures are well correlated with the results of Kusakabe et al. (1984). The main distinction is that a wider range of LH stage temperatures have been obtained from the current study.

Temperatures calculated from sulfur isotope geothermometry overlap with temperature estimates obtained from the fluid inclusion study (Table 9.2). The main exception is that temperatures of up to 600°C recorded from fluid inclusions were not

recorded from sulfur isotope geothermometry. The results of this sulfur isotope geothermometry study are limited by the fundamental assumption that the sulfide and sulfate species were precipitated in isotopic equilibrium. A lack of coprecipitation may be due sulfate or sulfide precipitation occurring in response to different physicochemical changes in the fluid, or potentially by mixing of oxidized and reduced sulfur sources which have not had time to isotopically equilibrate. Ohmoto and Goldhaber (1997) estimated that it takes less than a year for aqueous sulfate and sulfide to isotopically equilibrate in a 350°C acidic (pH <5) solution.

9.3   OXYGEN - HYDROGEN ISOTOPES

Introduction

Oxygen – deuterium (O-D) isotope geochemistry can help to constrain the sources of the mineralising fluids. Previous O-D isotopic studies of porphyry copper deposits unambiguously indicated that the early stages of mineralization are dominated by magmatic-derived fluids (e.g. Sheppard et al., 1969; Sheppard and Taylor, 1971; Taylor, 1997; Hedenquist et al., 1998). However, debate exists as to the nature of the fluids that formed the later sericite-bearing (phyllic) stages of porphyry copper deposits. Most early studies proposed that meteoric water played an important role in the formation of these alteration assemblages, based on O-D isotopic data from North and South American porphyry copper deposits (e.g., Sheppard et al., 1969; Taylor, 1974; Sheppard and Gustafson, 1976). In contrast, Kusakabe et al. (1984, 1990) found that phyllic alteration at El Teniente formed from a fluid with magmatic O-D isotopic composition. Kusakabe et al. (1984, 1990) also identified magmatic O-D fluid values from phyllic alteration at El Salvador by recalculating the data from Sheppard and Gustafson (1976) using different temperature estimates. Watanabe and Hedenquist (2001) proposed that the muscovite alteration at El Salvador was caused by a magmatic fluid, containing up to 20% meteoric water. Other recent studies have confirmed a continued magmatic input into the phyllic and advanced argillic stages of porphyry copper formation, with or without incorporation of external waters (e.g., Stein, 1988; Richards and Kerrich, 1993; Wolfe, 1994; Hedenquist et al., 1998; Harris and Golding, 2002).

Taylor (1992) calculated that the initial δD value of undegassed magmas ranges from -20 to -45‰ (felsic magma box, Fig. 9.7). An aqueous fluid exsolved from a fel-
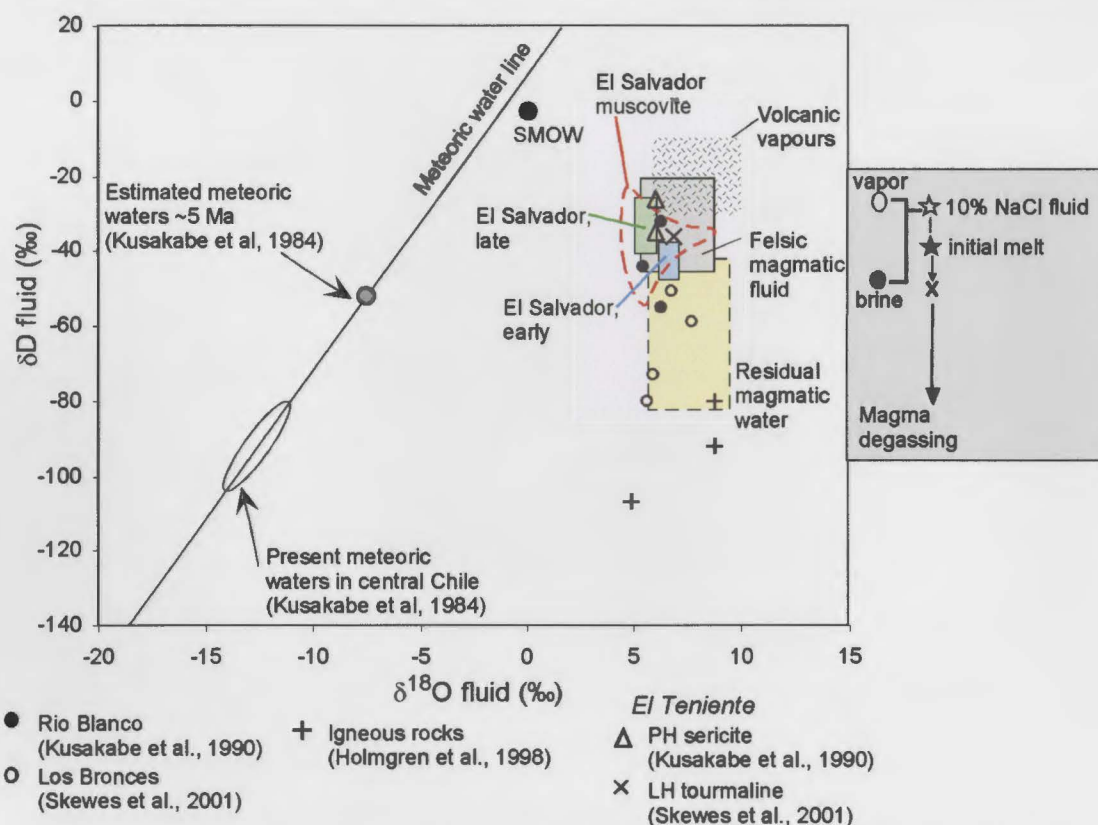
Figure 9.7. Published calculated $\delta^{18}O$ and δD fluid compositions for El Teniente, Rio Blanco, Los Bronces, and El Salvador (data from Shepard and Gustafson, 1976, Kusakabe et al., 1990; Skewes et al., 2001). The Rio Blanco samples are from the potassic zone with quartz-sericite alteration (top, average of 3), potassic-propylitic transitional zone (middle), and potassic zone (lower, average of 2; Kusakabe et al., 1990). The data are compared to the fields for felsic magmas prior to degassing, residual magmatic water, and volcanic vapours (Taylor, 1992; Giggenbach, 1992; Hedenquist et al., 1998). Analyses from unaltered intrusions from Los Bronces are also shown (Holmgren et al., 1988).

The shaded inset illustrates the deuterium fractionation associated with fluid exsolution and vapor separation (from Hedenquist et al., 1998). Assuming water dissolved in a magma has an initial δD composition of -40‰, exsolution of 50% isotopically heavy water (approximately -30‰ D) during crystallization will deplete deuterium in the bulk residual magmatic water by approximately 10‰, to -50‰ D. Further degassing in an open system leads to strongly depleted magmatic compositions. This explains the depleted D compositions of the igneous rocks from Los Bronces. Phase separation of the exsolved fluid results in further deuterium fractionation, involving estimated liquid-vapor fractionation of as much as -20‰ (Horita et al., 1995; Hedenquist et al., 1998).

sic magma will be enriched in deuterium approximately 15‰ to 20‰ compared to the melt (Taylor, 1992). Continued fluid exsolution results in deuterium depletion of the liquid remaining in the magma, driving it into the residual magmatic water field of Hedenquist et al. (1998; Fig. 9.7). If the exsolved aqueous fluid intersects its solvus and separates into liquid and vapor phases, additional deuterium enrichment of the vapour phase occurs (e.g., Horita et al., 1995; Hedenquist et al., 1998). Hedenquist et al. (1998) estimated that a vapour phase which has separated from a hypersaline magmatic brine is enriched in deuterium by up to 20‰ compared to the brine (inset, Fig. 9.7). Evidence for this process can be found in deuterium-enriched waters (δD = -20 ± 10‰) discharged through volcanic fumaroles, which were analysed by Giggenbach (1992; Fig. 9.7). Therefore, hydrous minerals formed in the presence of a vapour phase

or an evolved vapour phase may potentially be enriched in δD compared to the hydrous minerals formed from a one-phase liquid that has not undergone phase separation.

Previous work

Meteoric fluid composition

At El Teniente the modern day meteoric water has $\delta^{18}O$ values from $-11‰$ to $-14‰$ and δD values from -80 to -100‰ (Kusakabe et al., 1984; Fig. 9.7). Meteoric water compositions at the time of mineralization were probably enriched in $\delta^{18}O$ and δD compared to present day meteoric waters at Teniente, due to tectonic uplift that has occurred in the last five million years. Kusakabe et al. (1984) estimated that meteoric waters at the time of mineralization would have had $\delta^{18}O$ values of about -8‰ and δD values approximately -50‰ (Fig. 9.7).

Oxygen isotopes

Previous oxygen and hydrogen analyses from Teniente were undertaken by Kusakabe et al. (1984, 1990) and Skewes et al. (2001). Kusakabe et al. (1984, 1990) reported the results of oxygen isotope analyses on 28 anhydrite and 18 quartz samples from the LM, PH and LH stages (Fig. 9.8, Table 9.3). Quartz and anhydrite $\delta^{18}O_{mineral}$ values were mostly from 8.4‰ to 10.0‰ and 6.8‰ to 8.2‰ respectively. No lateral zonation in $\delta^{18}O_{mineral}$ values was detected, although one outlying value was obtained for a distal PH stage quartz vein of 2.6‰ (Fig. 9.8) that may have been due to involvement of meteoric fluids (Kusakabe et al., 1984). The $\delta^{18}O_{mineral}$ data from Skewes et al. (2001, n = 10) overlap with data from Kusakabe et al. (1984, 1990), except for relatively low $\delta^{18}O_{mineral}$ values for a single anhydrite analysis from a biotite breccia (1.2‰) and for LH stage scheelite (0.3‰) and barite (6.3‰; Table 9.3).

Kusakabe et al. (1984, 1990) calculated that $\delta^{18}O_{fluid}$ values at El Teniente were consistently around 6‰ based on temperatures obtained by sulfur isotope geothermometry, indicating a homogenous magmatic source for the hydrothermal fluids. $\delta^{18}O_{fluid}$ values from the data of Skewes et al. (2001) are between 6.8‰ and 10.9‰, also consistent with a magmatic source, with the exception of the LH stage barite and scheelite. Using the fractionation factors of Wesolowski and Ohmoto (1986) and Zheng (1999) respectively, and assuming a temperature of 330°C (± 60°C, from the
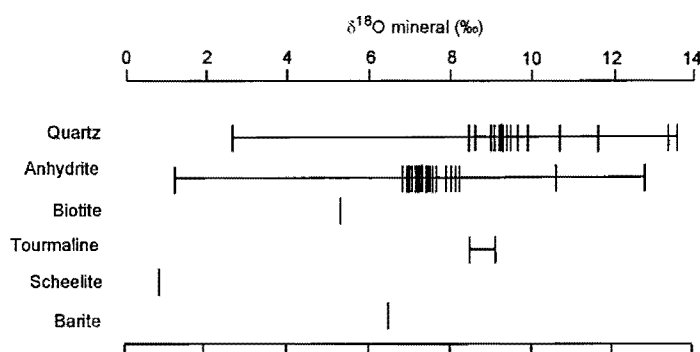
Figure 9.8. $\delta^{18}O_{mineral}$ values from El Teniente from Kusakabe et al. (1984), together with data from Skewes et al. (2001). Most of the data cluster at consistent $\delta^{18}O$ values, with little change between the LM, PH and LH stages. The outlying points are the barite and scheelite samples (LH stage), a low quartz sample (2.6‰) and a low anhydrite (1.2‰) sample. These may be analytical errors, or they may be due to involvement of meteoric waters at the edges of the system and/or in the latest stage veins.

Stage	$\delta^{18}O_{mineral}$ (‰)			Temperature	$\delta^{18}O_{fluid}$
	Quartz	Anhydrite	Other	estimate (°C)	(‰)
Kusakabe et al (1984)					
LM stage	Av = 8.9 (n = 6, range = 8.4 – 9.3)	Av = 7.1 (n = 10, range = 8.6 – 11.1)		456 ± 41	~6
PH stage	Av = 9.7 (n = 5, range = 9.2 – 9.9, excluding 1 value of 2.6)	Av = 7.5 (n=8, range = 7.1 – 7.9)		416 ± 31	~6
LH stage	Av = 9.5 (n=3, range = 9.3 – 9.7)	Av = 7.6 (n = 9, range = 9.8 – 12.5)		411 ± 35	~6
Postuma (type 4c/4d)	Av = 12.5 (n=2, range = 11.6 – 13.4)	10.6		360	6-8
Skewes et al. (2001)					
LM stage	10.6			500	8.4
LM stage biotite – anhydrite breccia	8.7	1.2	5.2 (biotite)	525	6.8
LH stage Marginal Breccia		12.9	9.1 (tourmaline) 8.4 (tourmaline)	400 400 400	10.9 7.6 6.9
LH stage Braden Pipe	13.5		6.3 (barite)	350 (330 ±60)	8.5 (3.8 ±1.0)
LH vein			0.8 (scheelite)	(330 ±60)	(3.1 ±1.0)

Table 9.3. Previous $\delta^{18}O$ analyses of vein minerals and breccia cements from El Teniente. The original temperature estimates and $\delta^{18}O$ fluid values calculated by the previous workers are also indicated. Skewes et al. (2001) do not calculate $\delta^{18}O$ fluid values for the anomalously low LM stage biotite and anhydrite analyses, or for the LH stage barite and scheelite analyses. The $\delta^{18}O$ fluid values in brackets were calculated in this study using the equations from Weselowski and Ohmoto (1986) and Zheng (1999) respectively, together with a temperature estimate of 330° ± 60°C.

fluid inclusion study) the scheelite and barite samples were precipitated from a fluid with $\delta^{18}O$ values of 3.1 to 3.8 ‰ (± 1.0 ‰; Table 9.3). These low values suggest the involvement of a meteoric component in the latest stage hydrothermal fluids.

Hydrogen isotopes

Three hydrogen isotopic analyses have been reported previously from Teniente, by Kusakabe et al. (1990) and Skewes et al. (2001; Table 9.4). Kusakabe et al. (1990) obtained two δD values of –53‰ and –62 ‰ from PH stage sericite. Using a temperature estimate of 416°C obtained from sulfide-sulfate geothermometry, they calculated a fluid δD composition of –26‰ and –35‰ respectively. Skewes et al. (2001) reported a single LH tourmaline value of –66‰, and calculated a δD_{fluid} value of –36‰ assuming a temperature of 400°C.

The calculated $\delta^{18}O$ and δD fluid values from previous workers at El Teniente indicate a predominance of magmatic fluids (Fig. 9.7). Also plotted on Figure 9.7 are fluid values calculated from Río Blanco (Kusakabe et al., 1990), Los Bronces (Holmgren et al., 1988; Skewes et al., 2002), and El Salvador (data from Sheppard and Gustafson, 1976, re-calculated by Kusakabe et al., 1990; Watanabe and Hedenquist, 2001). At Río Blanco, calculated δD fluid values increase from –55‰ in the potassic zone to -32‰ in the sericite alteration zone, whereas there is little change in the $\delta^{18}O$ fluid values (Kusakabe et al., 1990). Similarly at El Salvador, δD fluid values calculated from early biotite are lighter than those calculated from later sericite (Fig. 9.7, Kusakabe et al. 1990). In contrast δD fluid values of –40‰ ± 10‰ calculated from surface samples of muscovite by Watanabe and Hedenquist (2001) overlap with the early biotite-stable fluid values obtained by Kusakabe et al. (1990). Kusakabe et al. (1990) concluded that D enrichment in late-stage fluids at Teniente and Río Blanco was not due to interaction with isotopically heavy groundwaters, as suggested by Sheppard and Gustafson (1976) for El Salvador. This is because groundwaters at the time of formation would have been depleted in D compared to the hydrothermal fluids. Kusakabe et al. (1990) favored the interpretation that D enrichment in the sericite-stable fluids was due to closed system evolution of a magmatic-derived fluid which has previously formed a hydrous potassic assemblage.

This study

One tourmaline and three chlorite samples were selected for oxygen-hydrogen iso-topic analyses. The samples were analysed by Kurt Kyser and Kerry Klassen at Queens University. Samples were chosen from the propylitic zone and/or phyllic stage veins, in order to attempt to identify whether non-magmatic fluids existed in the Teniente hydrothermal system. Analytical methods are described in Appendix 6B.

Results

Measured $\delta^{18}O$ values of chlorite, sericite, and tourmaline range from 6.2 to 8.2‰ (Table 6.4; Fig. 9.9). Their δD values range from -53 to -90‰ (Table 6.4; Fig. 9.9). Assuming that isotopic equilibrium was attained between the fluid and the minerals, and using temperature estimates derived from fluid inclusions and sulfide-sulfate geo-thermometry with a ± 50°C error, calculated $\delta^{18}O_{fluid}$ and δD_{fluid} values are 4.9‰ to 7.7‰ and -56‰ to -6‰ respectively (Table 9.4; Fig. 9.9).

Mineral data from previous workers have been recalculated in the current study using temperature estimates obtained from the fluid inclusion study and fractionation equations detailed in Table 9.4. A temperature of 380°C was assumed for the PH seric-ite samples of Kusakabe et al. (1990), and 350°C for the LH tourmaline breccia sample of Skewes et al. (2001). The recalculated $\delta^{18}O_{fluid}$ values are 5.7 – 5.8‰ and δD_{fluid} val-ues are –18‰ to –28‰ (Table 9.4).

The O-D isotopic compositions of the fluids overlap with the fields for primary ungassed felsic magma and volcanic vapours (Fig. 9.9). Calculated $\delta^{18}O_{fluid}$ values are indistinguishable between the LM, PH, and LH stages. At face value this suggests that magmatic-derived fluids were predominant even at the deposit periphery and during the late stage phyllic alteration. However, circulating meteoric fluids may have isotopi-cally equilibrated with the igneous rocks of the Farellones Formation, thereby masking their isotopic signature. To test this possibility, modelling was undertaken of the $\delta^{18}O$ and δD compositions of a meteoric fluid undergoing isotopic exchange with the host rock andesites. The $\delta^{18}O$ and δD compositions of a meteoric fluid at various water/rock (W/R) ratios at 400°C are plotted on Figure 9.9. The original meteoric fluid is assumed to have $\delta^{18}O$ and δD isotopic composition of –8‰ and +50‰ respectively (Kusakabe et al., 1984). The modelled $\delta^{18}O$ and δD values of the unaltered wallrock andesites are

Sample (drillhole, depth)	Mineral	$\delta^{18}O_{min}$ (± 0.2 ‰)	δD_{min} ‰ (± 5 ‰)	Temp (°C)	$\delta^{18}O_{fluid}$ ‰	δD_{fluid} ‰
This study						
ET650 – LM-distal (DDH1698, 65.0m)	Chlorite	6.8	-73	450	7.7	-42
				400	**7.6**	**-41**
				350	7.2	-39
ET726 – LM-distal (DDH945, 560.9m)	Chlorite	6.2	-90	350	6.6	-56
				300	**6.0**	**-55**
				250	4.9	-52
ET728 - PH peripheral (DDH1319, 125.5m)	Chlorite	6.7	-70	400	7.5	-38
				350	**7.1**	**-36**
				300	6.5	-35
ET520 - LH peripheral (DDH1418, 322.1m)	Tourmaline	8.2	-61	400	7.2	-29
				350	**6.4**	**-19**
				300	5.4	-6.0
Kusakabe et al (1990)[&]						
98-PH	Sericite	8	-53	416	6	-26
			recalculated*	380	5.7	-18
148-PH	Sericite	8	-62	416	6	-35
			recalculated*	380	5.7	-27
Skewes et al. (2001)#						
LH	tourmaline	7.6	-66	400	6.9	-36
			recalculated*	350	5.8	-28

Table 9.4. Oxygen and hydrogen isotopic data for chlorite, tourmaline and sericite from El Teniente. Fractionation factors were calculated from Cole and Ripley (1998, oxygen chlorite-H_2O), Viglino et al. (1984, hydrogen chlorite-H_2O) and Zheng (1993, oxygen and hydrogen, tourmaline-H_2O). Temperature estimates, obtained from the fluid inclusion study and sulfur isotope geothermometry, are indicated in bold. The temperatures have an estimated error of ± 50°C, and fluid values have been calculated for 50°C above and below the estimated temperature accordingly. Original temperature estimates from Kusakabe et al. (1990) and Skewes et al. (2001) are indicated.

* - analyses have been recalculated using temperature estimates from this study, and fractionation factors as detailed above.

[&] - fractionation equations from Suzuoki and Epstein (1976).

- fractionation equations from Kotzer et al. (1993).

+6‰ and +50‰ respectively. The wallrock values were averaged from whole rock isotopic analyses of the SVZ between 33° and 34°S (Taylor, 1986).

The $\delta^{18}O$ and δD isotopic data from El Teniente are permissible of a minor to moderate meteoric component into the hydrothermal system. For example, meteoric water circulating through the wall rock andesites at 400°C at fluid/rock ratios of 0.1 would have an $\delta^{18}O$ composition of approximately 3‰ (Fig. 9.9). The fluid $\delta^{18}O$ values from El Teniente (Table 9.4) allow up to ~30% of an external water with this composition into the magmatic-hydrothermal system. Lesser percentages of external water are permissible if the fluid/rock ratios were higher and/or the temperatues were lower. However, the lack of variation or spatial zonation of the $\delta^{18}O$ fluid data is interpreted to in-
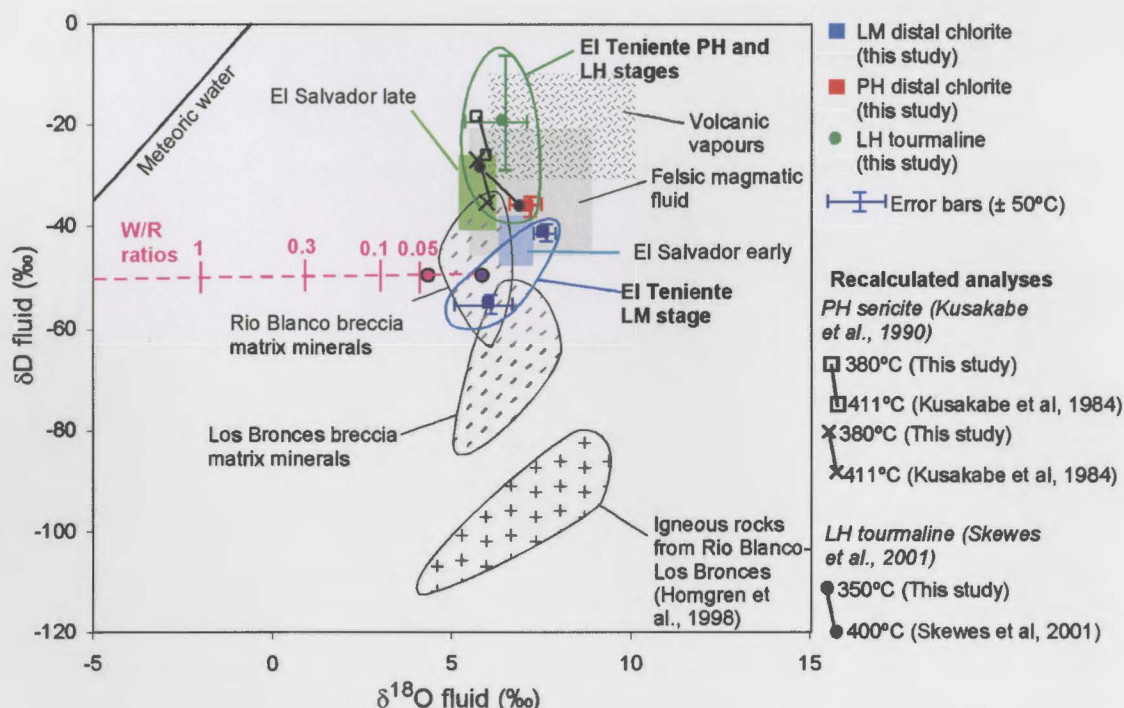
Figure 9.9. Calculated $\delta^{18}O$ and δD fluid compositions for El Teniente, compared to the datasets from Rio Blanco (Kusakabe et al., 1990), Los Bronces (Holmgren et al., 1998; Skewes et al., 2001), and El Salvador (Shepard and Gustafson, 1976; Kusakabe et al., 1990). This plot is magnified from Figure 9.6. Note that the igneous rocks from Los Bronces have δD values lighter than the corresponding fluid values, and that for all the deposits, significant δD variation occurs at relatively constant $\delta^{18}O$ values. Note also at Teniente, El Salvador, and at Rio Blanco (Kusakabe et al., 1984), the later sericite-stable fluid is more enriched in δD than the early biotite-stable fluid.

The pink line plots the modeled $\delta^{18}O$ and δD compositions of a meteoric fluid undergoing isotopic exchange with the host rock andesites at various water/rock (W/R) ratios at 400°C. Equations and fractionations are from Taylor (1977) and Criss and Taylor (1986). The modeled $\delta^{18}O$ and δD isotopic composition of the original meteoric fluid is –8‰ and 50‰ D respectively, (Kusakabe et al., 1984). The modelled $\delta^{18}O$ and δD values of the unaltered andesites are +6‰ and 50‰ respectively (marked by the purple dot, Taylor, 1986). The pink dot marks the isotopic composition of a water in equilibrium with feldspar in these rocks ($\Delta^{18}O_{feldspar-water}$ = +2). The line is horizontal as the modeled δD compositions of the meteoric fluid and the andesites are identical.

dicate a homogenous magmatic source, and that a significant meteoric input was not present in the Teniente magmatic-hydrothermal system.

Calculated δD fluid values for the phyllic PH and LH stage fluids are higher (-38‰ to -6‰) than those calculated for the LM fluids (-56 to -39‰, Fig. 9.9). As noted above, an increase in calculated δD values from the early potassic stage to the late phyllic stages also occurs at Río Blanco and El Salvador (Fig. 9.9). Overall, for the four deposits of central Chile, δD fluid values range widely (-81‰ to -6‰) which contrasts markedly with the restricted ranges of $\delta^{18}O$ fluid values (Fig. 9.9). The possible causes for this variation are discussed in section 9.5.

9.4   CARBON-OXYGEN ISOTOPES OF LH STAGE CARBONATES

Introduction and methods

Carbon isotope studies from vein deposits can provide information on the source of carbon and, when coupled with oxygen isotopic analysis, hydrothermal depositional processes. However, the carbon isotopic system is similar to the sulfur isotopic system in that it is complicated by aqueous speciation. There are several aqueous carbon species that can be predominant in hydrothermal fluids (e.g., H_2CO_3, HCO_3^-, $CO_{2(aq)}$, CO_3^{2-}, CH_4). Their relative abundances are sensitive to the temperature, pH, and fO_2 of the fluid (Ohmoto and Rye, 1979, Ohmoto and Goldhaber, 1997).

Carbonate minerals only occur in the LH stage at Teniente. A total of 22 carbonate samples were analysed for their carbon - oxygen (C-O) isotopic compositions. Analytical details are detailed in Appendix 6C. The analyses were performed by Keith Harris and Christine Cook at the Central Science Laboratory, University of Tasmania. The carbonate minerals were identified by a combination of geological criteria and staining with Alizarin red and potassium ferricyanide solution (Evamy, 1963). Carbon isotopes have not been previously analyzed from Teniente.

Results

Measured $\delta^{18}O$ values range from 8.3‰ to 15.8‰, and $\delta^{13}C$ values from -9.3‰ to -5.3‰ (Table 9.5; Fig. 9.10A). Dolomite and ankerite typically have higher $\delta^{18}O$ values and $\delta^{13}C$ values compared to calcite (Fig. 9.10A).

The array of C-O values in Figure 9.10A is consistent with calculated theoretical values for calcite precipitated from cooling of a magmatic fluid ($\delta^{13}C_{\Sigma C}$= -6‰; $\delta^{18}O_{fluid}$ = +6‰) from 520°C to 280°C (blue line; Fig. 9.10A). At face value, this cooling induced fractionation trend fits the observed data. However, theoretical temperatures on the cooling trend do not conform to the temperature estimates for the LH samples obtained from fluid inclusion and sulfur isotope geothermometry (Table 9.5). The samples which are enclosed in orange circles (Fig. 9.10A) are from within or close to geological units which intruded during the LH stage, such as late dacite dykes, the Braden pipe, and pebble dykes. However, these samples plot at the lower temperature end of the array of calculated values, whereas the samples located distally from from

Sample number	Drillhole, depth	vein stage	$\delta^{13}C_{min}$ (PDB) ‰ (± 0.1‰)	$\delta^{18}O_{min}$ (V-SMOW) ‰ (± 0.2‰)	Temp. est.(°C) (± 50°C)	δO_{fluid} ‰ ($\pm\sim1$‰)	$\delta^{13}C_{\Sigma C}$ ‰ ($\pm\sim1$‰)	Comments
Calcite								
ET520	1418, 332.1m	4a	-8.7	8.4	345	3.7	-7.5	
ET322	346.5m	4c	-8.0	9.3	380	5.7	-6.3	
ET418	1429, 73.2m	4c	-8.5	7.2	330	2.4	-7.6	
ET420	1429, 83.6m	4c	-7.3	10.0	330	5.2	-6.3	
ET473	1413, 396.5m	4c	-7.9	11.0	330	6.2	-7.0	
ET687	1889, 24.4m	4c	-9.3	12.7	330	7.9	-8.4	
ET778	1981, 274.5m	4c	-7.4	10.1	330	5.4	-6.4	
ET402	1423, 441.0	4cbx	-8.2	11.8	380	8.2	-6.5	Cement in pebble dyke
ET340	1486, 373.6m	4d	-7.6	8.3	330	3.6	-6.7	
ET497	1258, 233.3m	4d	-7.4	11.9	330	7.2	-6.5	Located in Braden Pipe
Dolomite								
ET123	1134, 143.3m	3/4c	-7.4	14.3	330	8.7	-6.8	
ET45	1738, 190.0m	4c	-5.6	9.9	330	4.3	-4.9	
ET459	1413, 54.6m	4c	-7.4	13.9	350	8.8	-6.5	Close to late dacite, stage 4c breccia zone
ET784	1079, 744.8m	4c	-7.6	12.9	400	9.1	-5.9	Deep in late dacite porphyry
ET793	1505, 55.7m	4c	-7.5	12.7	330	7.2	-6.9	Adjacent to Braden Pipe
ET303	1512, 163.8m	4c	-7.7	11.8	330	6.2	-7.1	
ET338	1486, 332.4m	4c	-7.0	12.9	330	7.3	-6.3	
ET755	1317, 7.0m	4c	-7.2	11.6	330	6.0	-6.6	
ET744	1272, 21.0m	4c	-7.9	15.5	330	9.9	-7.3	Adjacent to Braden Pipe
Ankerite								
ET698	1889, 170.8m	4c	-6.6	13.3	330	5.6		
ET193	1300, 342.2m	4d	-6.2	13.0	330	5.2		
ET478	1413, 259.6m	4d	-7.1	10.9	330	3.1		

Table 9.5. $\delta^{18}O$ and $\delta^{13}C$ isotopic analyses from LH-stage carbonates from this study. Calcite-water, dolomite-water and ankerite-water oxygen fractionation equations are from Zheng (1999). Calcite-CO_2 and dolomite-CO_2 fractionation equations are contained in Ohmoto and Goldhaber (1997). $\delta^{13}C_{\Sigma C}$ values for ankerite could not be calculated, due to the lack of suitable fractionation equations. Abbreviations: est = estimate, min = mineral, temp = temperature.

these geological units correspond to higher temperature precipitation. This trend is the opposite to that expected from hydrothermal fluids being focussed up through these geological units and structures, and migrating outwards from them. Alternatively, the array of values in Figure 9.10A can be explained by variation of the $\delta^{13}C_{\Sigma C}$ and $\delta^{18}O_{fluid}$ values of the hydrothermal fluids.

To calculate $\delta^{13}C_{\Sigma C}$ values, the physico-chemical conditions of the system must be estimated. Temperature estimates for the LH stage from sulfur isotope geothermometry range from 330° to 440°C and the fluid inclusion study indicates temperatures of 330°C ($\pm$ 60°C). For the individual samples without any thermometric information, a temperature of 330°C is assumed because the carbonate occurs as late void fill, so the lower end of the temperature range is considered most likely. The presence of sericite
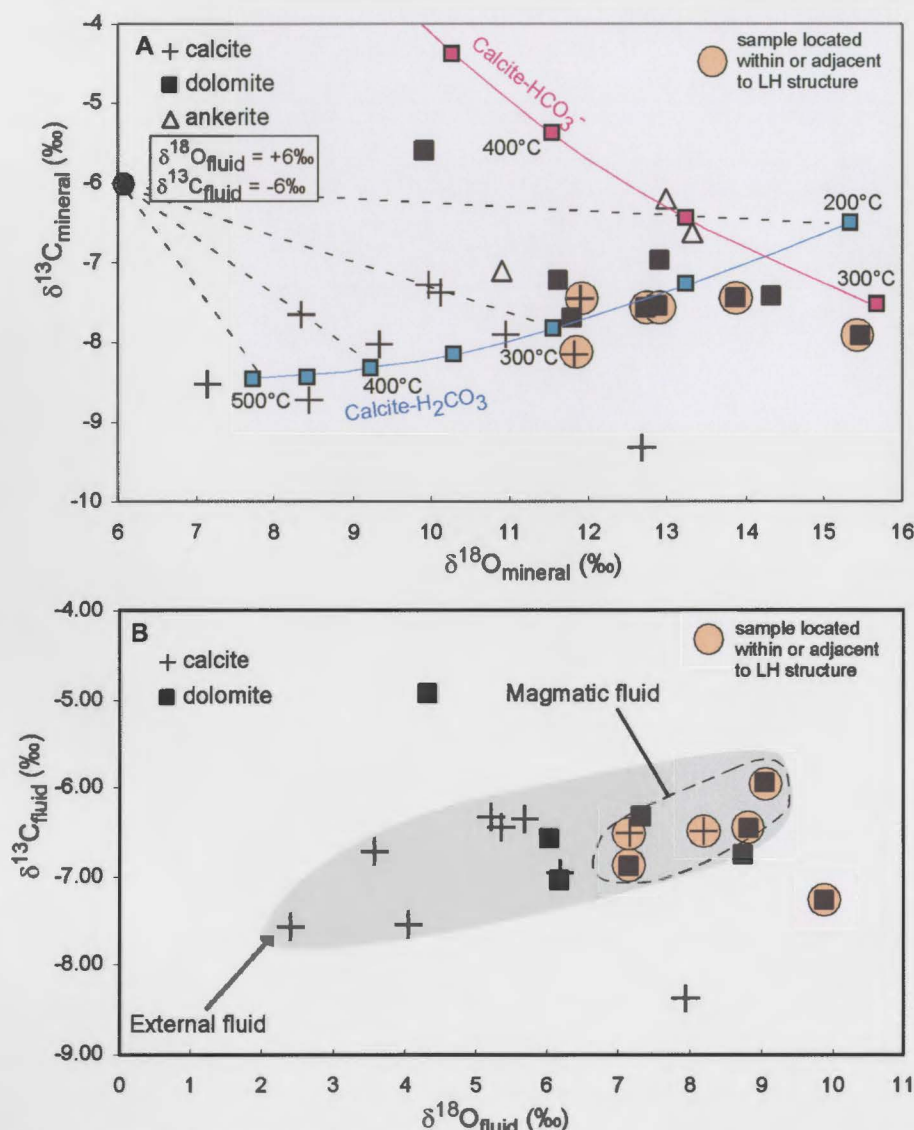
Figure 9.10. C-O isotopic data from LH stage carbonates.

A) Mineral $\delta^{18}O$ and $\delta^{13}C$ values. Also shown are the calcite-H_2CO_3 and calcite-HCO_3^- fractionation curves calculated using fractionation equations of Friedman and O'Neil (1977). Magmatic $\delta^{18}O$ and $\delta^{13}C$ fluid compositions are estimated to be +6‰ and -6‰ respectively.

B) Fluid $\delta^{18}O$ and $\delta^{13}C$ values calculated from LH-stage carbonates. The shaded region highlights a weakly defined coupled C-O isotopic trend. The circled points denote the samples which are located within or adjacent to LH-stage structures, either the Braden Pipe, late dacite dykes and associated type 4c breccia zones, or pebble dykes. Most of these samples have high $\delta^{18}O$ fluid values (between 7 and 10 ‰ - dashed line) consistent with a magmatic origin, and $\delta^{13}C_{\Sigma C}$ values between -7.0 and -6.0 ‰. Most of the samples away from the LH structures (uncircled) have $\delta^{18}O$ fluid values between 6.2 and 2.4 ‰, and $\delta^{13}C_{\Sigma C}$ from -8.4 to -6.3 ‰.

halos around the LH veins constrains the pH between approximately 3 and 5. The sulfur isotope systematics (see discussion below) indicate that oxidizing conditions prevailed (mCO_2/mCH_4 ratio >1). Under these conditions aqueous CO_2 or carbonic acid will be the dominant species in the aqueous phase ($H_2CO_{3\ approx} = H_2CO_3 + CO_{2aq}$). Therefore, minimal difference will exist between the $\delta^{13}C_{CO2}$ and $\delta^{13}C_{\Sigma C}$ values (Ohmoto and Rye, 1979; Ohmoto and Goldhaber, 1997). The calculated $\delta^{13}C_{\Sigma C}$ values

for Teniente carbonates are from -8.4‰ to -4.9‰ (Table 9.5), within the range of magmatic values (Ohmoto and Rye, 1979; Davidson, 1999). $\delta^{18}O_{fluid}$ values range from 2.4‰ to 9.9‰ (Table 9.5; Fig. 9.10B). An error of ± 50°C on the temperature estimates correlates to an error of ± ~1‰ for the calculated C-O isotopic fluid compositions.

The calculated $\delta^{18}O$ and $\delta^{13}C_{\Sigma C}$ fluid values define a linear trend (Figure 9.10B). Most samples from veins within or near LH geological units and structures have high $\delta^{18}O$ values (7‰ to 10 ‰) and $\delta^{13}C_{\Sigma C}$ values (predominantly -7.0‰ to -5.9‰), whereas the samples away from LH structures have lower $\delta^{18}O$ values (2.4‰ to 6.2‰) and slightly depleted $\delta^{13}C_{\Sigma C}$ values (-7.6‰ to -6.3‰). Considering the spatial association of the carbonate samples with respect to LH stage structures, the linear trend in C-O isotopic compositions can be interpreted to be due to mixing between two isotopic sources, rather than conductive cooling of a single homogeneous fluid. This is discussed further in section 9.5.

9.5 DISCUSSION OF STABLE ISOTOPES RESULTS

Oxygen-hydrogen isotope systematics

Fluids from Teniente, Rio-Blanco-Los Bronces and El Salvador have significant variation in calculated δD compositions (-81 to -6‰) at consistent magmatic $\delta^{18}O$ values (4.9‰ to 7.7‰, Fig. 9.9). This is likely to have been caused by deuterium enrichment during magma degassing and subsequent enrichment of the vapour phase during boiling (Taylor, 1997; Hedenquist et al., 1998; Harris and Golding, 2002). Open system fractionation due to magma degassing is considered most likely to explain the depleted δD compositions of the Los Bronces igneous rocks, compared to the enriched δD values calculated for hydrothermal fluids from the same deposit.

The observed shift in δD_{fluid} values from the LM stage (-56‰ to -39‰) to later PH stage (-38‰ to -6‰) at constant $\delta^{18}O_{fluid}$ values at Teniente is consistent with the calculated deuterium enrichment of the vapour phase as an aqueous fluid intersects its solvus (Horita et al., 1995; Hedenquist et al., 1998). It is postulated that the PH and LH sericite-chlorite alteration may have formed from a vapour phase, whereas the LM stage hydrous minerals were precipitated in the absence of vapour, either prior to vapour separation or from the residual brine. This interpretation is supported by the

abundance of vapour-rich fluid inclusions observed in the PH and LH stages (chapter 8). In contrast, evidence for phase separation (boiling) is rare in the LM stage quartz, and most of the fluid inclusions (>95%) homogenize to liquid.

In summary, δD and $\delta^{18}O$ data from this study support a model in which the later stage sericite-stable alteration and vein stages were generated from a magmatic-derived fluid that was isotopically similar to that which formed the early biotite-stable alteration stages. Enriched δD fluid values at constant $\delta^{18}O$ fluid values in the sericite-stable stages may be explained by separation of a vapour phase. The deuterium-enriched vapour phase was most likely involved in the formation of sericite, chlorite and tourmaline. Deuterium enrichment of sericite-stable fluid, compared to biotite-stable fluid, is also evident from the Río Blanco and El Salvador datasets (Kusakabe et al., 1990). This dataset supports the proposal of Harris and Golding (2002) and Mein-ert et al. (2003) that the transition from biotite to sericite alteration does not necessarily require the input of meteoric water, but can occur due to cooling of a magmatic-derived fluid. This model contrasts with the previous genetic association of phyllic alteration with invasion of meteoric waters (e.g. Henley and McNabb, 1978; Taylor, 1997).

Source of the hydrothermal fluids

Oxygen isotopes are sensitive to the involvement of meteoric fluids (e.g., Campbell and Larson, 1998). $\delta^{18}O$ fluid compositions, from this study and from previous studies, remained constant (between 5‰ and 7‰) during the LM, PH, and early LH (stage 4a marginal breccia) stages (Fig. 9.11). This is interpreted to indicate a homogenous magmatic source of oxygen. The calculated δD_{fluid} values from the LM, PH, and LH stages are also consistent with a magmatic fluid source. Hydrous minerals, even from the deposit periphery, formed from waters with O-D isotopic compositions overlapping with felsic magma and volcanic vapour (Fig. 9.9), precluding the involvement of significant proportions of meteoric fluids. There is evidence for meteoric water involvement late in the LH stage (Fig. 9.11). The broad peak in $\delta^{18}O$ fluid values from 2-10‰ suggests fluid heterogeneity and mixing between magmatic and meteoric fluids. Assuming meteoric water with $\delta^{18}O$ and δD values of -8‰ and -50‰, respectively (Kusakabe et al., 1984), a simple mass balance calculation suggests that up to 30% of the water in the latest vein stages (stage 4c and 4d) was meteoric in origin. This pro-
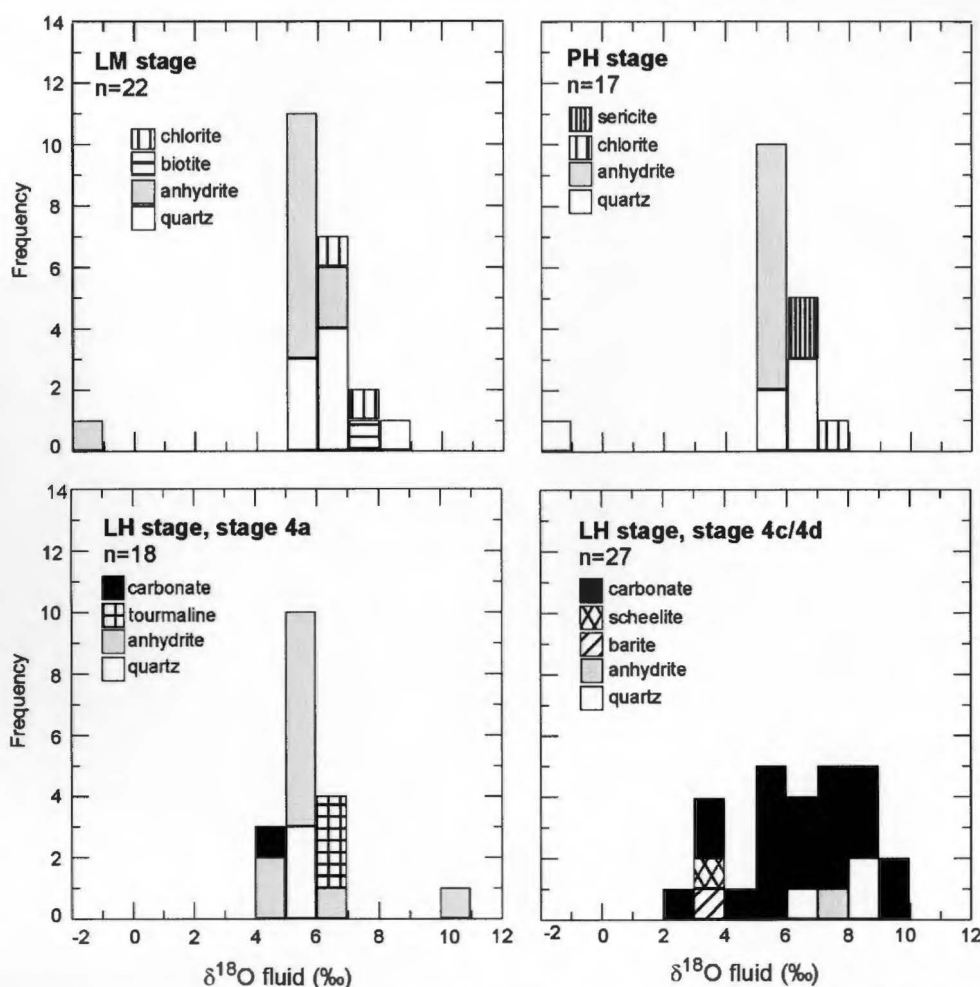
Figure 9.11. Compilation of $\delta^{18}O_{fluid}$ values obtained from different minerals at El Teniente. Data from Kusakabe et al (1984), Skewes et al. (2001) and the current study. Note in both the LM and PH stage datasets, a single low $\delta^{18}O$ fluid value suggests the possibility of meteoric fluid involvement, however the lack of a intermediate values suggests that the outlier points are anomalies. Only $\delta^{18}O_{fluid}$ values (mainly from carbonates) from the stage 4c and 4d veins indicate the existence of significant meteoric waters in the hydrothermal system, recording heterogeneous $\delta^{18}O_{fluid}$ values from 2-10 ‰.

portion may be significantly greater, as external waters may have partially equilibrated with the igneous wall rocks at high temperatures, shifting their $\delta^{18}O$ values towards magmatic values (Fig. 9.9).

Spatial zonation of sulfur isotopes

Total sulfur composition ($\delta^{34}S_{\sum S}$) and SO_4/H_2S ratio of the fluids

In order to determine the $\delta^{34}S_{\sum S}$ fluid value for the Teniente system, the observed $\delta^{34}S_{sulfide}$ and $\delta^{34}S_{sulfate}$ mineral values for co-existing mineral pairs have been plotted against their corresponding temperature estimates obtained from sulfide-sulfate geo-thermometry (Fig. 9.12A). If sulfides and sulfates are precipitated from a cooling, iso-topically homogenous fluid, then they will have covarying $\delta^{34}S$ values which plot on
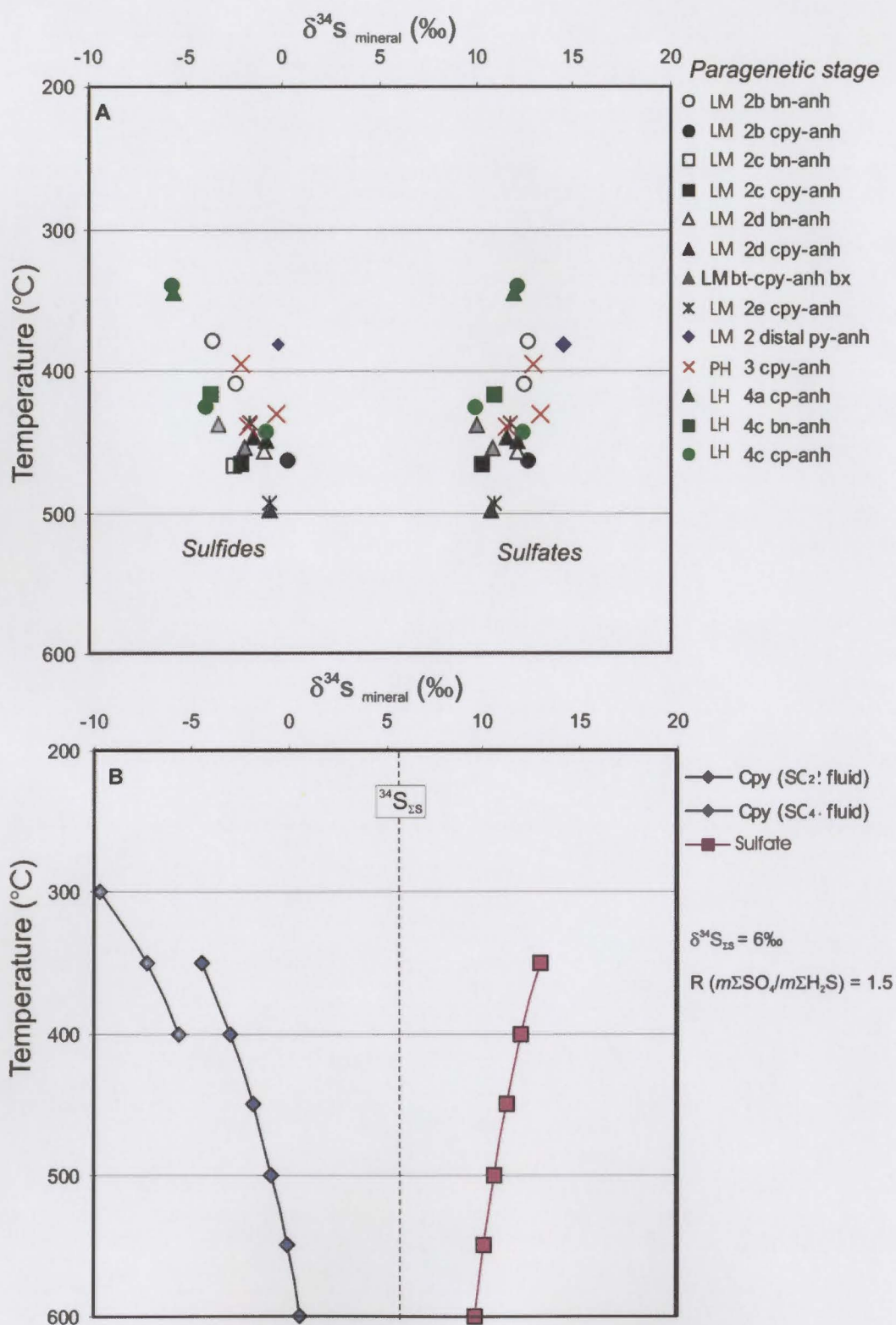
Figure 9.12. Measured and modeled $\delta^{34}S$ compositions from the Teniente deposit.

A) Measured $\delta^{34}S$ values for co-existing sulfide and sulfate mineral pairs from the different paragenetic stages plotted against their calculated temperatures obtained from sulfide-sulfate geothermometry.

B) Modelled $\delta^{34}S$ values for sulfate and sulfides precipitated in equilibrium from a cooling fluid with $\delta^{34}S_{\Sigma S}$ composition of 6‰ and SO_4/H_2S ratio of 1.5:1. Equations from Ohmoto and Goldhaber (1997).

Abbreviations: anh = anhydrite, bn = bornite, bx = breccia, cpy = chalcopyrite, py = pyrite

linear trendlines. The $\Delta\delta^{34}S_{sulfate-sulfide}$ values increase with degree of cooling. The cooling trend of sulfide and sulfate $\delta^{34}S$ values is dependent on the SO_4/H_2S ratio of the fluid and bulk sulfur composition ($\delta^{34}S_{\Sigma S}$). Modelling of sulfide and sulfate values, assuming conditions of isotopic equilibrium, indicate that the observed $\delta^{34}S$ compositions (Fig. 9.12A) can be approximated by cooling of a fluid with a bulk sulfur value of 6‰ and a SO_4/H_2S ratio of 1.5 (Fig. 9.12B). The bulk sulfur estimate, although higher than most magmatic sulfur values (0 ± 5‰; e.g., Ohmoto and Rye, 1979), is similar to the value of 3.3‰ for fresh granitoids from the Teniente region (Sasaki et. al., 1984). The scatter of data in Figure 9.12A suggests either that the redox state or the $\delta^{34}S_{\Sigma S}$ of the hydrothermal fluids varied, or that isotopic equilibrium was not reached between the sulfide and sulfate species in all of the analysed samples.

LM stage

The spatial variation (Fig. 9.3) in the Teniente $\delta^{34}S$ sulfide data from the LM stage may be due to several factors (Ohmoto and Goldhaber, 1997; Wilson, 2003):

1) Equilibrium fractionation between the fluid and sulfide species (Ohmoto and Goldhaber, 1997).

2) Redox gradients within the fluid

3) Mixing of sulfur reservoirs

In reference to point 1), a well-developed sulfide zonation exists at Teniente. Bornite is stable proximal to the dacite porphyry and pipes, passing out to a domain where chalcopyrite is stable, and then to a peripheral pyrite zone (Fig. 4.2). Fluid inclusion and sulfur isotope geothermometry indicate that temperatures varied from approximately 500°C in the deposit centre to 350°C at the deposit periphery. The calculated fractionations between copper-iron sulfides precipitated in equilibrium at 500°C, 400°C and 350°C is shown in Table 9.6, from the equations of Ohmoto and Rye (1979). If the zoned sulfide minerals at Teniente were all precipitated in equilibrium from a chemically homogenous fluid with a constant $\delta^{34}S_{\Sigma S}$, then the difference in $\delta^{34}S$ values between the central bornite and peripheral pyrite (Δ_{bn-py}) would be -1.08‰ at 500°C, or -1.67‰ at 350°C (Table 9.6). From Figure 9.3, the observed difference in $\delta^{34}S$ values from the central bornite (~ -5‰) to peripheral pyrite zone (~ 0‰) is on the order of 5‰, significantly greater than these equilibrium fractionation values. There-

fore, it is concluded that the spatial variation of $\delta^{34}S$ values is too great to be explained by equilibrium fractionation between different sulfide species.

Temperature (°C)	Δ_{bn-cpy}	Δ_{cpy-py}	Δ_{bn-py}
500	-0.33	-0.75	-1.08
400	-0.44	-0.99	-1.43
350	-0.51	-1.16	-1.66

Table 9.6. fractionations between copper-iron sulfide minerals calculated at 500°C, 400°C and 350°C from the equations of Ohmoto and Rye (1979). This temperature range is applicable to the Teniente hydrothermal system based on sulfur isotope geothermometry, and fluid inclusion temperature estimates.

A variation in the redox state of the fluid is interpreted to be the most likely cause for the zonation in the LM sulfide values. Assuming that the bulk sulfur composition remained constant, spatial variations of $\delta^{34}S$ sulfide values reflect changes in the temperature and oxidation state of the fluid. As the fluid cooled the $\delta^{34}S$ sulfide values progressively decreased. The magnitude of this shift is greater under oxidizing conditions. Reduction of the fluid causes $\delta^{34}S$ fractionation between the fluid and the sulfide species to decrease, assuming equilibrium between oxidized and reduced fluids is maintained (Ohmoto and Goldhaber, 1997). Therefore, reduction of an oxidized fluid can produce an increase in $\delta^{34}S_{sulfide}$ values.

The most negative $\delta^{34}S_{sulfide}$ values (-3.0‰ to -5.9‰) have been obtained from bornite and chalcopyrite from the Na-K-feldspar alteration zone in the centre of the deposit. No anhydrite from this domain was analysed. Assuming $\delta^{34}S_{\Sigma S} = 6‰$ (from the covariance of the sulfide-sulfate $\delta^{34}S$ values in Fig. 9.12B), and temperatures of ~500°C (from fluid inclusion microthermometry), using the calculations contained in Ohmoto and Goldhaber (1997) an $SO_4:H_2S$ ratio of 6:1 is obtained, indicating strongly oxidizing conditions existed in the Na-K-feldspar alteration zone. These oxidising fluids are interpreted to have migrated outwards and upwards, where they underwent progressive reduction due to either interaction with the magnetite-stable wall rock or with reduced fluids. As the oxidised fluids migrated outwards, reduction caused $\delta^{34}S_{sulfide}$ values to increase, outstripping the competing effect of cooling, which would decrease $\delta^{34}S_{sulfide}$ values. This could explain the observed array of increasing $\delta^{34}S_{sulfide}$ values towards the deposit periphery.

An alternative mechanism that could produce the observed zonation of $\delta^{34}S$ values at El Teniente is by introduction of enriched ^{34}S from an external source, i.e. changing the bulk sulfur isotopic composition of the fluid. The igneous host rocks of the Teniente host sequence would be expected to have near zero $\delta^{34}S$ values; however, the host rock sequence is considered too sulfur-deficient to be able to supply sulfur for the huge volume of distal pyritic alteration. Alternatively an external fluid with enriched ^{34}S is required. Evaporates, composed of isotopically heavy sulfur (Taylor, 1986) occur in the Jurassic sequences exposed east of Teniente in the Principal Cordillera, and it is possible that a deep circulating fluid dissolved isotopically heavy sulfur and was then focused up into the Teniente deposit. Although feasible, this model is not preferred as mixing between two isotopically distinct fluid sources would be expected to produce more variation in the $\delta^{34}S$ values.

PH and LH stages

For the PH and LH stages sulfides, the zonation to lighter $\delta^{34}S_{sulfide}$ and heavier $\delta^{34}S_{sulfate}$ values at higher elevations (Fig. 9.4) can be explained, like the LM spatial zonation, by variation in the temperature and/or the oxidation state of the fluids. Both cooling of the fluid and an increase in the fluid $SO_4:H_2S$ ratio can generate more negative $\delta^{34}S$ sulfide values.

The variation of PH and LH $\delta^{34}S_{sulfide}$ and $\delta^{34}S_{sulfate}$ values with respect to elevation is consistent with precipitation of sulfides from a cooling fluid. The observed antithetic zonation of LH sulfide and sulfate $\delta^{34}S$ values is modelled in Figure 9.13. Assuming a bulk sulfur composition of 6‰, the observed LH stage $\delta^{34}S_{sulfide}$ and $\delta^{34}S_{sulfate}$ data can be produced by cooling from ~470°C to 320°C of a fluid with $SO_4:H_2S$ ratio of 3:1. This model is validated by the good agreement between modelled temperatures and temperatures obtained by sulfur isotope geothermometry (enclosed in green boxes on Fig. 9.13) and the fluid inclusion study.

The PH $\delta^{34}S$ data are poorly constrained as the $\delta^{34}S_{sulfate}$ values from three PH samples do not lie on a linear trend. The modelled values in Fig. 9.13A are for cooling of a fluid with $SO_4:H_2S$ ratio of 2:1 from 450° to 375°C. Two of the three temperature calculations obtained by sulfide-sulfate geothermometry (enclosed in red boxes in Fig. 9.13A) agree with the modelled temperatures. However, a similar data fit could be ob-
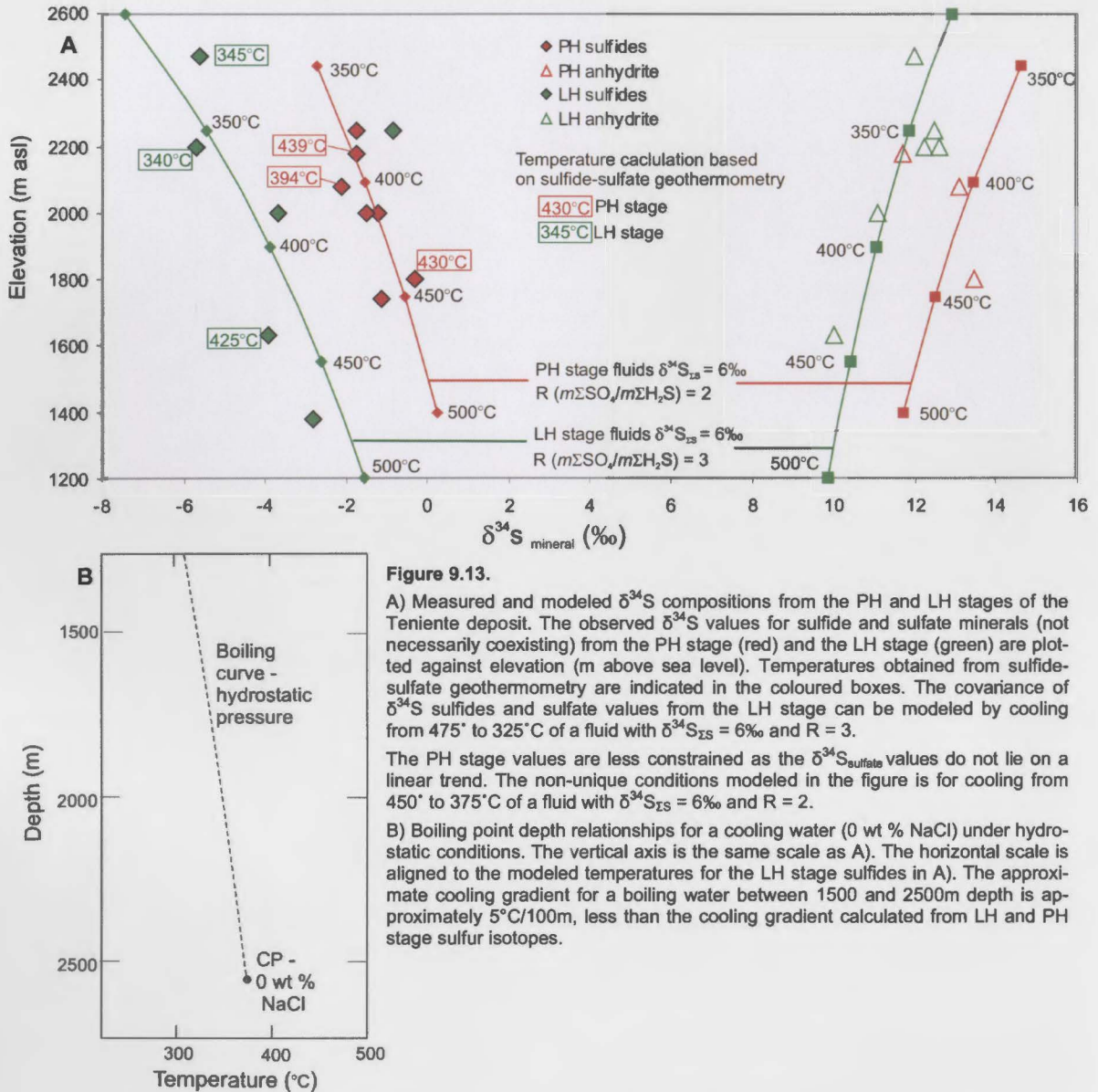
252

Figure 9.13.

A) Measured and modeled $\delta^{34}S$ compositions from the PH and LH stages of the Teniente deposit. The observed $\delta^{34}S$ values for sulfide and sulfate minerals (not necessarily coexisting) from the PH stage (red) and the LH stage (green) are plotted against elevation (m above sea level). Temperatures obtained from sulfide-sulfate geothermometry are indicated in the coloured boxes. The covariance of $\delta^{34}S$ sulfides and sulfate values from the LH stage can be modeled by cooling from 475° to 325°C of a fluid with $\delta^{34}S_{\Sigma S} = 6‰$ and R = 3.

The PH stage values are less constrained as the $\delta^{34}S_{sulfate}$ values do not lie on a linear trend. The non-unique conditions modeled in the figure is for cooling from 450° to 375°C of a fluid with $\delta^{34}S_{\Sigma S} = 6‰$ and R = 2.

B) Boiling point depth relationships for a cooling water (0 wt % NaCl) under hydrostatic conditions. The vertical axis is the same scale as A). The horizontal scale is aligned to the modeled temperatures for the LH stage sulfides in A). The approximate cooling gradient for a boiling water between 1500 and 2500m depth is approximately 5°C/100m, less than the cooling gradient calculated from LH and PH stage sulfur isotopes.

tained from a slightly different temperature range from a fluid with different $SO_4:H_2S$ ratio. Therefore, the model shown in Fig. 9.13 for the PH $\delta^{34}S$ values represents a non-unique solution.

Assuming the observed PH and LH $\delta^{34}S$ values are due to cooling of fluid with a constant bulk sulfur composition and $SO_4:H_2S$ ratio then the temperature varied by approximately 150°C over 1,000m elevation. This corresponds to an average vertical temperature gradient of 15°C/100m during the LH and the PH stages. The LH $\delta^{34}S_{sulfide}$ values are consistently 3‰ lighter than the PH values (Fig. 9. 13A). This shift can be interpreted to be due to more oxidizing conditions and/or cooler temperatures and/or shallower depths during the LH stage.

The calculated temperature gradient of 15°C/100m is too high to be a product of conductive cooling alone (e.g., Hochstein and Browne, 2000). Heat transfer from the liquid to the vapour phase during boiling is a more efficient cooling process for water than conductive cooling. The boiling point – depth relationship for water under hydrostatic pressure is shown in Figure 9.13B. The cooling curve modelled for the LH data (Fig. 13A) is significantly shallower than that of boiling water. This indicates that conductive cooling and boiling-induced cooling cannot account for the high temperature gradients determined for the LH and PH stages. These high temperature gradients may have been produced by mixing with a cooler external fluid, or transient thermal disequilibrium during fracture propagation from hot to cold rock.

The observed variation in $\delta^{34}S$ values of PH and LH sulfides could have been caused by a transition to more oxidizing fluid conditions at higher levels. The O-D isotopic composition of minerals from the deposit periphery precludes the involvement of large volumes of meteoric waters. However, it is feasible that oxidized magmatic vapours condensed into groundwater at high levels, generating an oxidized, acidic, hybrid liquid. This interpretation was proposed by Frikken (2003) and Frikken et al. (submitted) for the Sur-Sur tourmaline breccia, based on a similar sulfur isotope pattern in conjunction with a mineralogical zonation from magnetite stability at depth to hematite stability at higher elevations. These authors proposed that sulfides were precipitated from a reduced brine phase as it was oxidized during ascent due to interaction with the hybrid liquid. The transition from reduced to oxidized conditions is inferred to have resulted in a 5‰ shift to lower $\delta^{34}S$ values in sulfides over 300m vertically. Although there are no vertical zonations of PH or LH stage redox minerals at El Teniente, this model is supported by the presence of zones of pervasive PH and LH sericitic alteration occurring mainly above 2100m asl, fluid inclusion evidence that boiling was occurring in the PH and LH stages, and the magmatic vapour-like O-D isotopic composition of the PH and LH fluids.

Carbon – oxygen isotopic variation in LH stage carbonates

For the latest LH stage (stage 4c and 4d veins), as noted above, $\delta^{18}O$ data indicate the involvement of up to approximately 30% meteoric water into the hydrothermal system. Calculated fluid values from LH stage carbonates (Fig. 9.10B) indicate a mixing trend between a magmatic-derived fluid ($\delta^{18}O$ fluid = 7‰ to 10‰, $\delta^{13}C$ = –7.0‰

254

to -5.6‰) and a source with lower $\delta^{18}O$ values (2.4‰ to 6.2‰) and $\delta^{13}C$ values (-7.6‰ to –6.3‰). This positive coupled trend may be caused by;

1) Fluid-wallrock interaction (e.g., Davidson, 1999)

2) Mixing between two fluids (e.g., Zheng and Hoefs, 1993)

3) Redox gradients in the fluid (Ohmoto and Goldhaber, 1997)

Option 1 can be eliminated, as the predominantly mafic igneous wall rocks contain virtually no carbon; therefore, they would not be able to change the bulk carbon composition of the fluid. Furthermore, the predominantly igneous wall rocks should not have $\delta^{18}O$ values <5 ‰. Conversely, mixing between a magmatic derived fluid ($\delta^{18}O$ = 7 to 10‰), emanating from LH structures at depth, supplying most of the carbon ($\delta^{13}C_{\Sigma C}$ = -7 ‰ to –6 ‰) and a meteoric fluid ($\delta^{18}O$ = -8 ‰; Kusakabe et al., 1990; and $\delta^{13}C_{\Sigma C}$ <-7‰) may explain the trend. Meteoric fluids with $\delta^{13}C$ values down to and less than -8.4 ‰ may be due to near-surface interaction of the fluids with soil-derived organic carbon or leaching of light carbon in sedimentary rocks in the fluid pathway (e.g., Ohmoto and Goldhaber, 1997). Alternatively, Ohmoto and Goldhaber (1997) note that oxidation of a fluid (option 3), assuming that equilibrium is maintained between the reduced and oxidized species, will increase the $\delta^{13}C$ fractionation between the fluid and the precipitating minerals, leading to more negative $\delta^{13}C$ mineral values.

In conclusion it is considered most likely that the coupled trend between $\delta^{18}O$ and $\delta^{13}C$ fluid values calculated from LH carbonates is due to mixing of magmatic and external waters, and associated cooling and oxidation of the hydrothermal fluids. Scatter in the dataset is probably due in part to inaccuracies in the temperature estimates, and due to a combination of process occurring in the hydrothermal system.

9.6 RADIOGENIC ISOTOPES

Introduction

The radiogenic isotopes of Sr-Nd and lead provide information regarding the source of the igneous rocks and hydrothermal minerals and can be used to identify mixing trends between different sources (e.g., Tosdal et al., 1999). Sr-Nd and lead isotope studies can also be utilized to investigate the interaction between hydrothermal fluids and wall rocks (e.g., Farmer and DePaolo, 1987; Tosdal et al., 1999). Lead iso-

topes are a particularly useful in ore deposit research as lead is generally coupled with other metals of economic interest such as copper and zinc (e.g., Tosdal et al., 1999). Strontium isotopes can also be used to infer the source of elements with a chemical affinity to strontium, such as calcium, barium, and even sodium and potassium (Richards and Noble, 1998).

Sr-Nd isotopes are sensitive indicators of any contamination of magma that has occurred during its emplacement (e.g., Kesler et al., 1975; Kay et al., 1999). Magmas that have not been contaminated during their ascent through the crust have depleted mantle-like $^{87}Sr/^{86}Sr$ ratios (<0.7045). Potential contaminants include continental crust, components from the subducted slab, or enriched lithospheric mantle. The affinity of parent rubidium with the continental crust has resulted in elevated daughter ^{87}Sr, and higher $^{87}Sr/^{86}Sr$ ratios compared to mantle-derived rocks (Rollinson, 1993). In contrast, the Sm-Nd isotopic systematics are opposite to the Sr-Rb system, in that parent samarium has a mantle affinity. Therefore, mantle-derived magmas have high $^{87}Sr/^{86}Sr$ and low εNd values (measured relative to a chondritic uniform reservoir reference value of 0.512638; Skewes and Stern, 1996), and magmas derived from or contaminated by the crust have low $^{87}Sr/^{86}Sr$ and high εNd values. Several workers have unsuccessfully attempted to identify systematic Sr-Nd isotopic differences between productive and barren porphyry-related intrusive complexes (Farmer and DePaolo, 1984; Lang and Titley, 1998). These authors concluded that mantle or lower crustal regions were important in the magma-genesis of porphyry-related complexes. However, many porphyry systems in continental arc settings have isotopic evidence for extensive involvement of upper crustal material (Hedenquist and Richards, 1998).

Lead isotopic data are typically displayed on uranogenic ($^{207}Pb/^{204}Pb$ vs $^{206}Pb/^{204}Pb$) and thorogenic ($^{208}Pb/^{204}Pb$ vs $^{206}Pb/^{204}Pb$) diagrams. The uranogenic diagram plots the radiogenic daughter (^{207}Pb, as a ratio of the non-radiogenic ^{204}Pb isotope) of the ^{235}U isotope versus the radiogenic daughter (^{206}Pb) of the ^{238}U isotope (Tosdal et al., 1999). Due to the abundance of ^{235}U in the Archaean rocks, elevated $^{207}Pb/^{204}Pb$ ratios indicate the involvement of old crustal lead. Lower $^{207}Pb/^{204}Pb$ ratios indicate a lack of old lead, suggesting a source that was isolated from the old radiogenic crust, such as the mantle. The thorogenic diagram plots the radiogenic daughter of thorium (^{208}Pb) versus the radiogenic daughter of the most abundant uranium isotope (^{206}Pb). Elevated $^{208}Pb/^{204}Pb$ (high thorium/uranium) and $^{206}Pb/^{204}Pb$ values indi-

cate a radiogenic upper crustal source, whereas depleted $^{208}Pb/^{204}Pb$ and $^{206}Pb/^{204}Pb$ ratios are characteristic of a primitive mantle source. Kay et al. (1999) interpret high $^{208}Pb/^{204}Pb$ and low $^{206}Pb/^{204}Pb$ values from the basement in Peru to indicate a lower crustal source.

Lead isotopic data are also presented and discussed on the plumbotectonics model of Doe and Zartman (1979) and Zartman and Haines (1988). This model has utilized the distinct uranium-thorium-lead characteristics of different reservoirs of the evolving Earth to identify three idealized reservoirs, the mantle, lower crust, and upper crust (Doe and Zartman, 1979). Mixing of these reservoirs through deformation, magmatism, sedimentation and metamorphism results in a fourth reservoir referred to as the orogene (Doe and Zartman, 1979).

Lead isotopic studies of porphyry systems have tended to obtain equivocal results, with isotopic compositions indicating a mixture of sources including MORB, lower continental crust, and pelagic sediment (Hedenquist and Richards, 1998). Porphyry copper deposits, and batholiths in general, tend to have homogenous lead isotopic compositions within a given district, though these compositions vary from one district to another (Hedenquist and Richards, 1998; Tosdal and Munizaga, 2003). This may be explained in part by isotopic homogenization in the lower crust due to circulation of brines (McCullogh and Woodhead, 1993), partly explaining the mixed isotopic signatures of porphyry deposits. Further complexity occurs during ascent of the magma through the upper crust. Due to the high lead concentration in crustal rocks (10-30 ppm) compared to the mantle (1-2 ppm), a small amount of crustal contamination can significantly alter the isotopic composition of a mantle-derived melt (Tosdal et. al., 1999), especially in continental arc porphyry systems (Tosdal and Munizaga, 2003).

Methods

Seven vein and breccia samples of anhydrite and one epidote sample were submitted for Sr-Nd and lead isotopic analysis. Samples were selected in order to cover the paragenesis of the Teniente system. They were also selected to provide a spatial coverage from the centre to the deposit periphery. Analyses have been conducted to trace fluid sources and potential spatial or temporal fluid evolution. Analytical techniques are described in Appendix 6D.

The following assumptions have been made for this study:

1) No radiogenic daughter isotopes (e.g. ^{206}Pb, ^{207}Pb, ^{208}Pb, ^{87}Sr, ^{144}Nd) have been added to the mineral by radiogenic decay of the parent (e.g. ^{238}U, ^{235}U, ^{232}Th, ^{87}Rb, ^{147}Sm respectively), due to the young age (5.7 - 4.7 Ma) of the samples (Richards and Noble, 1998).

2) There has been no fractionation of non-radiogenic isotopes (e.g., ^{204}Pb) compared to radiogenic isotopes (e.g., ^{208}Pb, ^{207}Pb, ^{206}Pb) during precipitation of anhydrite from hydrothermal fluids, as isotopic fractionation of elements with high atomic mass is negligible (Richards and Noble, 1998).

3) Based on assumptions 1) and 2), the lead, strontium and neodymium isotopic ratios for the gangue minerals are inherited directly from the fluids that precipitated them.

Sr-Nd isotopes

Previous work

The Cenozoic volcanic arc of the Andes displays notable geographical and temporal variations in the Sr-Nd isotopic signatures and REE patterns of the erupted magmas (e.g. Hildreth and Moorbath, 1988; Stern and Skewes, 1995; Kay et al., 1999; Hollings et al., submitted). It is debatable whether this variation is due to intracrustal contamination of depleted mantle-derived magmas, or due to contamination of the magma source region underlying the crust (Kay et al., 1999).

Sr-Nd isotopic data from Nystrom et al. (1993), Skewes and Stern (1996), Kay et al., (1999), and Hollings et al. (submitted) display a trend towards depleted MORB-like values until the Cretaceous, followed by a reversal and a trend back to more crustally-enriched values through to the Miocene. This trend of Sr-Nd values is paralleled by whole rock geochemical trends (e.g., Kay et al., 1999). In the region of El Teniente, the Coya-Machalí Formation has the most MORB-like, least crustally-contaminated Sr-Nd isotopic composition (Nystrom, 1993; Fig. 9.14A), consistent with its tholeiitic geochemical affinities and an interpreted formation in an extensional back-arc basin (Kay and Kurtz, 1995; Charrier et al., 2002). The younger Farellones Formation (Teniente volcanic complex) and Teniente plutonic complex have progressively enriched $^{87}Sr/^{86}Sr$ and depleted εNd compositions. Late hornblende dykes from
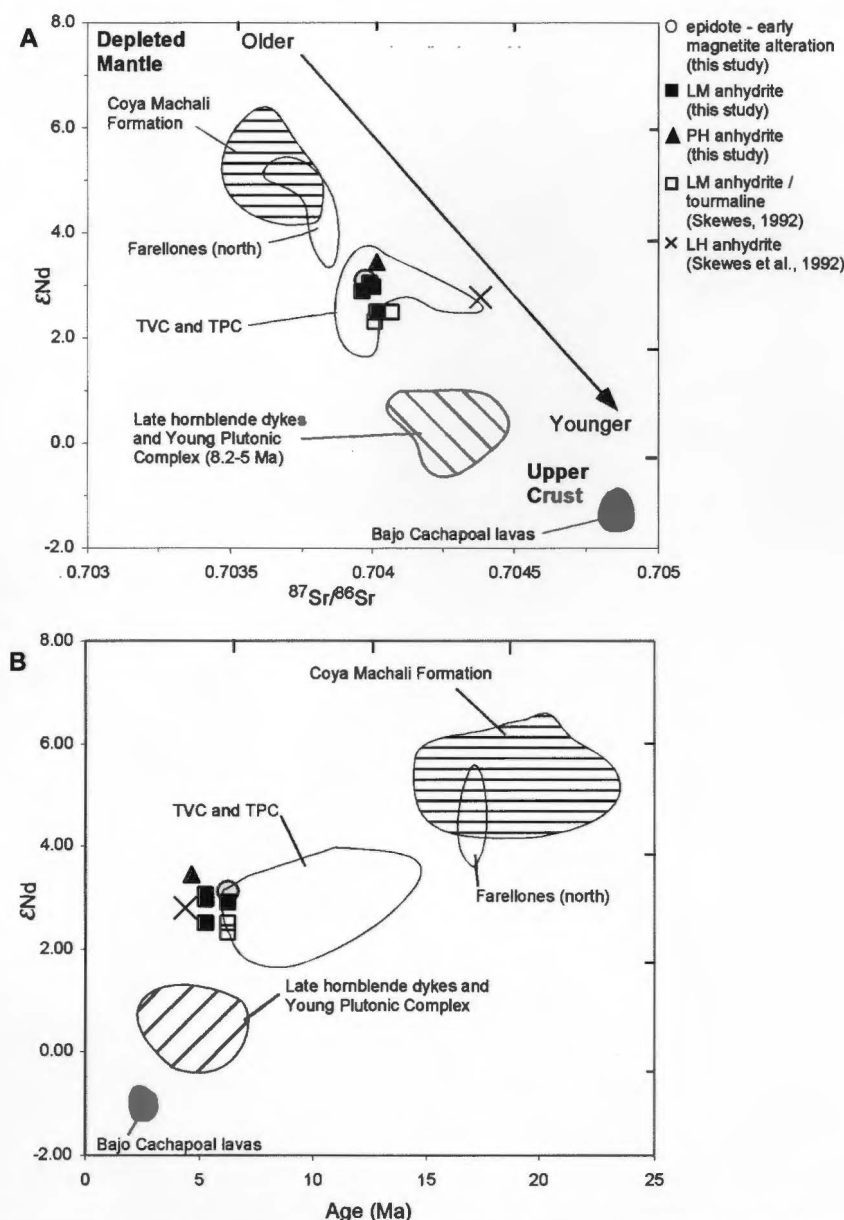
Figure 9.14. Sr-Nd data for El Teniente hydrothermal minerals from this study, and from Skewes (1992). The dataset is superimposed on the fields for the Oligocene to Pliocene igneous units in the Teniente district from Kay and Kurtz (1995).

A) $^{87}Sr/^{86}Sr$ and εNd

B) εNd vs. age

Abbreviations: TVC = Teniente volcanic complex, TPC = Teniente plutonic complex

the Teniente deposit, and the calc-alkaline dacitic Young plutonic complex have en-riched $^{87}Sr/^{86}Sr$ and depleted εNd values (Fig. 9.14A). Dacites of the Teniente intrusive complex have not been analysed for Sr-Nd isotopic compositions. However, the Young plutonic complex is dated at the same age as the Teniente intrusive complex, and has similar geochemistry and REE patterns (Chapter 7). In this study the Teniente intrusive complex units are assumed to have similar crustally-enriched Sr-Nd values as

the Young plutonic complex (Kay and Kurtz, 1995).

Hildreth and Moorbath (1988) found that in the recent southern volcanic zone (33°
- 38° 30' S) the $^{87}Sr/^{86}Sr$ and $^{143}Nd/^{144}Nd$ values are depleted in the south (0.7036 and
0.5129 respectively) in the south, where the crust is 30-40km thick. In contrast, the
crust is enriched in the north (0.7057 and 0.5125 respectively) where subduction of the
Juan Fernandez Ridge has resulted in crustal thickness of 45-60km. The mantle mag-
mas were probably contaminated by lower crustal material through the melting, as-
similation, storage, homogenisation (MASH) processes (Hildreth and Moorbath,
1988). These authors, together with Davidson et al. (1991) and Kay et al. (1991, 1999)
concluded that intra-crustal processes exerted a fundamental control on magma evolu-
tion in the central Andes.

In contrast, Stern (1989), Stern and Skewes (1995), and Hollings et al. (submitted)
concluded that temporal and spatial changes in the isotopic values of Miocene to Plio-
cene lavas in central Chile were influenced by contamination of the sub-arc mantle.
They argued that a decreasing subduction angle and the subduction of the Juan Fernan-
dez Ridge caused an increase in the rate of subduction erosion and source region con-
tamination below the Miocene-Pliocene arc. Kay and Abbruzzi (1996), and Kay et al.
(1999) suggest that Tertiary Main Cordilleran, Precordilleran, and Pampean magmas
north of 33°S were sourced from sub-arc mantle which was contaminated by continen-
tal lithosphere due to delamination, lithosphere boundary erosion, and subduction ero-
sion processes, and further contaminated during ascent through thickened crust.

Skewes (1992) and Skewes and Stern (1996) analysed Sr-Nd isotopes from pre-
and post-mineralization porphyries and from breccia cement minerals from El
Teniente, Río Blanco-Los Bronces, and Los Pelambres. Two samples of LM stage
tourmaline and anhydrite breccia cement have Sr-Nd values similar to the pre-
mineralization Teniente volcanic complex and Teniente plutonic complex host rocks
(Table 9.6). A single tourmaline sample from the LH marginal breccia has a $^{87}Sr/^{86}Sr$
value closer to the post-mineralization igneous rocks, and an εNd value overlapping
with the range of pre-mineralization rocks (Fig. 9.14). A single biotite sample with an
anomalous strontium ratio was discarded as analytical error (Skewes, 1992; Table 9.6).
At all three of the giant porphyry copper deposits, Skewes (1992) found that the brec-
cia minerals have Sr-Nd isotope compositions that are intermediate between the pre-

and post-mineral porphyries, and lie on a poorly defined mixing curve (Skewes and Stern, 1996). Skewes and Stern (1996) noted that the εNd values for breccia cements are similar to the pre-mineralization wall rocks, whereas the $^{87}Sr/^{86}Sr$ values vary between the compositions of pre- and post-mineral igneous rocks. Strontium has a high solubility compared to neodymium in hydrothermal fluids (Farmer and DePaolo, 1987). Therefore, Skewes and Stern (1996) argued that the observed mixing curve is not consistent with Sr-Nd exchange between a magmatic-derived fluid and the wall rock. Rather, they concluded that the breccia-forming fluids were exsolved from magmas that are not exposed at the current mine levels that had isotopic compositions intermediate between the pre- and post-mineral igneous rocks.

Results

$^{87}Sr/^{86}Sr$ results from the current study are tightly grouped, ranging from 0.70396 to 0.70404 (Table 9.7; Fig 9.14A). This contrasts with the values obtained from Skewes (1992) which range from 0.70401 - 0.70438 (Table 9.7; Fig 9.14A). The εNd

Sample no.	Vein stage	Age (Ma)	mineral	$^{87}Sr/^{86}Sr$	Nd (ppm)	Sm (ppm)	$^{143}Nd/^{144}Nd$	εNd
This study								
et234	stage 1, early magnetite alteration	6.3?	epidote	0.70398	16	11.5	0.51280	3.10
et825	LM anh/sulf/bt bx	5.7	anhydrite	0.70396	9	69.3	0.51279	2.89
et638	stage 2c	5.5	anhydrite	0.70401	13	36.1	0.51276	2.48
et669	stage 2d anh bx	5.5	anhydrite	0.70401	8	73.0	0.51279	2.97
et151	stage 2, distal	5.5	anhydrite	0.70399	10	15.4	0.51279	3.04
et605	stage 3 PH	4.9	anhydrite	0.70401	9	41.8	0.51281	3.45
et418	stage 4c LH	4.7	anhydrite	0.70404		0.1	*	
et497	stage 4c LH	4.7	anhydrite	0.70400	2.4	0.5	#	
Skewes (1992), Skewes and Stern (1996)								
	LM anh/bt/tour bx	5.7	biotite	0.70641^			0.51276	2.6
	LM anh/bt/tour bx	5.7	anhydrite	0.70401			0.51275	2.3
	LM anh/bt/tour bx	5.7	tourmaline	0.70407			0.51276	2.5
	stage 4a (marg. bx)	4.7	tourmaline	0.70438			0.51278	2.8

Table 9.7. Sr-Nd isotopic data for El Teniente vein minerals from this study. Included are three breccia gangue minerals from Skewes (1992). εNd values were calculated using a present day chondritic uniform reservoir (CHUR) reference value of 0.512638 (Skewes and Stern, 1996). * Sm-Nd too small to measure. # Sm-Nd concentrations unsatisfactory. ^ Anomalously high $^{87}Sr/^{86}Sr$ value due to analytical error (Skewes, 1992).

Abbreviations: anh = anhydrite, bt = biotite, bx = breccia, marg. = marginal, tour = tourmaline, sulf = sulfide

values from this study range from 2.48 to 3.45, overlapping with the range of Skewes (1992). Note that two LH samples did not record satisfactory Sm-Nd concentrations; hence, they are not reported in Table 9.7.

The Sr-Nd isotopic data from vein and breccia minerals at El Teniente correlate well with whole rock data from the Teniente volcanic complex and Teniente plutonic complex (Fig. 9.14A), The only sample lying outside the field is one LH sample from Skewes (1992). Sr-Nd isotopic values from the current study are distinct from the Young plutonic complex and late hornblende dykes. Figure 7.14B plots the εNd values against the age of the samples, illustrating the lack of systematic temporal variation of the Sr-Nd data.

The most likely explanation for this isotopic dataset is that the strontium and neo-dymium were scavenged from the wall rocks. Abundant evidence for alteration of pri-mary plagioclase in the Teniente host sequence (Fig. 4.10A) supports this interpreta-tion. No systematic variation in Sr-Nd values was detected from the center to the pe-riphery of the deposit, suggesting the wall rock Sr-Nd signature swamped the or-thomagmatic signature. An alternative interpretation is that strontium and neodymium were sourced from a separate fluid that was in equilibrium with the wall rocks and then mixed with the magmatic-derived fluid. These two models cannot be discriminated on the basis of the current Sr-Nd isotope database alone.

Lead isotopes

Previous work

Previous studies of the lead isotope systematics of central Chile are contained in Harmon et al. (1984), Puig (1988), Hildreth and Moorbath (1988), Davidson et al. (1991), Kay and Kurtz (1995), Kay and Abruzzi (1996), Kay et al. (1999), and Tosdal and Munizaga (2003). Their data are summarized in Figure. 9.15.

In contrast to the strontium and neodymium isotopic data, the lead isotopic compo-sitions of igneous rocks from the SVZ, CVZ, and Chilean flat slab zone are tightly grouped (Fig. 9.15). These values have enriched (high $^{208}Pb/^{204}Pb$, $^{207}Pb/^{204}Pb$, and $^{206}Pb/^{204}Pb$ ratios), upper crustal-like signatures (Kay and Abruzzi, 1996). Figure 7.15A suggests that the isotopic composition of the arc magmas have not been influ-enced by contribution from the subducted Nazca Plate (Hildreth and Moorbath, 1988);

hence, the lead isotopic enrichment is most likely due to interaction of the magmas with continental crust, either in the sub-arc region, or during ascent through the crust (eg. Harmon et al., 1984; Hildreth and Moorbath, 1988). The homogenous, enriched lead signature may be due to swamping the mantle-derived lead by assimilation of crustal fluids and materials with much higher lead concentrations than the primitive magma (Hildreth and Moorbath, 1988). The lead isotopic compositional ranges for the latest Miocene - Pliocene intrusives, and for the Teniente Volcanic Complex and Teniente Plutonic Complex from Kay and Kurtz (1995), are tightly clustered enclosed within the fields for SVZ, CVZ and flat slab lavas (Fig. 9.15). The La Obra Pluton, which has geochemical affinities to the Coya-Machalí Formation (Kay and Kurtz, 1995), plots at more depleted $^{207}Pb/^{204}Pb$, and $^{206}Pb/^{204}Pb$ values than the recent and flat slab volcanics.

The Precordilleran basement of central Chile has depleted $^{208}Pb/^{204}Pb$, $^{207}Pb/^{204}Pb$, and $^{206}Pb/^{204}Pb$ ratios, inherited from a primitive source such as the mantle (Kay and Abruzzi, 1996). Lead compositions from Miocene Precordilleran rocks and the Sierra Pampeanas (in the back-arc region of Main Cordillera in the flat slab zone) can be modelled as a mixture of magma with lead compositions similar to the recent SVZ and CVZ magmas from the Main Cordillera contaminated with lead from the Precordilleran basement (Kay and Ambruzzi, 1996).

Puig (1988) analyzed lead isotope compositions of 81 galena samples from 48 Chilean ore deposits of Palaeozoic to Miocene age. The restricted range of values obtained (Fig. 9.15) was interpreted to be due to thorough mixing of different lead reservoirs during Andean orogenic processes (Harmon et al., 1984; Puig, 1988). The lead isotope values from deposits hosted by Tertiary rocks was found to be more variable than the lead from deposits hosted in Mesozoic rocks, reflecting the influence from mixed lead sources in a more evolved and thickened crust (Puig, 1988). No obvious correlation was recognized between the lead isotopic composition and the age of the mineralizing or intrusive events; however, the lead compositions correlated with the age of the country rock. This suggests that the lead was derived from the wall rocks, or that the wall rocks and ore systems had common lead sources (Puig, 1988).

Frikken (2003) and Frikken et al. (submitted) analysed four samples of pre-ore anhydrite for their lead isotope compositions from the Río Blanco deposit. They
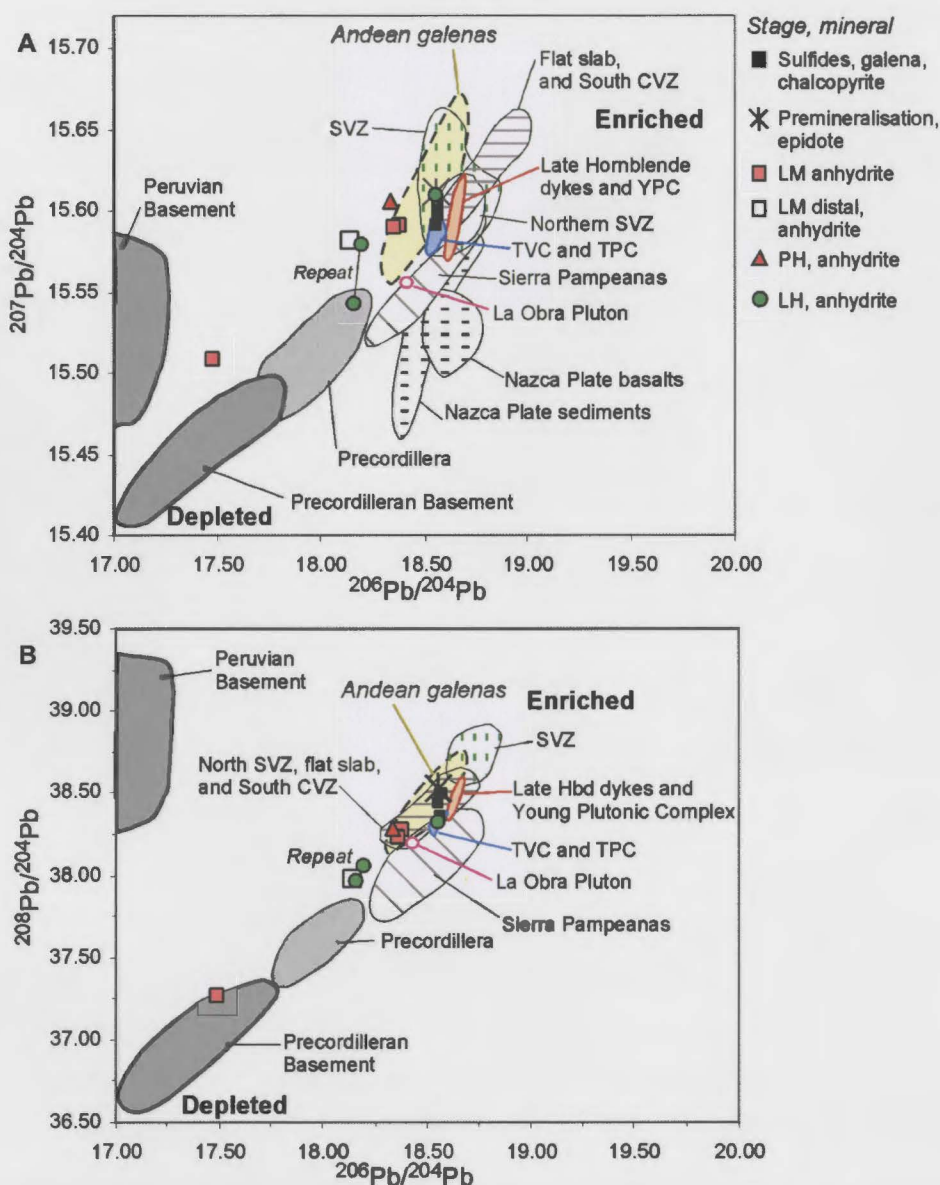
Figure 9.15. Uranogenic (A) and, thorogenic (B) diagrams showing Pb isotope composition for the regional rocks in Central Chile. The "flat slab" data are from the Miocene arc and back-arc rocks, and overlap with volcanics from the Quaternary SVZ and CVZ. Fields from Kay and Abruzzi (1996). Fields for igneous rocks are from Hildreth and Moorbath (1988, and references therein), Kay and Kurtz (1995) and Kay et al., (1999). Teniente sulfide values are from LH stage galena (x3) and chalcopyrite (x1), from Puig (1988), Zentilli et al. (1988), and Tosdal et al. (1999). The field of Andean galenas (Puig, 1988) is from 81 analyses from 48 mining areas.

Abbreviations: CVZ = Central Volcanic Zone, Hbd = hornblende, SVZ = Southern Volcanic Zone, TPC = Teniente plutonic complex, TVC = Teniente volcanic complex, YPC = Young plutonic complex.

found that the anhydrite lead isotopic compositions varied widely (e.g., $^{206}Pb/^{204}Pb$ from 17.558 – 18.479), in contrast to the sulfide lead isotope compositions ($^{206}Pb/^{204}Pb$ from 18.552 – 18.627) from previous authors (Tilton, 1979; Puig, 1988; Zentilli et al. 1988; Tosdal et al., 1999). On a thorogenic diagram, the anhydrite lead compositions plot on linear trend lines. The most enriched compositions overlap with the sulfide

264

lead isotopic values and fields for central Chilean Tertiary igneous rocks, whereas the most depleted compositions are similar to the Precordillera and Precordilleran basement values. To explain this dataset, Frikken (2003) and Frikken et al. (submitted) proposed that anhydrite was precipitated by mixing of magmatic vapours containing SO_2, and a deep circulating water which supplied external primitive lead. In contrast, sulfides were precipitated from isotopically homogenized magmatic brines which ascended into the breccias after the vapour phase (Frikken, 2003; Frikken et al., submitted).

Only four previous lead isotopic analyses of sulfides from Teniente have been obtained to date (Puig, 1988; Zentilli et al. 1988; Tosdal et al., 1999). They are clustered at enriched compositions overlapping with the fields for the Teniente volcanic complex and Teniente plutonic complex within which the deposit is hosted, the Young plutonic complex, and late hornblende dykes (Fig. 9.15).

Results

$^{208}Pb/^{204}Pb$ ratios of anhydrite and lead from El Teniente range from 37.264 to 38.530, $^{207}Pb/^{204}Pb$ values range from 15.509 to 15.612, and $^{206}Pb/^{204}Pb$ values vary between 17.490 and 18.559 (Table 9.8; Fig. 9.15). The epidote sample from an early magnetite alteration assemblage and an LH anhydrite sample have a crustally-enriched lead isotopic composition similar to the Teniente sulfides and pre-, syn-, and post-mineral host rocks (Fig. 9.15). Two LM and the single PH anhydrite samples have more depleted lead ratios, and overlap with the lowest values for the SVZ/flat slab lavas. The distal LM sample, and a LH-stage vein from outside of the Braden Pipe have more depleted lead isotopic values than any analysed igneous rocks in the Teniente district. The anhydrite sample associated with the early grey porphyry in the southeast corner of the deposit has a strongly depleted lead isotope composition similar to the Precordilleran basement.

Anhydrite has a wide range of lead isotope values compared to the tightly grouped values for the Teniente host rocks and sulfides. The anhydrite lead isotope compositions span the entire range of central Chilean igneous rocks and sulfides (Fig. 9.15), largely due to the strongly depleted lead isotopic composition of a single anhydrite analysis from a LM anhydrite-biotite-sulfide breccia adjacent to the grey porphyry.

Sample no.	Vein stage	Age	mineral	Pb * (ppm)	$^{208}Pb/^{204}Pb$	$^{207}Pb/^{204}Pb$	$^{206}Pb/^{204}Pb$
This study							
et234	stage 1, early magnetite alteration	6.3?	epidote	14.3	38.530	15.612	18.558
et825	LM anhydrite – biotite -sulfide breccia	5.7	anhydrite	1.49	37.264	15.509	17.490
et638	stage 2c	5.5	anhydrite	4.63	38.271	15.590	18.381
et669	stage 2d anh bx	5.5	anhydrite	1.31	38.229	15.589	18.361
et151	stage 2, distal	5.5	anhydrite	5.41	37.970	15.581	18.146
et605	stage 3 PH	4.9	anhydrite	1.13	38.287	15.606	18.339
et418	stage 4c LH non-magmatic	4.7	anhydrite	0.5	37.963	15.542	18.164
replicate				0.5	38.055	15.579	18.120
et497	stage 4c LH magmatic (from Braden Pipe)	4.7	anhydrite	24.3	38.320	15.610	18.559
Zentilli et al., 1988							
BRD-ET‡	stage 4 LH stage	4.7	Galena		38.493	15.605	18.565
Puig, 1988, average of 2							
TTE 3	stage 4 LH stage	4.7	Galena		38.493	15.600	18.570
Tosdal et al., 1999							
TEN-11-95-3	stage 4 LH stage	4.7	Chalcopyrite		38.432	15.591	18.559
Replicate					38.354	15.597	18.566

Table 9.8. Pb isotopic data for Teniente gangue minerals. ET418 has large 2σ errors, as indicated by the lack of correlation between the original and the replicate sample. Excluding ET418 the 2se mass spectrometer measurement errors are < 89 for $^{208}Pb/^{204}Pb$, < 37 for $^{207}Pb/^{204}Pb$, and < 42 for $^{206}Pb/^{204}Pb$. In the vein stage column for et418 and et497, "magmatic" and "non-magmatic" refers to the $\delta^{18}O$ fluid values calculated for these samples (chapter 9.4).

* Pb concentrations were obtained by solution – inductively coupled plasma mass spectrometry (ICPMS) analyses, at the University of Tasmania, performed by Leonid Danyshevsky.

The lead isotope data plotted on the plumbotectonics model of Doe and Zartman (1979) indicate that the Precordillera and Precordilleran basement contain a significant mantle-derived lead component (Fig. 9.16). The Miocene to Quaternary volcanics of the flat slab, SVZ and CVZ have orogenic lead isotope ratios, that have been further contaminated with upper crustal material. Most of the gangue and sulfide minerals plot on or slightly above the orogene curve. The LM anhydrite associated with the grey porphyry is an outlier. It is shifted away from the orogene curve and plots towards primitive mantle values (Fig. 9.16).
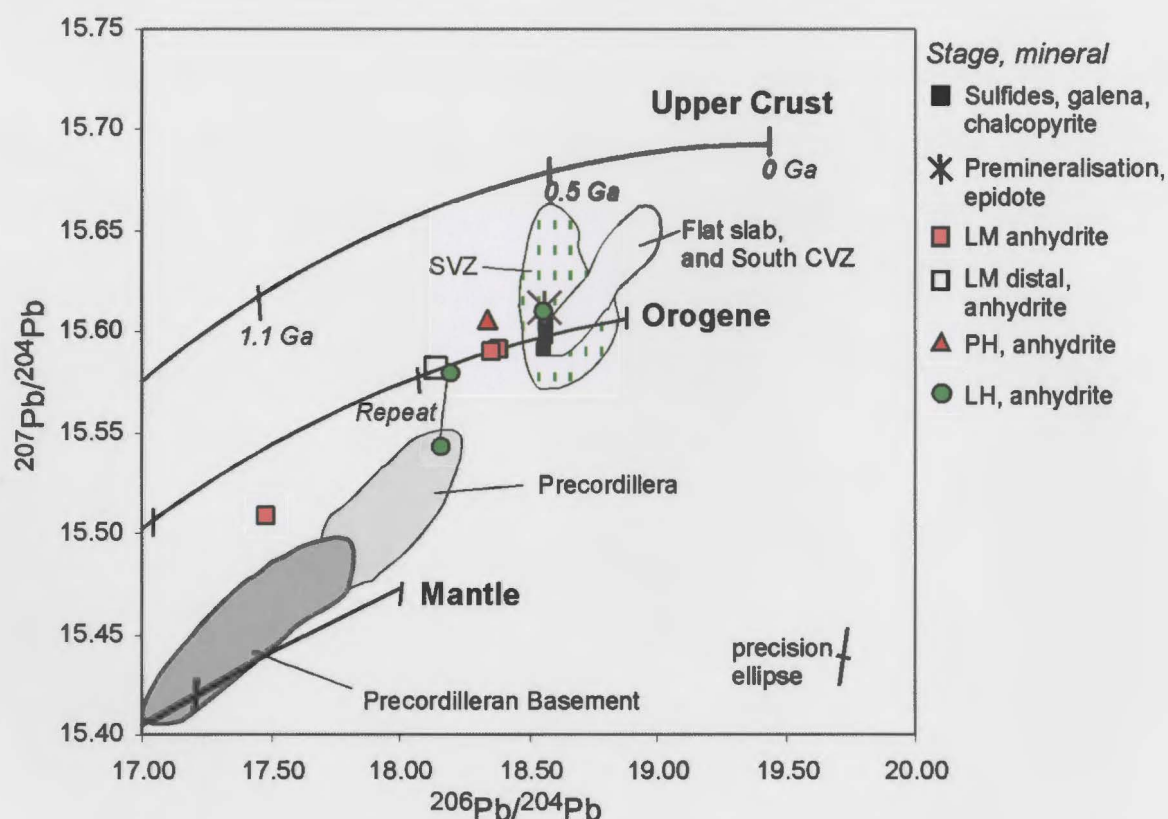
Figure 9.16. Lead isotope data for gangue minerals (this study), sulfides (Puig, 1988; Zentilli et al., 1988; Tosdal et al., 1999), and regional rocks of central Chile (Kay and Ambruzzi, 1996) plotted on the "plumbotectonics" model of Doe and Zartman (1979) with growth curves representing different reservoirs. The orogene curve is due to mixing of crustal and mantle reservoirs during the orogenic processes. The lower crust growth curve plots below the bottom axis of this diagram. The precision ellipse refers to the gangue minerals from this study.

Abbreviations: CVZ = Central volcanic zone, SVZ = Southern volcanic zone.

Radiogenic isotope discussion

Lead systematics

In contrast to the Sr-Nd values, the lead isotopic compositions of anhydrite from Teniente vary widely, from enriched compositions similar to the wall rock values to depleted values indicating a primitive mantle component. The wide range of values for anhydrite contrasts with the restricted range of reported sulfide lead isotopic values from Teniente (Fig. 9.15). All the lead isotopic analyses of sulfides from Teniente were performed on galena and chalcopyrite from the LH stage (Puig, 1988; Zentilli et al., 1988; Tosdal et al., 1999). Therefore, the lead isotopic composition of the LM and PH sulfides are unknown. However, the dataset of Puig (1988) indicates relatively homogenous enriched sulfide lead values from 48 deposits throughout Chile. Furthermore, a similar lead isotopic dataset was reported by Frikken (2003) from the Río Blanco deposit. Anhydrites forming breccia cements have depleted to enriched lead isotopic values, similar to the range of anhydrite values from Teniente, whereas sul-

fides have homogenous enriched lead isotopic values (Frikken, 2003). Therefore, by analogy with other Chilean porphyry copper deposits it is considered unlikely, though not impossible, that early sulfides at Teniente have depleted lead isotopic values similar to the anhydrite.

To assess the possible effect that radiogenic lead may have had on the present day lead isotopic composition of the samples, the concentration of lead in the samples was plotted against the $^{206}Pb/^{204}Pb$ ratio (Fig. 9.17; e.g., Gulson et al., 1987; Wilson, 2003). Galena has a high lead content; therefore, the addition of radiogenic ^{206}Pb from the radioactive decay of ^{235}U is minimal. Therefore, galena records the lead isotopic composition of the source region. Higher $^{206}Pb/^{204}Pb$ values in lead-poor minerals than in galena may be due to the addition of radiogenic ^{206}Pb to the present day $^{206}Pb/^{204}Pb$ value (Gulson et al., 1987). All the anhydrite values from this study contain between 0.5 and 24.4ppm lead, and plot at lower $^{206}Pb/^{204}Pb$ ratios than the galena (Fig. 9.17). This indicates that addition of radiogenic lead cannot account for the strongly depleted lead isotopic compositions of anhydrite from Teniente. Furthermore, considering the young age of the Teniente deposit (5.7 – 4.7 Ma) it is unlikely that the present day $^{206}Pb/^{204}Pb$, $^{207}Pb/^{204}Pb$ and $^{208}Pb/^{204}Pb$ values have been modified by addition of radiogenic lead (e.g., Richards and Noble, 1998).

Figure 9.18 illustrates the wide variation of the $^{206}Pb/^{204}Pb$ ratios of the Teniente gangue minerals compared to the sulfide minerals and host rocks, plotted against interpreted age. The oldest anhydrite sample from the LM anhydrite – biotite – sulfide breccia zone surrounding the grey porphyry has the most depleted lead composition. The primitive lead in anhydrite from this breccia may have been contributed by either:

1) magmatic-hydrothermal fluids from the grey porphyry,

2) an external lead source

It is possible that the grey porphyry originated from a source region depleted in radiogenic Pb, such as the mantle or Precordilleran lower crust, and was able to ascend with minimal contamination from the upper crust. The intermediate chemistry and shallow REE slopes of the grey porphyry are also consistent with a primitive source. However, this theory assumes that sulfides associated with the grey porphyry also have primitive lead isotopic compositions, which as discussed above is considered unlikely, though not impossible. This theory could be tested by lead isotopic analyses of sulfides from the biotite-sulfide-anhydrite breccia which surrounds the grey porphyry.
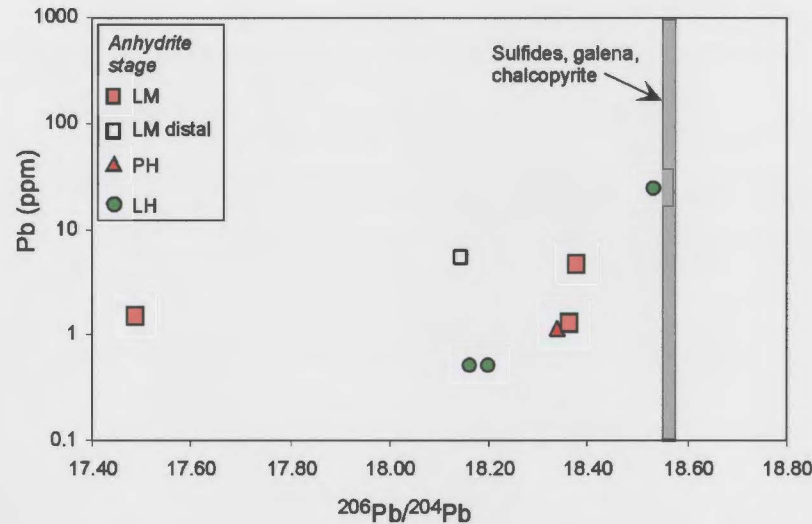
Figure 9.17. Variation of $^{206}Pb/^{204}Pb$ with respect to total lead content for anhydrites and sulfides from Teniente (from data in Table 9.8). The low-lead samples have $^{206}Pb/^{204}Pb$ values lower than the sulfides, indicating that their lead isotopic compositions have not been modified by radioactive decay.
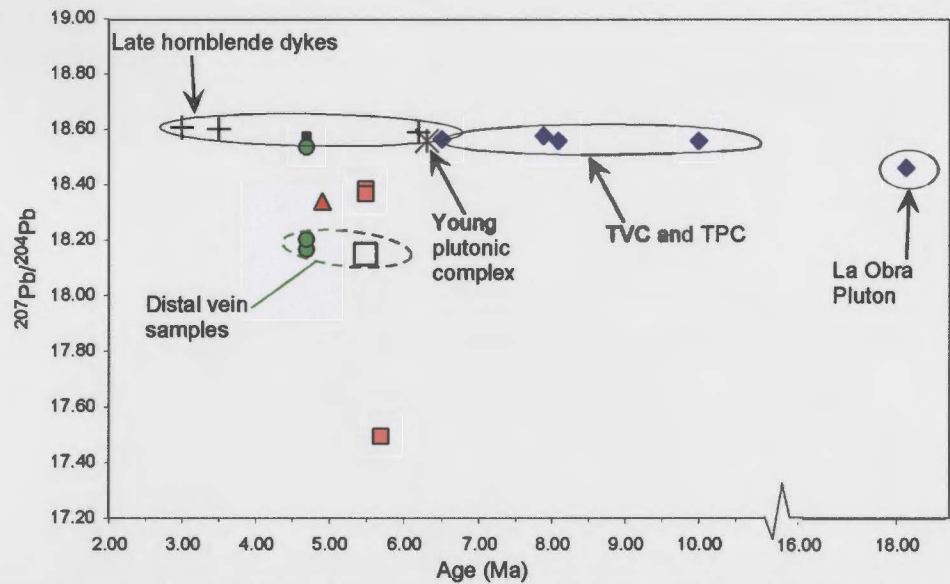

Figure 9.18. Age vs. $^{206}Pb/^{204}Pb$ ratio for the Teniente gangue minerals (this study), sulfides (Puig, 1988, Zentilli et al., 1988, Tosdal et al., 1999) and the local wall rocks (Kay and Kurtz, 1995). Note the wide range of lead values for anhydrite compared to the sulfides and wall rocks.

Abbreviations: TPC = Teniente plutonic complex, TVC = Teniente volcanic complex.

It is considered more likely that the variability of anhydrite lead isotopic values in the deposit may be due to mixing between two different sources of lead. In support of this option, there is a broad spatial zonation to lower anhydrite lead isotopic values towards the deposit periphery (Fig. 9.19). As the wall rocks have crustally enriched lead compositions, this zonation cannot be explained by fluid-rock interaction. The observed zonation is consistent with mixing between an external fluid containing primitive lead sourced from deep in the crust and a magmatic-hydrothermal fluid derived
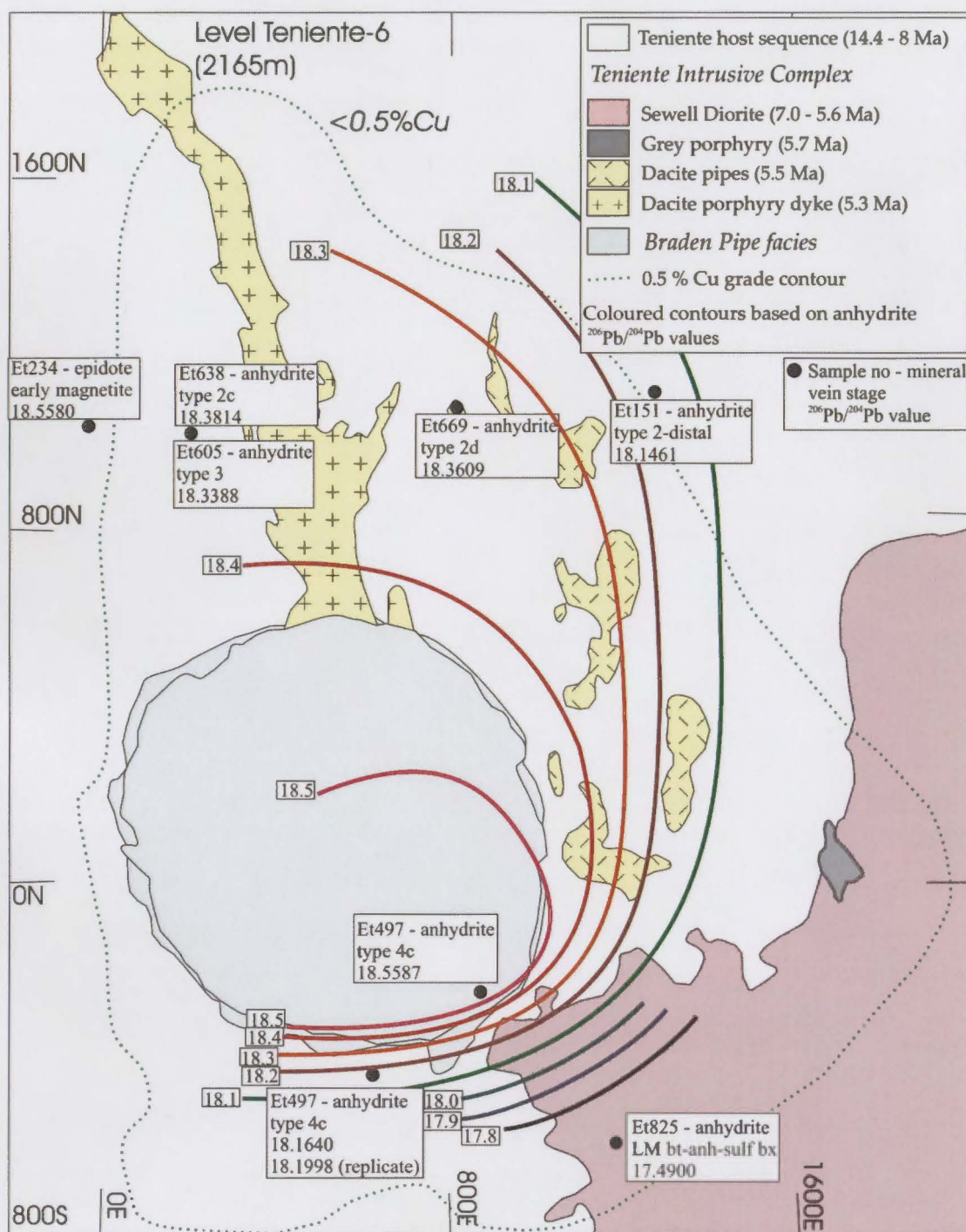
Figure 9.19. Spatial zonation of [206]Pb/[204]Pb values for the Teniente gangue minerals analysed during this study, projected onto the geology of the deposit through the Ten-6 level (2,165m asl). Anhydrite [206]Pb/[204]Pb values are enriched in the centre of the deposit, and most depleted distally from the dacitic intrusions and Braden Pipe. Note that the lead isotopic value of epidote does not fit this zonation.

from the crustally contaminated Teniente intrusive complex. The zonation also co-incides roughly with the sulfur isotope zonation around the dacite porphyry (Fig. 9.3).

The source of the primitive lead is speculative. Figure 9.15 indicates that the de-pleted end member lead has a composition similar to the Precordilleran basement. Primitive geochemical and isotopic signatures from Tertiary volcanics in central Chile are rare; however, they have been reported from the Las Maquinas basalts in the Sierra Pampeanas, the Segerstrom (CVZ back arc), and from the Colbun area (SVZ; Kay and Ambruzzi, 1996; Vergara et al., 1999). Although lead isotopic analyses of the Coya Machali Formation have not been performed, it is postulated that this formation may also have depleted lead isotopic values, based on its primitive Sr-Nd ratios (Fig. 9.14), shallow REE patterns, and tholeiitic affinites (Chapter 7) due to formation in thinned crust in an extensional basin (e.g. Kay et al., 1999; Charrier et al., 2002; Hollings et al., submitted). This contention is supported by a single analysis of the La Obra Pluton, the intrusive correlate of the Coya Machali Formation (Kay and Kurtz, 1995) which plots at relatively depleted lead isotopic compositions (Fig. 9.15).

In conclusion, due to the complex tectonic evolution of central Chile, there are do-mains that are depleted and enriched with respect to lead isotopic values within the upper and lower crust. It is speculated that deep-circulating connate, metamorphic or hydrothermal fluids may potentially have leached depleted lead from these primitive sources and were then focused up into the Teniente deposit via deep-seated structural pathways. As these upwelling fluids entered the Teniente magmatic-hydrothermal sys-tem, they partially equilibrated with magmatic-hydrothermal fluids and/or the upper crustal wall rocks with enriched lead compositions to generate the array of lead com-positions observed in Figure 9.15. The pronounced spatial zonation of lead isotopic compositions within the Teniente host sequence (Fig. 9.19) suggests mixing between primitive and enriched lead sources.

Sulfide and sulfate lead and sulfur isotope systematics

Irrespective of the source of the primitive lead, one of the most perplexing aspects of the Teniente isotopic dataset is that sulfides and sulfates were precipitated from SO_2 $_{(aq)}$ and $H_2S_{(aq)}$ in apparent sulfur isotopic equilibrium, implying formation from a com-mon fluid. However, the sulfides and sulfates have very different lead isotope sys-tematics, implying different fluid sources.

To explain a similar dataset at Río Blanco, Frikken (2003) and Frikken et al. (submitted) was able to temporally separate the anhydrite and sulfide stages of the breccia systems. He proposed that the anhydrite was precipitated from a hybrid fluid generated by mixing of magmatic vapours containing SO_2, and a deep-circulating water which supplied external primitive lead. In contrast, sulfides were precipitated from magmatic brines which ascended after the vapour phase. However, at Teniente the sulfide and anhydrite show evidence for textural equilibrium (Fig. 9.5) and sulfur isotopic equilibrium (Section 9.2), implying they were precipitated from a single magmatic-hydrothermal fluid. Furthermore, condensation of a vapour phase is expected to create a highly corrosive solution and resultant sericitic alteration of the wall rocks. The absence of phyllic alteration halos associated with anhydrite, and the scarcity of vapour-rich fluid inclusions in the LM stage veins and breccias argues against this mechanism operating during the LM stage at Teniente.

Due to the reverse solubility of anhydrite, cooling of a fluid results in increased anhydrite solubility, whereas heating leads to anhydrite precipitation (e.g. Rimstidt, 1997). In contrast sulfides are precipitated from a cooling fluid. Anhydrite precipitation from a sulfate-bearing fluid can also occur due to depressurisation, leaching calcium from the wall rocks to force anhydrite saturation, or mixing with a reduced calcium-rich fluid (e.g., Rimstidt, 1997). It is difficult to envisage co-precipitation mechanisms for anhydrite and sulfides that are in apparent equilibrium, yet have widely different lead isotopic values.

There is currently insufficient information to fully assess this paradoxical dataset, and no conclusive explanation is proposed in this study. A study integrating detailed petrology, further sulfur and lead isotopic analyses, and thermodynamics is required to resolve the lead and sulfur isotopic systematics of sulfides and sulfates in the central Chilean ore deposits.

9.7 SUMMARY

Stable and radiogenic isotope analyses have been able to constrain the physico-chemical conditions of alteration and mineralization and the sources of the fluids in the Teniente magmatic-hydrothermal system. Modelling of sulfur isotope values from co-existing sulfide-sulfate pairs indicates that the bulk sulfur composition of the fluid was

6‰, and oxidized conditions prevailed. LM sulfide $\delta^{34}S$ compositions are zoned from a core of −5‰ to values near 0% at the deposit periphery. Thus zonation is inferred to be due to progressive reduction of oxidized magmatic-hydrothermal fluids by the wall rocks or a reduced external fluid with magmatic-like $\delta^{18}O$ values.

In contrast, sulfides in the PH and LH veins have $\delta^{34}S$ values closer to zero at depth, and are more negative at higher elevations. The observed data can be modelled from cooling of a fluid with bulk sulfur $\delta^{34}S$ composition of 6‰ and SO_4:H_2S ratio of 3:1 for the LH stage and 2:1 for the PH stage, with a calculated vertical temperature gradient of ~ 15°C/100m. This cooling gradient is greater than can be achieved by boiling-induced cooling under hydrostatic pressure at ~2,000m depth, suggesting that fluid cooling was at least in part facilitated by fluid mixing, or by transient thermal disequilibrium occurring during fracture propogation. Alternatively, the sulfur isotopic zonation may be caused by more oxidizing conditions prevailing at higher elevations, possibly by condensation of oxidized magmatic vapours at higher levels in the system. Oxidation and cooling of the more reduced brine as it ascends and mixes with the condensed liquids could theoretically account for the observed shift in $\delta^{34}S$ values. Frikken (2003) and Frikken et al. (submitted) proposed this explanation for sulfur isotopic zonation in the Sur-Sur breccia at Río Blanco.

Stable isotopic evidence indicates that the fluids responsible for alteration and mineralization at Teniente were predominantly of magmatic origin. Calculated O-D fluid compositions for the LM stage fall in the felsic magmatic field of Taylor (1992), whereas isotopic compositions of the PH and LH stage fluids are similar to those for volcanic vapours (Giggenbach, 1992). The δD enrichment at constant magmatic oxygen values in the PH and LH sericite-stable fluids suggests that they were composed of magmatic vapours. There is no O-D isotopic evidence to indicate the involvement of meteoric fluids, even in the peripheral areas of the LM, PH and early LH stages of the Teniente deposit, although a volumetrically minor component cannot be discounted. Only late stage minerals from the LH stage such as carbonates, barite, and scheelite provide detectable evidence for the existence of meteoric fluids in the Teniente hydrothermal system, with $\delta^{18}O$ fluid values ranging down to 2.4‰. These $\delta^{18}O$ fluid values allow up to 30% meteoric water involvement in the latest stages of the Teniente magmatic-hydrothermal system.

Anhydrite and epidote from all stages of the Teniente hydrothermal system have a restricted range of Sr-Nd isotopic compositions that are indistinguishable from the Teniente volcanic complex and Teniente plutonic complex wall rocks, and different to the syn- and post-mineral igneous rocks. This suggests that these elements (and by analogy calcium?) were most likely leached from the altered wallrocks.

Limited lead isotopic analyses of sulfides from Teniente have homogenous enriched lead compositions overlapping with the pre- and post - mineral host rocks. In contrast, lead isotopic compositions of anhydrite are highly variable. The anhydrite lead isotopic values trend from enriched values similar to the sulfide lead compositions, to values at the deposit periphery that are more depleted than any igneous rocks from the Teniente district. The anhydrite may have been precipitated from a deep circulating fluid with a primitive isotopic signature inherited from a lead-depleted source. This interpretation requires that anhydrite and sulfide were precipitated from different fluids, whereas the sulfur isotopes and textural evidence suggests this was not the case. Despite the seemingly paradoxical isotopic datasets, the primitive lead signature in anhydrite implies the presence of a deep crustal scale structural pathway that focussed primitive components into the upper crust with minimal interaction with continental crust.

CHAPTER 10

CONCLUSIONS AND GENETIC MODEL

10.1 INTRODUCTION

The aim of this study has been to investigate the genesis of the Teniente copper - molybdenum porphyry deposit, the largest known copper resource in the world. This chapter discusses the major findings and their implications in three sections. The first section summarises the regional-scale features and processes that were important in the genesis of the Teniente deposit. In the second section the fluid inclusions, stable isotopes, and radiogenic isotopes are integrated in order to assess the origins of the fluids involved, the manner in which they interacted, and ultimately, the processes that caused copper precipitation. The third and concluding section integrates all of the preceding chapters into a genetic model for the Teniente deposit and compares the genetic model of this study to those proposed by previous authors.

Previous genetic models for the Teniente deposit

Previous workers (with the exception of Skewes et al., 2002) have advocated a classical porphyry model for El Teniente, with alteration and mineralisation zoned around a central lower grade felsic porphyry (Camus, 1975, 2003; Villalobos, 1975; Ojeda et al., 1980; Kusakabe et al., 1984; Cuadra, 1986; Maksaev et al., 2002, 2004) These workers related LM stage mineralisation and alteration to the intrusion of the Sewell Diorite stock and the dacite porphyry dyke, despite an apparent age difference of several million years. Zúñiga (1980) and Arévalo and Floody (1995) documented the zonation in the intensity of the biotite and sericite alteration around the dacite porphyry, supporting the interpretation of mineralisation related to felsic intrusions.

Most previous workers (e.g., Camus, 1975; Ojeda, 1980; Arévalo and Floody, 1995) have assumed that the PH and LH stages were caused by cooling of the LM stage fluids or ingress of meteoric fluids into the system, in accordance with the model of Sheppard et al. (1971) and Sheppard and Gustafson (1976). However, O-D, sulfur, and Sr-Nd isotopic studies by Kusakabe et al. (1984, 1990), Skewes (1992), and Skewes et al. (2001, 2002) indicate a magmatic origin for the LM, PH, and LH compo-

275

nents, with no evidence for a meteoric component.

Kusakabe et al. (1984, 1990) are the only authors to have addressed potential copper depositional mechanisms. Based on sulfur isotope geothermometry, and the temporal zonation from early biotite-stable to late sericite-stable alteration assemblages, they suggested that cooling of the fluids from ~500° to 350°C was the main mechanism for ore precipitation.

Mathur et al. (2001), Maksaev et al. (2002, 2004), and Munizaga et al. (2002) have confirmed a temporal link between the felsic intrusions and mineralisation by obtaining coincident U-Pb dates from the Teniente intrusive complex units (6.3 Ma, 5.7 – 5.5 Ma, 5.3 Ma, and 4.8 Ma; Table 6.1) and Re-Os dates from the molybdenite (6.3 Ma, 5.9 Ma, 4.8Ma, and 4.4 Ma; Table 6.2). These authors avoided the LM, PH, and LH terminology and instead favoured a model linking multiple generations of mineralisation with episodic magmatic pulses.

Skewes (1998, 2001) and Skewes et al. (2001, 2002) suggested an alternative to the classical porphyry model for El Teniente. They described the deposit to be primarily a breccia-hosted deposit, similar to Río Blanco/Los Bronces (Serrano et al., 1996) and Los Pelambres/El Pachón (Atkinson et al., 1996). They proposed that most of the copper mineralisation was emplaced in a series of early biotite breccias, which predated intrusion of the Sewell Diorite and the dacite porphyries. In support of this, they described mineralised veins and breccias which are cut by the Sewell Diorite. They inferred that intrusion of the dacite porphyry resulted in minor redistribution of the metals *into* the intrusive phase to create the central bornite zone (Skewes et al., 2002). Skewes et al. (op. cit.) confirmed a magmatic source of fluids based on additional stable isotopic and fluid inclusion information.

10.2 REGIONAL GEODYNAMICS

The following key points of the regional-scale and district-scale architecture are relevant to the genesis of the Teniente deposit.

Regional-scale crustal evolution

- Kay and Kurtz (1995) and Kay et al. (1999) proposed that the Teniente deposit, and indeed all of the porphyry deposits in central Chile, formed in the final stages

of an episode of compression and crustal thickening that started in the mid Miocene at approximately 15 Ma (e.g., Godoy, 1992). The early-mid Miocene Coya-Machalí Formation accumulated in an extensional basin above thin crust (~35 - 40km; Kay et al., 1991; Charrier, et al., 2002). Due to an increase in plate convergence rates, there was a transition to compressional tectonics, resulting in deformation of the Coya-Machalí Formation, reverse faulting, and crustal thickening (Fig. 2.3). Subsequently extruded lavas of the Farellones Formation have REE patterns reflecting a higher-pressure amphibole residual mineralogy. The Farellones Formation remained undeformed as it was thrust above the Coya-Machalí Formation (Godoy, 1994).

- Eventually volcanism ceased and plutons accumulated in the shallow crust beneath the remnant arc. The productive Teniente intrusive complex was emplaced during the latest Miocene – early Pliocene. These intrusions are some of the youngest and most evolved magmas in the region. The Young plutonic complex has a similar age and geochemistry as the Teniente intrusive complex and is highlighted as an attractive exploration target. These intrusions have REE patterns indicating a high pressure garnet-bearing residuum when the arc was at its thickest (~55 - 65 km, Kay et al., 1991; Kay and Kurtz, 1995). A trend to increasing $^{87}Sr/^{86}Sr$ ratios and decreasing εNd values with time for Miocene to Pliocene magmas (Fig. 9.14) testify to their increased crustal interaction with time, due to intrusion through a progressively thicker crust.

- Crustal thickening during the Miocene - Pliocene in central Chile appears to have been controlled by flattening of the slab due to subduction of the Juan Fernandez Ridge (e.g., Kay et al., 1999; Yañez et al., 2002). Oblique convergence, combined with the NE trend of the subducted ridge segment, resulted in southward migration of the deformation and associated crustal thickening with time. In contrast to the model of gradual crustal thickening proposed by Kay et al. (1999), Hollings et al. (submitted) argued that ridge subduction and slab flattening occurred abruptly in the Late Miocene, generating rapid uplift, magmas with anomalous compositions due to contamination from the slab, and, ultimately, giant ore deposit formation.

- It is speculated that tectonic inversion generated a stratigraphy conducive to trapping of fractionating magma chambers within the upper crust. In particular, the

thick flat lying Farellones Formation has the potential to trap magmas and act as a pressurising lid on the evolving magmatic-hydrothermal system. The normal faults which underwent tectonic inversion (e.g. El Fierro fault, Pocura fault, Triassic basement faults) may have been able to provide access to the upper crust for syntectonic magmas and fluids (Fig. 2.3).

- At the deposit scale, the Teniente host sequence is a strongly biotite-altered sequence of interpreted subvolcanic intrusions, extrusives, and volcaniclastic rocks. The intrusions have a basaltic to basaltic andesite composition. Although the sequence has not been dated, the intrusives are possibly correlatable with 11 – 9 Ma volcanic centres along the Codegua Fault (Fig. 2.4).

- The intermediate to mafic intrusives in the Teniente host sequence are geochemically anomalous in comparison to other late Miocene igneous rocks of Central Chile. Despite strong alteration this sequence has retained many of its primitive geochemical characteristics such as a tholeiitic affinity and shallow REE patterns suggesting formation in a thin crust. The Teniente host sequence intrusions have similar REE characteristics as the Coya-Machalí Formation which formed prior to compression above a thin crust (e.g., Kay and Kurtz, 1995). The primitive nature of the Teniente host sequence suggests either that regional compression was not initiated until after emplacement of the Teniente host sequence intrusions, or, more likely, that localised areas of extension existed within an overall compressive setting.

- Volcanism recommenced during the Pliocene. A new magmatic arc formed approximately 40km to the east of the extinct arc (Fig. 1.2). This occurred after formation of the Teniente deposit.

District-scale structural control

- At the district scale, El Teniente is located at the intersection of the crustal scale NNW-trending Codegua Fault and the NE trending Teniente Fault Zone (TFZ; Fig. 2.4). The Codegua Fault appears to have exerted a fundamental control on the localisation of volcano-sedimentary facies in the Teniente district (Rivera and Falcón, 1998; P. Gow, pers. comm., 2001). NNW trending structures form a persistent fabric evident at the largest scale in the central and northern Chilean Cordillera (Rivera

et al., 2000). These structures are believed to have been be caused by reactivation of Mesozoic basement faults (Fig. 2.3E; Rivera and Falcón, 1998; Rivera et al. 2000; Gow, 2000). Similar arc-transverse structures have also played an important role in localising mineralisation in other porphyry copper belts around the world, for example the Lachlan Transverse Zone in central NSW (e.g., Glen and Walshe, 1999) and transfer structures in the PNG-Irian Jaya region (Gow and Walshe, submitted).

- The TFZ has controlled argillic alteration and intrusion of the Sewell Diorite intrusive complex to the south-west of El Teniente (Fig. 2.5). Koeppen and Godoy (1994) proposed that the TFZ acted as a transform zone in central Chile to accomodate differences in convergence rates to the south and north.

- Consequently both the TFZ and the Codegua Fault may have been able to provide localised extensional settings such as grabens or pull apart basins which were favourable for emplacement of magmas. Considering the location of the deposit close to the intersection of these structures, it is considered likely that interference between the two structures generated a dilational setting into which magmas and fluids were focussed at the district scale.

- Structurally focussed and compartmentalised advanced argillic and phyllic (sericitic) alteration has occurred within in a 20 x 20km district-scale alteration system around El Teniente (Fig. 2.6). These alteration assemblages have overprinted a background regional propylitic alteration assemblage. It is tentatively proposed that the outline of the alteration systems may define the subsurface limits of deep magmatic-hydrothermal convection systems and/or upflow zones. They may highlight structures that have focused hydrothermal fluid flow and hence are important exploration targets.

10.3 FLUID RESERVOIRS AND ORE PRECIPITATION

El Teniente contains abundant evidence for the involvement of magmatic-hydrothermal fluids. However, some datasets cannot be fully explained by magmatic-hydrothermal fluids alone and require the input of external components. This section summarises the evidence for sources of the mineralising fluids, as deduced from the mineralogical, fluid inclusion, and isotopic studies, and highlights the evidence for non-magmatic fluids in the Teniente deposit. This information will then be used to as-

sess the physico-chemical gradients in the deposit in order to investigate processes of copper and molybdenum precipitation.

Fluid inclusions

The most abundant fluid inclusion type in the deposit are the low to moderate salinity liquid-rich (± opaque) type 1 fluid inclusions (Fig. 8.3A) which have copper contents up to several weight percent. Primary type 1 fluid inclusion populations are predominant in USTs and wavy-edged early quartz veins within the dacite intrusions, where they coexist with silicate melt inclusions. Based on this observation, these fluid inclusions are interpreted to have trapped a one-phase magmatic-hydrothermal liquid (Fig. 8.22). Sporadic decompression in tensional veins and breccias resulted in this fluid entering the two-phase region, whereupon it separated into a brine (which was trapped in the fluid inclusions), and a vapour phase which buoyantly ascended out of the ore-forming environment. Zoning of the salinities and maximum homogenisation temperatures of the inclusions suggest that magmatic-hydrothermal brines were sourced from the felsic intrusions (Fig. 8.18) and cooled as they migrated laterally.

In addition to these magmatic-hydrothermal fluids, low salinity, low temperature (200 – 300°C) fluid inclusion populations mainly in veins from the potassic and propylitic zones (Fig. 8.18C and D) indicate the involvement of an external water. Data trends suggest that this water mixed with the brine (e.g., Fig. 8.9C). Unfortunately none of the water inclusions were analysed by PIXE; however, a single brine inclusion from a LM vein from the propylitic zone, and three brine inclusions from a PH vein returned higher lead, zinc, arsenic and calcium concentrations than LM inclusions from the deposit centre. These elements may have been enriched due to mixing of the brine with small amounts of an external water in the peripheral LM and PH veins.

Stable isotopes

The oxygen-deuterium isotope compositions of LM, PH and LH hydrous vein and alteration products (this study; Kusakabe et al., 1984; Skewes et al., 2001) overlap with the felsic magmatic fluid and magmatic vapour fields (Fig. 9.9). No evidence for the involvement of meteoric water exists in the dataset, even in the distal propylitic and late stage phyllic veins. However, isotopic modelling shows that at low fluid/rock ratios, a meteoric water would isotopically equilibrate towards Farellones Formation

isotopic compositions and would be difficult to detect. It is speculated that up to 30% partially equilibrated meteoric water is permissible in the oxygen-deuterium data. Deuterium enrichment is interpreted to be a due to fractionation during fluid exsolution from the felsic melt and subsequent separation of a vapour phase.

Sulfur isotopic values for sulfides and anhydrite indicate the $H_2S_{(aq)}$ and $SO_{4\ (aq)}$ were in isotopic equilibrium and were derived from the same source (Fig. 9.12). The calculated bulk sulfur isotopic composition is 6‰, which is higher than most magmatic values but still consistent with a magmatic source (Ohmoto, 1986). Sulfur isotopes are zoned from most negative values in the centre of the deposit close to the dacite porphyry and pipes, to values near zero at the deposit margins. The most likely interpretation of this dataset invokes an oxidised magmatic fluid sourced from the dacites which was reduced and cooled as it migrated outwards to the deposit periphery.

Variation in calculated oxygen isotopic fluid values from LH carbonates suggests predominantly magmatic-hydrothermal fluids close to and within the Braden pipe, late dacite dykes, and pebble dykes, and the incorporation of up to 30% meteoric water in veins located distally from these rock types.

Radiogenic isotopes

The analysed Sr-Nd isotopic values of anhydrite and epidote gangue overlap with the values of the Teniente volcanic complex and Teniente plutonic complex (Fig. 9.14), and distinct from the syn- and post-mineral intrusions. This suggests that the strontium and neodymium (and by association calcium) is sourced from the wall rocks, and not from the felsic intrusions.

Lead isotopic compositions of sulfides from Teniente are similar to the crustally-enriched signatures of the igneous rocks from Teniente district and region (Fig. 9.15), implying a well-homogenised upper crustal lead reservoir. In contrast, the lead isotopic values for vein and breccia anhydrite are variable. They span a range from enriched upper-crustal values to strongly depleted values indicating an influence from a primitive source such as the Precordilleran basement. A pronounced spatial zonation exists in the anhydrite lead isotopic values, with the most depleted values occurring at the deposit periphery, and the most enriched values occurring in the centre of the deposit, proximal to the felsic intrusions (Fig. 9.19).

$^{187}Os/^{188}Os$ ratios of chalcopyrite and galena from the LH stage from Teniente also record primitive mantle-like ratios (Mathur et al. 2000), implying that osmium may be derived from a similar source as the lead. Mathur et al. (2000) proposed the existence of deep crustal pathways, so that this primitive osmium signature could be preserved.

Characteristics and origin of the external water

The points detailed above indicate that although the mineralising fluids at Teniente were predominantly magmatic in origin, some datasets indicate the involvement of a non-magmatic external water. Constraints can be placed on the nature of this external water. At the mine levels it had a temperature of around 200° to 250°C and a low salinity (< 5 wt% NaCl). The water was in equilibrium with the magnetite-stable wall rocks and was reduced in comparison to the oxidised magmatic fluids. Oxygen-deuterium isotopes indicate no evidence of a meteoric input. It possibly carried significant lead, zinc and arsenic. Importantly, it had lead and osmium isotopic signatures suggestive of a primitive source. Strontium, neodymium, and calcium may have either been contributed by the water, or leached from the wall rocks.

The source of this external water is speculative. One possibility is that it is a deep-sourced metamorphic liquid released during the breakdown of amphibole to garnet in the zone of magma generation at the base of the thickening crust, as proposed by Kay et al. (1999). Alternatively, this fluid could be a low salinity fluid derived from the underlying Jurassic-Cretaceous sedimentary rocks, which was trapped during crustal thickening and released during generation of out-of-sequence thrusting (Kay and Kurtz, 1995). The timing of fluid release in both of these interpretations is broadly synchronous with ore deposit formation. It is interpreted that this deep-circulating liquid was focussed along the regional-scale thrust planes and inherited a depleted lead isotopic signature due to interaction with either the Coya-Machalí Formation or a deeper primitive igneous unit, prior to bring channelled up into the Codegua Fault – TFZ structural system.

The regionally distributed early magnetite alteration assemblage (composed of magnetite - Ca-plagioclase - quartz - actinolite - rare epidote) may speculatively have been formed from a deep-circulating primitive water. However, the lead isotopic composition of epidote from an early magnetite alteration assemblage from the deposit periphery is similar to that of the homogenised upper crustal lead reservoir (Fig. 9.15).

Nonetheless, it is feasible that the epidote was precipitated from later magma-derived fluids which overprinted the early magnetite assemblage. Further lead isotopic analyses of anhydrite from the early magnetite alteration assemblage is recommended to assess the nature of the fluids which caused this alteration.

Ore depositional processes

Late Magmatic stage

At El Teniente, hypersaline fluid inclusions from the Na-K-feldspar alteration zone close to a dacite pipe contain up to 4 wt% copper. Hypersaline fluid inclusions from LM veins in the peripheral domain contain 0.01 wt% copper, indicating close to 100 % efficiency in copper precipitation over this interval. Relatively constant grades (between 0.5 and 1.2 % copper) over the ~1,000m interval from the deposit centre to the deposit periphery are consistent with a gradual, yet sustained physico-chemical gradient causing copper precipitation. This section summarises the gradients identified at El Teniente which may have caused copper precipitation.

Cooling: Fluid cooling below 400°C has been proposed as the main mechanism for copper precipitation at Bajo de la Alumbrera (Ulrich, et al., 2002), and Bingham Canyon (Redmond et al., 2004). The fluid inclusion dataset, and sulfur isotope geothermometry, indicate cooling of the mineralising brine from 520°C (± 80C) in the Na-K-feldspar altered zone to 400° (± 80°C) in the propylitic zone (Fig. 8.18).

SO₂ disproportionation: SO$_2$ disproportionation occurs at approximately 400°C (Rye et al., 1993; Ohmoto and Lasaga, 1997), and it is likely that at least some of the sulfide deposition at El Teniente was caused by an increase in the abundance of H$_2$S below this temperature.

Fluid reduction: Modelling of the sulfur isotopic values from a dacite pipe on section-83 indicates the orthomagmatic fluid had an SO$_4$/H$_2$S ratio of approximately 6:1, which was reduced to < 1.5:1 as the fluid migrated laterally (Section 9.5). This inferred redox zonation is consistent with the sulfide zonation in the deposit from innermost bornite (oxidised), through chalcopyrite, to outermost pyrite containing pyrrhotite inclusions (reduced; Figs. 4.1, 4.2). The general alteration zoning around the dacite pipes has been plotted schematically on log oxygen fugacity versus composition diagrams (Fig. 10.1A and B). The zonation from pervasive Na-K-feldspar alteration close to the
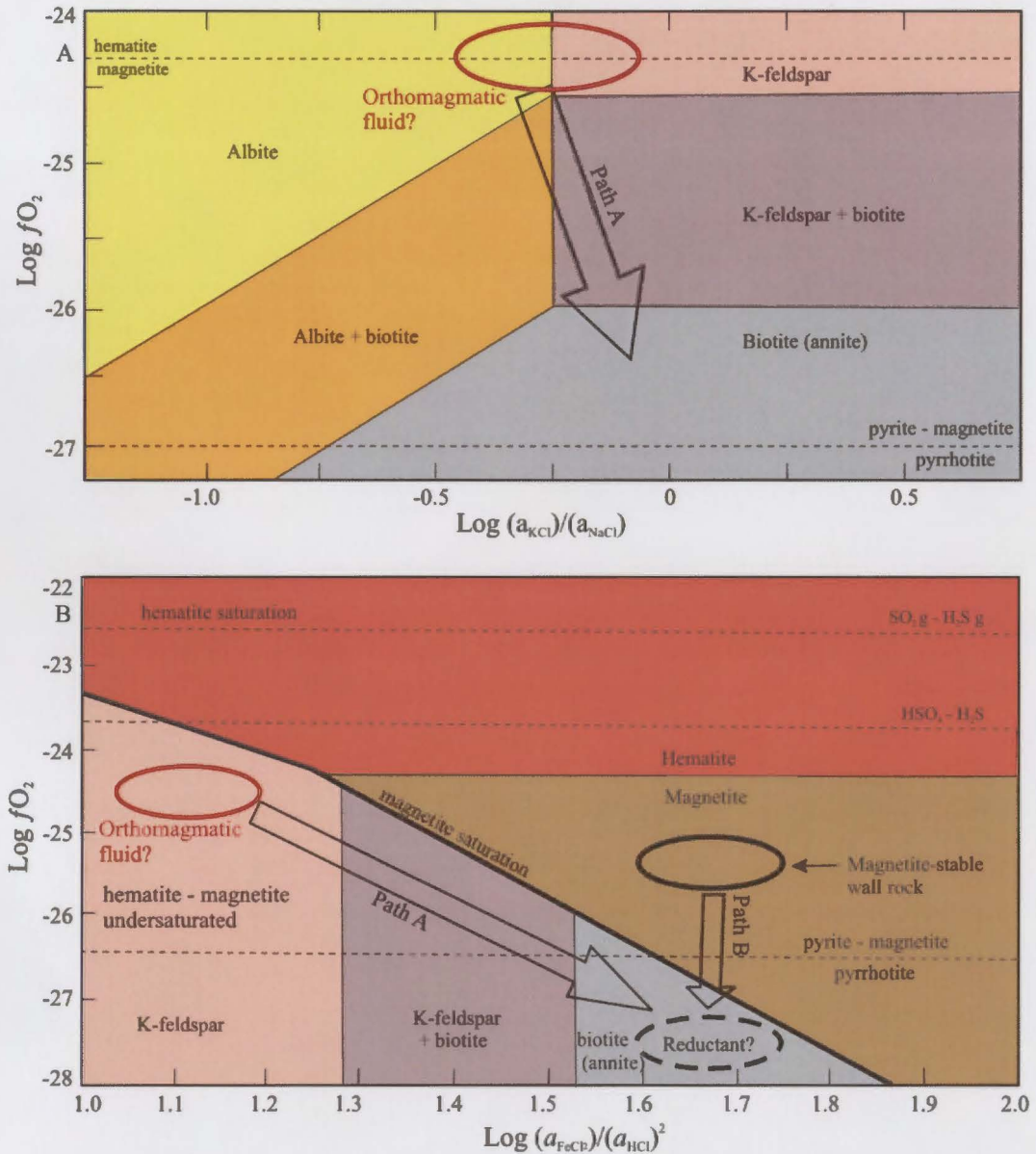
283

Figure 10.1. Phase diagrams illustrating the interpreted physico-chemical evolution of the Teniente orthomagmatic fluids as they were reduced due to interaction with the magnetite-stable Teniente host sequence (modified from Walshe et al., 2002). Diagrams were constructed at 400°C and 500 bars. Equilibrium constants calculated using HCH (Shavarov and Bastrakov, 1999), except for the annite data that was taken from SUPCRT95.

A) Log fO_2 versus Log $aKCl/aNaCl$. The orthomagmatic fluid was stable with respect to albite and K-feldspar close to the productive dacite pipes and porphyry, resulting in Na-K-feldspar alteration. As it migrated laterally it was reduced into the biotite-stable domain. Pyrite with pyrrhotite inclusions only seen outside the 0.5 % Cu deposit limits indicate that the hydrothermal fluid was further reduced in the peripheral domains.

B) Log fO_2 versus Log $aFeCl/(aHCl)^2$. The absence of iron oxides in the Na-K-feldspar alteration assemblage indicates that the orthomagmatic hydrothermal fluid was undersaturated with respect to hematite and magnetite (below the heavy line). This diagram is plotted using a high KCl/NaCl ratio, however at lower ratios albite predominates over K-feldspar (as shown in Fig. 10.1A). As the orthomagmatic fluid interacts with magnetite in the wall rock assemblage it is reduced and becomes biotite stable, synchronous with biotite replacement of the wall rock magnetite. No iron-oxides were precipitated in the Na-K-feldspar altered zones due to the high H_2S and low iron content of the mineralising fluid. This fluid is proposed to have been hematite- and magnetite-undersaturated, in the K-feldspar field (± albite – biotite) below the magnetite saturation line on Figure 10.1B.

dacite pipes to biotite alteration away from the pipes is consistent with reduction of an oxidised orthomagmatic fluid (Fig. 10.1A, path A). The nature of the reductant is open to interpretation, as the wallrocks do not show any evidence of oxidation. Wallrock magnetite has been replaced by biotite, which as indicated on Figure 10.1B (path B) involved reduction of the magnetite. Alternatively, the oxidised magmatic-hydrothermal fluid may have been reduced due to mixing with the reduced, deep-seated external fluid.

Fluid mixing: Mixing arrays in the temperature – salinity data of the fluid inclusion populations indicate fluid mixing was a common process in the deposit. Evidence for the reduced (below the pyrite + magnetite - pyrrhotite buffer; Fig. 10.1B), deep-circulating external water also exists in the radiogenic isotope datasets and mineralogical zonations. Mixing between a reduced, low salinity, and low temperature water and a hot, oxidised metalliferous aqueous solution can result in sulfide precipitation by abrupt cooling, dilution, and reduction.

Principal Hydrothermal and Late Hydrothermal stages

The sulfide-rich nature of the PH-LH stage veins, and low copper concentrations in interpreted "spent" fluid inclusions (< 0.12 wt% copper) imply that the ore depositional mechanisms acting during the PH and LH stages were highly efficient. The transition from the LM stage to the PH stage was marked by an abrupt change from lithostatic to hydrostatic conditions, possibly due to rupturing of the lithostatic seal. This resulted in a pressure and temperature decrease and phase separation of the magmatic-hydrothermal fluids. A change to hydrostatic conditions may also have allowed ingress of an external (non-meteoric) water into the magmatic-hydrothermal system. This is supported by the presence of low temperature and low salinity fluid inclusion populations in all of the analysed PH and LH vein samples. A vertical fluid temperature gradient of 15°C/100m has been estimated from sulfur isotopic modelling (Fig. 9.13). This temperature gradient is greater than the cooling rates predicted from conductive cooling or fluid boiling, and it could be explained by mixing with cooler, external, deep-circulating fluids, or by transient thermal disequilibrium during vein formation.

Summary

Metal precipitation during the LM stage appears to have been due to cooling and reduction of oxidised magmatic-hydrothermal fluid, either due to mixing with a deep-circulating external fluid, or wall rock interaction. The processes responsible for metal precipitation during the PH and LH stages are probably related at least in part to a change from lithostatic to hydrostatic confining pressures due to rupturing of the lithostatic seal, and fluid mixing due to ingress of external water.

10.4 EL TENIENTE GENETIC MODEL

Premineralisation stage

Early magnetite vein and alteration (magnetite – Ca-plagioclase – quartz – actino-lite) was the earliest hydrothermal event at El Teniente (Fig. 10.2). Early magnetite alteration occurred throughout the Teniente district, and has also been reported from the Río Blanco deposit (Serrano et al., 1996; Frikken, 2003). Epidote from the early magnetite alteration assemblage has a crustally enriched lead isotopic signature, similar to the Teniente wall rocks.
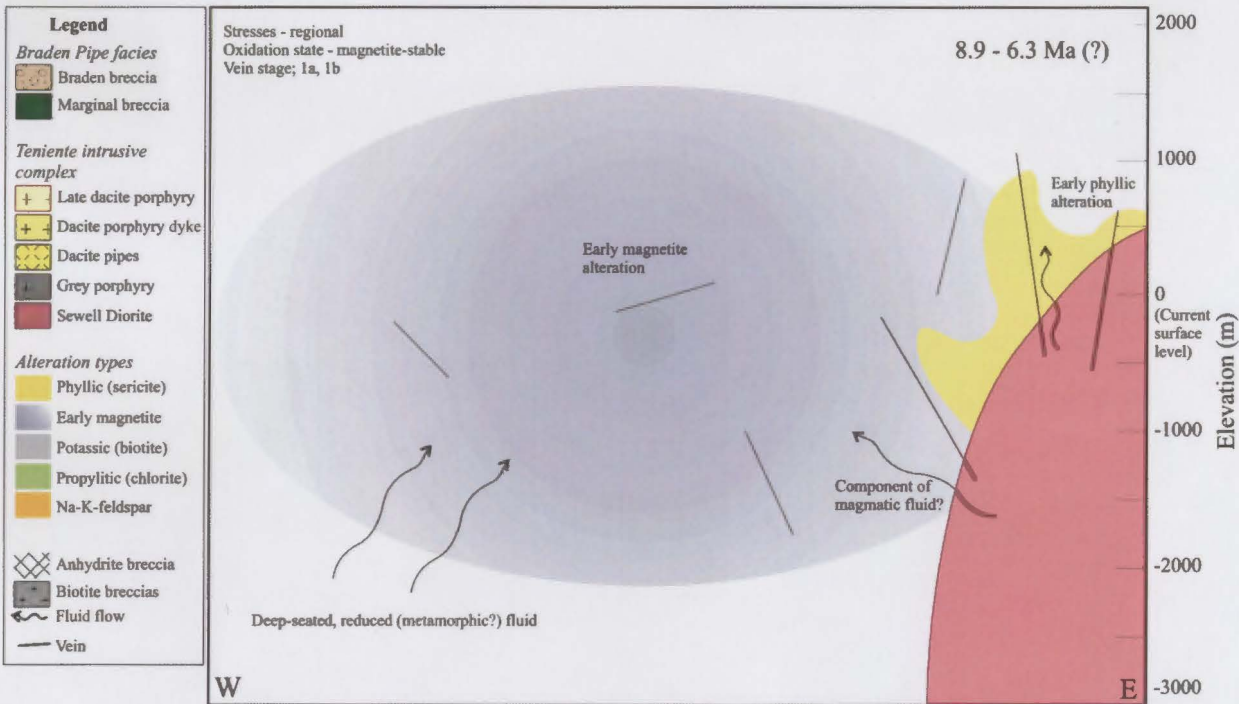

Figure 10.2. Diagram showing the features of the premineralisation stage of the Teniente deposit. The vertical axis plots elevation with respect to the current surface level at 0m. The horizontal axis is not to scale, and is schematically based on the section-124 (100N), looking north. Intrusive and volcanosedimentary units of the Teniente host sequence are not shown.

Early phyllic (+ tourmaline) alteration is spatially associated with the Sewell Diorite. Early magnetite alteration may have been formed from fluids with a magmatic component, or from deep-circulating, inward-migrating fluids.

The equigranular 8.9 – 7 Ma Sewell Diorite complex intruded prior to the LM stage. Early phyllic (tourmaline + sericite, chlorite, magnetite) alteration formed adjacent to the Sewell Diorite, locally associated with thick, barren quartz veins. No copper or molybdenum was associated with the premineralisation hydrothermal stages.

Late Magmatic stage

A large calc-alkaline magma body was emplaced at approximately 6.3 Ma, probably at depths of 4-6 km below the palaeosurface (Fig. 10.3A). This magma chamber sourced the individual phases of the Teniente intrusive complex units and controlled the magmatic-hydrothermal evolution of the deposit for the next 2 million years.

Crystallisation in an ascending and cooling parent magma chamber can lead to the separation of an aqueous fluid phase into which volatiles and metals are readily partitioned (e.g., Henley and McNabb, 1978; Burnham, 1979, 1985). These aqueous phases migrate to the apical portions of the magma chamber and pond beneath the crystallising carapace. As crystallisation proceeds, the fluid pressures build up and eventually exceed the lithostatic confining pressures, resulting in rupturing of the carapace and adjacent wallrock. This allows formation of stockwork veins and/or breccias (if the mechanical energy is sufficient; Burnham, 1985; Fournier, 1999).

Despite the location of El Teniente at a structural intersection, the deposit-scale stresses were controlled by the parent magma chamber. Stresses localised around the intruding magma chamber were greater than the regional stresses, resulting in the formation of the LM vein stockworks with orientations predominantly radial and concentric to the parent chamber. Explosive fragmentation resulted in formation of localised biotite (± copper-iron sulfides) cemented breccias early during the LM stage.

High confining pressure in the parent magma chamber resulted in the exsolution of a one-phase supercritical magmatic-hydrothermal liquid from the deep parent chamber. High confining pressures may have been due to the presence of a lithostatic seal above the deposit. The exsolved liquid was maintained in the one-phase field as it ascended to the current El Teniente mine level, greater than 2,500m depth below the palaeosurface. This aqueous low salinity liquid was approximately 500°C (± 100°C) and contained up to 4 wt% copper in solution. Local decompression in dilational veins resulted in phase separation and generation of a brine phase and a vapour phase.
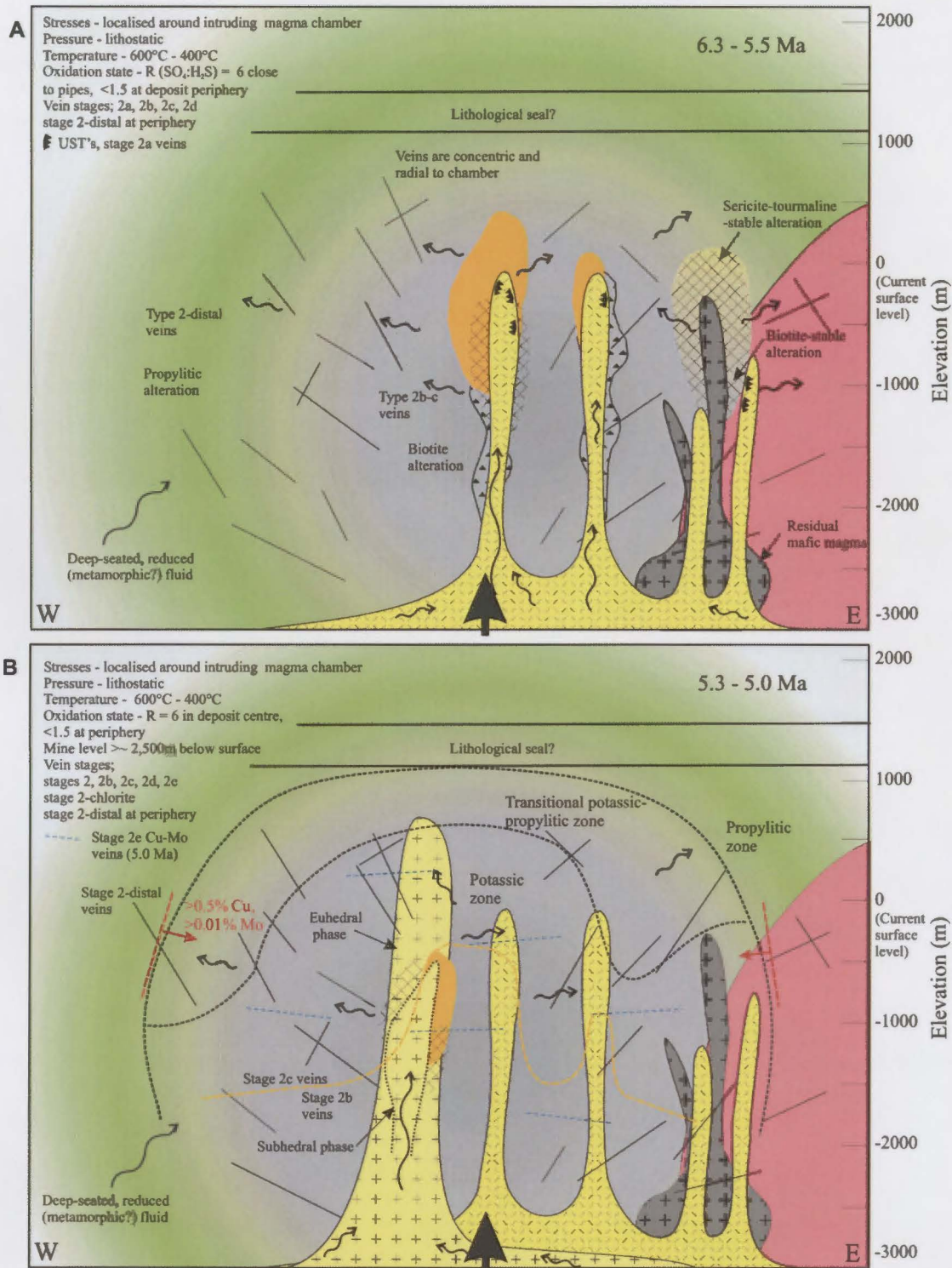
Figure 10.3. Late magmatic stage of the Teniente deposit. Geological legend is explained in Figure 10.2.

A) Dacitic pipes were sourced from a postulated deep magma chamber that controlled the stresses and resultant vein orientations in the deposit. Magmatic-hydrothermal fluids during the LM stage migrated laterally, due to the interpreted presence of a lithological seal that maintained high fluid pressures and restricted fluid boiling. Fluids focussed up through the dacite pipes formed proximal Na-K-feldspar alteration, passing outwards to biotite and peripheral propylitic alteration. Localised anhydrite breccias and biotite breccias occur near the intrusive contacts

B) The multiphase dacite porphyry intruded from the deep magma chamber after the dacite pipes. Type 2b veins predominate at higher elevations, whereas type 2c veins predominate at depth, closer to the parent chamber. Subhorizontal type 2e Cu-Mo veins post date vein types 2a-d and the LM intrusions. 0.5% Cu and 0.01% Mo contours are indicated by the red dashed lines at the mine elevation.

288

Pulses of magma intruded from the deep-seated magma body between 5.7 and 5.5 Ma (Fig. 10.3A). The first intrusion was the grey porphyry (5.7 Ma; Table 3.2), one of several intermediate pipes which intruded into the Sewell Diorite contact zone. They probably crystallised from a residual intermediate magma that co-existed with the felsic magmas. High intrusive and fluid pressures ruptured the wall rock surrounding the grey porphyry. Chalcopyrite, anhydrite, biotite ± tourmaline precipitated from magmatic-hydrothermal fluids, forming the breccia cement. Molybdenite from this body returned ages of 5.9 Ma (this study) and 6.3 and 5.7 Ma (Maksaev et al., 2004).

Biotite alteration (vein-controlled, microfracture-controlled, and pervasive) of the unaltered and early-magnetite altered Teniente host sequence occurred during emplacement of the intrusions. Biotite alteration grades outwards to transitional potassic-propylitic alteration, and to outermost chlorite-stable propylitic alteration (Figs. 10.3A and B).

A series of dacite pipes intruded into the Teniente host sequence, and into the contact zone with the Sewell Diorite, dated between 5.6 and 5.5 Ma (Maksaev et al., 2002; Fig. 10.3A). Some of the dacite pipes contain wavy-edged stage 2a veins and USTs, linking fluid exsolution with late stage crystallisation of the pipes. The small volume of the dacite pipes compared to the huge volume of altered and mineralised rock implies that the mineralising fluids were sourced from the deep parent chamber, and channelled up into the dacite pipes. A mineralised, pervasive Na-K-feldspar alteration assemblage formed around the productive dacitic pipes, and overprinted the biotite alteration assemblage. Stage 2b and 2c veins (composed of quartz – anhydrite - sulphide - Na-K-feldspar - biotite) and stage 2d anhydrite - sulfide breccias cut and were cut by individual dacite intrusions, indicating that multiple vein- and breccia-forming events overlapping with the intrusion of the dacites. Based on sulfide and gangue mineral zonations and crosscutting relationships, it is inferred that veining, alteration and copper - molybdenum mineralisation occurred synchronously with some, but not all of the dacitic pipes.

Alteration and vein patterns in the deposit are broadly zoned around the dacite porphyry, implying that it intruded into the hydrothermal and structural core of the deposit from the underlying magma chamber (Fig. 10.3B). The central 'subhedral' phase of the dacite porphyry intruded at 5.3 Ma (Maksaev et al., 2002). It caused veining, min-

eralisation and localised development of anhydrite breccias and Na-K feldspar altera-
tion at its contacts. The central bornite core of the deposit is largely restricted to within
and around the subhedral phase (Fig. 4.2), implicating its role in ore formation. De-
spite the geological features which link the dacite porphyry to mineralisation, no Re-
Os ages on molybdenite have been correlated with the 5.3 Ma dacite porphyry age.
The earlier 'euhedral' phase of the dacite porphyry, which is undated, is an elongate
body that is cut by the alteration zones, sulfide zones, and 0.5 % Cu contour in the
north of the deposit (Figs. 3.1, 4.2, and 4.3). It is interpreted to be a pre-mineral wall-
rock.

The stage 2b and 2c veins comprise the bulk of the LM stockwork in the potassic
alteration zone in the Teniente host sequence. In the transitional and propylitic zones,
chlorite-sericite-stable stage 2f-chlorite and stage 2-distal veins predominate. These
veins are interpreted to be temporally equivalent to the Na-K-feldspar / biotite-stable
stage 2 veins in the deposit core. It is estimated that approximately 60% of the copper
in the deposit is hosted in LM stage veins, breccias and alteration assemblages.

Late-stage 2e (quartz-sulfide) veins are continuous, have parallel walls and sulfide
seams and selvages. This vein stage hosts a significant proportion of the molybdenun
in the deposit, which has been dated at between 5.01 and 4.95 Ma. These veins do not
have any spatial or temporal relationship to any felsic intrusion identified within the
deposit, indicating that some pulses of hydrothermal fluids were released from the par-
ent chamber without accompanying felsic intrusion at the level of the ore deposit.

Principal Hydrothermal stage

The beginning of the PH stage was marked by breaching of the brittle-ductile tran-
sition at 4.95 Ma due to continued uplift and exhumation to a depth less than 2,500m
below the water table (Fig. 10.4). Pressures dropped from lithostatic to hydrostatic
(e.g., Fournier, 1999), and the magmatic-hydrothermal fluid abruptly underwent de-
compression and entered the two-phase field to generate a brine and vapour. PH stage
veins are wider, straighter, and more continuous than LM veins, reflecting the brittle
conditions under which they formed. They have chalcopyrite rich seams (± anhydrite -
quartz - molybdenite - pyrite) and sericite-quartz (± chlorite) halos. PH vein orienta-
tions are unchanged from the LM stage, indicating the prevalence of high magmatic-
controlled stresses. Despite the low PH vein abundances in most of the deposit (mostly

<5 veins/m core), and the short duration of the PH stage (< 100,000 years), approximately 30% of the copper in the deposit is estimated to have been precipitated during this stage.

Deuterium isotopic enrichment implies the involvement of magmatic vapours in the formation of the PH and LH stage minerals, and magmatic oxygen isotopic values preclude the presence of significant meteoric water. Temperatures were between 450°C and 350°C in the PH stage. A vertical zonation of sulfur isotopes can be modelled by cooling of the ascending hydrothermal fluid by, on average, 15°C/100m (Fig. 9.13). This cooling rate cannot be achieved by conductive cooling or boiling of the fluid, and can be interpreted to indicate fluid mixing, or thermal disequilibrium in the wallrocks. The degree of sericitisation of the wall rocks around the PH veins in general increases with elevation (Fig. 4.19) and appears to be related to cooling of the fluids below ~400°C. Acidity could have been generated by $HCl_{(g)}$ dissociation and/or SO_2 disproportionation in the cooling fluid (Rye et al., 1993). The acidity and temperature of the fluid did not evolve to conditions favourable for argillic or advanced argillic alteration, at least at the current mine levels.
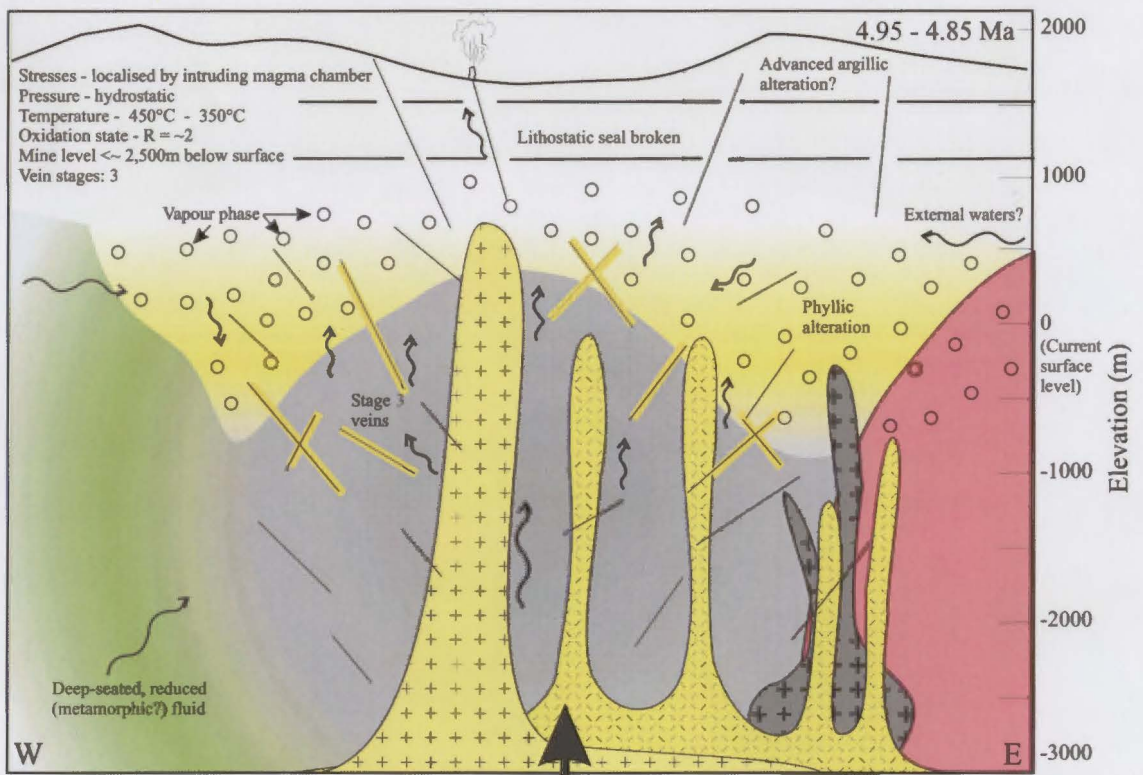

Figure 10.4. Principal Hydrothermal stage of the Teniente deposit. Geological legend is explained in Figure 10.2.
The lithological seal was ruptured during the PH stage, probably due to reduction of the lithostatic pressure due to uplift and erosion. Depressurisation resulted in boiling of the magmatic-hydrothermal fluids. Vein controlled and pervasive phyllic (sericitic) alteration occurred mainly at higher elevations in the deposit. No intrusive activity has been correlated with the PH stage.

The sulfur isotopic zonation could alternatively be explained by more oxidising conditions at higher elevations, possibly due to condensation of magmatic vapours at high levels to form an acidic fluid that caused pervasive sericite alteration. However, no redox mineralogical variations have been identified to support this interpretation.

Late Hydrothermal stage

The LH stage was a second sericite-stable stage related to the intrusion of the Braden pipe and late dacite intrusions. The LH stage began approximately 4.85 Ma, when the mine level was less than ~1700m below the palaeowater table (Fig. 10.5A). LH veins are distinguished from PH veins by a diverse ore and gangue mineralogy, including base metal sulfides and sulfosalts, and quartz, sulfates, carbonates, and tourmaline. An increase in the acidity of the fluid is indicated by the presence of illite and kaolinite, and pyrophyllite, which was reported by Camus (1975). Sulfur isotopic modelling indicates oxidised fluid conditions ($SO_2/H_2S = ~3$) and temperatures varying from approximately 470°C at depth to 320°C at the mine level, with an apparent temperature gradient of ~15°C/100m of vertical elevation. Enriched deuterium isotopic fluid values calculated from sericite and tourmaline indicate that magmatic vapours were involved in their formation, whereas low oxygen isotopic fluid values from carbonates, between 2‰ and 10‰, indicate the involvement of meteoric waters.

The LH stage paragenesis is summarised below in three stages; pre-Braden breccia, Braden breccia formation, and post-pipe stages.

Pre-Braden breccia stages

The first LH event was formation of the tourmaline – anhydrite – chalcopyrite – bornite – tennantite-tetrahedrite cemented Marginal breccia, and co-genetic stage 4a veins and breccias (Fig. 10.5A). The open-space fill textures of the these veins and breccias suggest that they filled dilational openings. The Marginal breccia forms an inward-dipping incomplete cone sheet concentric to the deep magma chamber. This paragenetic stage was probably caused by volatile release from the magma chamber, possibly accompanied by late dacite intrusion (Fig. 10.5A).

The most abundant LH veins are stage 4c veins, containing a diverse mineralogy including sulfides (bornite, chalcopyrite, pyrite, galena, sphalerite, stibnite, molybdenite), sulfosalts (tennantite-tetrahedrite), carbonates (calcite, dolomite, ankerite), sul-
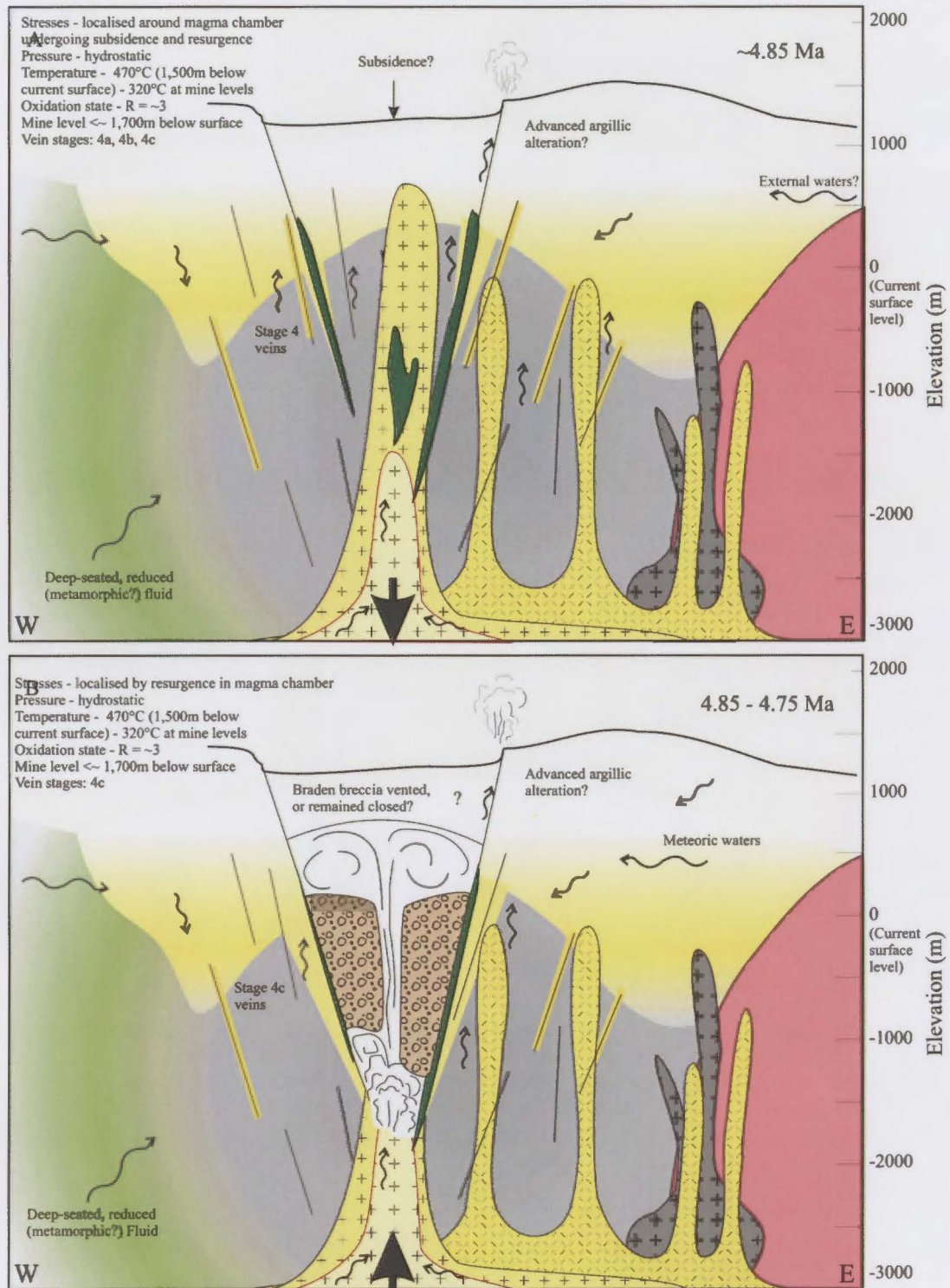
Figure 10.5. Late Hydrothermal stage of the Teniente deposit. Geological legend is explained in Figure 10.2.

A) LH stage structures are steeply-inward dipping, in contrast to the LM and PH stage veins, imply they were formed during relaxation of intrusive magmatic pressures. Approximately 800m of erosion is estimated to have occurred in the short interval between the start of the PH stage and the end of the LH stage. The first LH stage was formation of the Marginal breccia, possibly related to intrusion of a late dacite stock.

B) Braden breccia formation occurred due to the combined fluid and magmatic pressures exceeding the lithostatic confining pressures. Wall rock material was pulverised and fluidised and settled out to form a variably stratified rock flour matrix breccia. The Braden breccia utilised the concentric Marginal breccia fracture zone for emplacement. Brecciation may have been facilitated by phreatomagmatic explosion caused by ingressing cool external waters interacting with the late dacite magma, and/or fast rates of uplift and erosion.

fates (anhydrite, gypsum, barite), quartz, and tourmaline. These veins overlapped temporally with formation of the Braden pipe.

Braden breccia formation

The Braden breccia is interpreted to be related to intrusion of dacitic ring dykes (late dacite) and stocks sourced from the deep-seated parent magma chamber. Molybenite from the contact zone of a late dacite stock at depth returned an age of 4.85 Ma (this study), in good agreement with a U-Pb age of 4.82 Ma (Maksaev et al., 2004) for a late dacite dyke. Depth estimates from PH and LH fluid inclusions indicate rapid uplift and erosion was occurring (~2.4 mm/yr) during the PH and LH stages, reducing the lithostatic load above the magma chamber.

Combined fluid and magmatic pressures associated with the emplacement and cooling of a late dacite stock is inferred to have eventually exceeded the lithostatic pressure, resulting in brecciation, and generation of the Braden breccia (Fig. 10.5B). Sillitoe (1985) interpreted the Braden pipe to be phreatomagmatic in origin; however, direct evidence for this process (i.e., wispy clasts from the parent magma) is lacking. The Braden breccia utilized the concentric fractures occupied by the Marginal breccia phase, resulting in the characteristic funnel shaped Braden breccia partially bordered by the early-formed Marginal breccia (Fig. 10.5B). The entrained material was fluidized, resulting in clast rounding, thorough mixing, stratification, and crosscutting breccia units, consistent with the simulated models of McCallum (1985). The sericitic alteration rims around the outer edge of most clasts indicate the involvement of acidic hydrothermal fluids in the fluidisation process. Sericite at a clast margin has been dated at 4.75 Ma (± 0.10 Ma) by $^{40}Ar/^{39}Ar$ geochronology (Maksaev et. al., 2004). Large blocks of late dacite were incorporated into the pipe, which may have been blocks of wall rock transported downwards, or parts of the causative late dacite stock transported upwards, or a brecciated intra-pipe intrusion. No unambiguous evidence was observed to indicate if the pipe vented to the surface or remained closed.

Post-pipe stages

After formation of the Braden pipe, minor late dacite dykes and pebble dykes intruded, locally associated with anhydrite/sulfide breccia zones and phyllic alteration (Fig. 10.6). A stage 4c anhydrite sulfide breccia spatially associated with a late dacite

dyke returned a molybdenite age of 4.7 Ma. The last veins to form in the deposit were predominantly unmineralised stage 4d gypsum – chlorite dominated veins.

Late stage tourmaline and chalcopyrite were deposited from fluids passing through concentric fractures in the pipe and along its margins. This hydrothermal activity is responsible for the localised gradual transition between the Marginal breccia and the Braden breccia (Floody, 2000; Fig. 10.6). The last stage in the pipe genesis was the formation of giant gypsum crystals filling open spaces in gas and/or liquid pockets in the Braden breccia.

LH veins differ from LM and PH veins in their orientation. They have steeply-inward dipping concentric orientations around the parent magma chamber. Stereonets of LH vein data and fault data indicate the absence of radial structures. This implies that the fractures were formed in response to a period of subsidence or magma with-drawal from the parent chamber. Other stage 4c and 4d veins are NE-trending, parallel to the district-scale TFZ, indicating that they were influenced by far field stresses ex-ceeding localised magmatic stresses (Fig. 10.6). The orientations of LH structures indi-
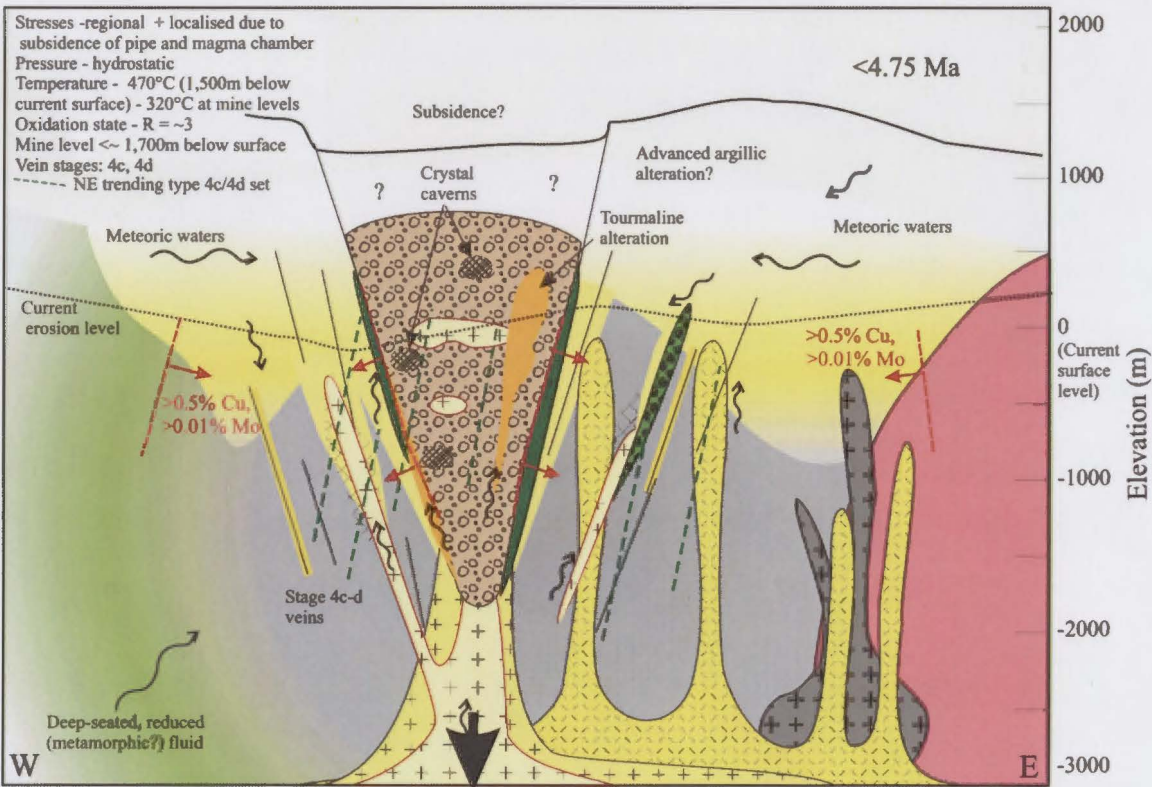

Figure 10.6. Late Hydrothermal stage of the Teniente deposit. Geological legend is explained in Figure 10.2.

The post-pipe stages include intrusion of late dacite dykes, associated phyllic alteration and anhydrite breccias, minor pebble dykes, and tourmaline (+ minor Cu) alteration along the margins and internally in the pipe. A set of post-pipe, NE trending LH stage veins reflect the influence of far field stresses, due to depressurisation of the parent magma chamber during brecciation.

cate that brecciation and formation of the Braden pipe depressurised the parent magma chamber, and in doing so dissipated the high magmatic pressures which controlled the LM and PH stages of fracturing in the deposit.

Ar-Ar and K-Ar ages from biotite and sericite are mostly from 4.81 - 4.37 Ma. A lateral and vertical zonation of cooling ages indicates that they do not represent precipitation ages but instead ages of cooling below ~300 - 350°C. The late dacite body underneath the Braden pipe was the thermal centre of the magmatic-hydrothermal system during the LH stage. The biotite closure isotherm is estimated to have descended at approximately 100m/10,000 years (10 mm/yr). This is an order of magnitude greater than uplift rates calculated from the Teniente deposit (0.4 to 2.4 mm/yr; this study, Chapter 8; 0.15 to 3mm/yr from Skewes and Holmgren, 1993; Kurtz et al., 1997). Considering the thermal gradient of 15°C/100m calculated from the sulfur isotope modelling, this indicates that the late-stage magmatic-hydrothermal system at Teniente cooled at ~15°C/10,000 years. This fast cooling rate indicates that cooling of the hydrothermal system took place by thermal conduction, and probably also phase separation and fluid convection.

Comparison with previous models for El Teniente

The results of this study are not consistent with the model of Skewes et al. (2001, 2002), who postulated that El Teniente is a mega-breccia-hosted deposit. Skewes et al. (op. cit.) proposed that copper at El Teniente was initially deposited with widespread biotite brecciation and alteration, and was either remobilized or eliminated by the later intrusive events. Several points from the current study are incompatible with this model. No textural evidence has been observed for the dissolution and remobilization of early-formed copper sulfides during the intrusion of the dacite porphyry and pipes. If Skewes et al. (2002) are correct, then the LM and PH vein halos would be sulfide-deficient compared to the pervasive biotite altered wall rock, and high vein densities would correlate to low copper grades. In both cases the opposite relationship is observed, indicating that copper was introduced into the host rock through the veins.

Skewes et al. (2002) argued that the dacite porphyry is low grade compared to the Teniente host sequence because it postdated the biotite breccias and copper mineralisation. This study has shown that biotite breccias locally cut the dacites. Furthermore, the low copper grade of the dacite porphyry (a feature common to many porphyry cop-

per deposits; e.g. Sillitoe, 2000), may simply reflect its intra-mineral timing, the presence of as-yet undiscriminated late-mineral dacite porphyry phases that have diluted grade, or a lack of a suitable physicochemical gradient to precipitate copper or molybdenum in the central, hottest parts of the system. Based on drill core observations, it is concluded that the biotite breccias and associated widespread biotite alteration are temporally and spatially linked to the dacite intrusions, and are not a discrete hydrothermal event that preceded dacite emplacement by up to several million years (as suggested by Skewes et al., 2002).

Skewes et al. (2002) classified El Teniente as a breccia-hosted deposit. The current study for the first time has mapped out individual lithofacies on cross sections, and we confirm that breccias, including biotite-cemented breccias, anhydrite-cemented breccias, and the Marginal breccia facies of the Braden pipe do host high-grade ore at El Teniente. However, the breccias are volumetrically minor in comparison to the several cubic kilometers of felsic intrusions and andesitic host rocks which contain the pervasively developed vein stockwork that hosts the bulk of the ore at El Teniente.

Our research, and the geochronology of Maksaev et al. (2002, 2004), Cannell et al. (2002), and Stein et al. (in prep), confirms the findings of Howell and Molloy (1960), Camus (1975), Ojeda (1980), and Cuadra (1986) that the mineralisation, veining and alteration at El Teniente are intimately linked to felsic intrusions. Vein overprinting relationships indicate that the LM stage vein-hosted mineralisation overlapped temporally with the multi-stage dacite intrusions. The dacite pipes, the southern end of the dacite porphyry dyke and the grey porphyry appear to have acted as fluid conduits, and focused veining, brecciation, and high-grade mineralisation proximal to their contacts. The pervasive alteration assemblages, sulfide assemblages, and LM vein assemblages and intensities all vary systematically both outward and upward from the dacite porphyry to the deposit periphery.

The interpretation in the current study differs from the above authors in that it is speculated that a large parent magma chamber exists below the level of the mine. The predominance of concentric and radial vein orientations in all stages of mineralisation at El Teniente indicates that the emplacement of this large parent magma chamber localised stresses and controlled vein formation throughout the life of the hydrothermal system, from early stages of stockwork development to later stages of brecciation to form the Braden Pipe. This intrusion is interpreted to have sourced both the felsic in-

trusions and mineralising fluids. Re-Os molybdenite dates and SHRIMP U-Pb zircon dates from the porphyries indicate broadly synchronous mineralisation and high level felsic intrusion, spanning a time interval of at least 1.5 Ma. Clusters of Re-Os ages that do not correlate with known felsic intrusion U-Pb ages indicate that episodes of mineralisation may have been generated from the deep magma chamber that were not accompanied by high level intrusion. Episodes of magma intrusion and withdrawal, coupled with decreasing depths and pressures due to tectonic uplift and concomitant erosion, are proposed to account for differences between the three main stages of mineralisation at El Teniente.

El Teniente has many features typical of porphyry copper-molybdenum deposits. It is characterised by multiple phases of weakly to strongly altered felsic intrusions. It has an alteration paragenesis and distribution typical of other porphyry copper deposits (e.g., Lowell and Guilbert, 1970). Its vein paragenesis is similar to El Salvador (Gustafson and Hunt, 1975). It has an association with a large, late-stage breccia pipe, similar to deposits such as Batu Hijau (Garwin, 2002). El Teniente is the largest known copper resource in the world; however, no single empirical feature of the deposit has been identified in this study to account for its anomalous size, or distinguish it from porphyry copper deposits that contain less copper.

10.5 FUTURE WORK

Several unresolved questions that are considered to warrant further investigations are highlighted below:

• Structural mapping at the district scale to identify movement directions, the temporal relationship between the Codegua Fault and TFZ, and the alteration assemblages associated with these structures.

• Further detailed logging (and underground mapping?) of the Teniente host sequence, involving petrographic studies, to delineate intrusive and volcano-sedimentary lithofacies.

• Underground mapping of biotite breccia bodies to determine their morphology, spatial distribution, and relationships to the various intrusions at El Teniente.

• Paragenetically controlled underground structural mapping to preferred orienta-

tions and structural controls on individual vein generations.

- Further geochemical analyses (or a compilation of pre-existing data) of Teniente host sequence, to determine i) major and trace element immobility during alteration, ii) the presence of different igneous suites, iii) the geochemical relationship with the regional units of the Farellones Formation and Coya Machali Formation.

- Geochemical and petrographic study of the grey porphyry to assess if it i) represents coeval intermediate and felsic magmatism in the deposit, or ii) formed by contamination of a felsic protolith with mafic Teniente host sequence wallrock.

- Further U-Pb dating of Teniente complex intrusions, in particular the subhedral phase of the dacite porphyry, to investigate the temporal relationship between felsic intrusion and molybdenum mineralisation.

- Mapping of the distribution of redox-sensitive minerals, such as anhydrite, magnetite, and hematite to investigate redox zonation in the deposit more thoroughly.

- Investigation of silicate melt inclusions and their relationship to aqueous fluid inclusions.

- Cathode luminescence studies to assist in determining the paragenetic relationship between the high and low salinity fluid inclusions, and the silicate melt inclusions.

- Quantitative micro-analyses (e.g., PIXE or LA-ICPMS) of the low temperature, low salinity fluid inclusions which trapped the interpreted external water to determine compositional information, and possible source.

- Further lead isotopic analyses to investigate the decoupled lead isotope systematics in anhydrite and sulfides at Teniente. In particular re-analyse the early magnetite alteration assemblage to assess the nature of the fluids which formed this assemblage.